Criteria and Tools for Determining Drainage Divide Stability

Adam M. Forte[1]* & Kelin X. Whipple[2]

[1]Department of Geology and Geophysics, Louisiana State University, Baton Rouge, LA
[2]School of Earth and Space Exploration, Arizona State University, Tempe AZ

*Corresponding author email: aforte8@lsu.edu

Abstract

Watersheds are the fundamental organizing units in landscapes and thus the controls on drainage divide location and mobility are an essential facet of landscape evolution. Additionally, many common topographic analyses fundamentally assume that river network topology and divide locations are largely static, allowing channel profile form to be interpreted in terms of spatio-temporal patterns of rock uplift rate relative to base level, climate, or rock properties. Recently however, it has been suggested that drainage divides are more mobile than previously thought and that divide mobility, and resulting changes in drainage area, could potentially confound interpretations of river profiles. Ultimately, reliable metrics are needed to diagnose the mobility of divides as part of routine landscape analyses. One such recently proposed metric is cross-divide contrasts in χ, a proxy for steady-state channel elevation, but cross-divide contrasts in a number of topographic metrics show promise. Here we use a series of landscape evolution simulations in which we induce divide mobility under different conditions to test the utility of a suite of topographic metrics of divide mobility and for comparison with natural examples in the eastern Greater Caucasus Mountains, the Kars Volcanic Plateau, and the western San Bernadino Mountains. Specifically, we test cross-divide contrasts in mean gradient, mean local relief, channel bed elevation, and χ all measured at, or averaged upstream of, a reference drainage area. Our results highlight that cross-divide contrasts in χ only faithfully reflect current divide mobility when uplift, rock erodibility, climate, and catchment outlet

elevation are uniform across both river networks on either side of the divide, otherwise a χ-anomaly only indicates a possible future divide instability. The other metrics appear to be more reliable representations of current divide motion, but in natural landscapes, only cross-divide contrasts in mean gradient and local relief appear to consistently provide useful information. Multiple divide metrics should be considered simultaneously and across-divide values of all metrics examined quantitatively as visual assessment is not sufficiently reliable in many cases. We provide a series of Matlab tools built using TopoToolbox to facilitate routine analysis.

1. Introduction

Drainage divides are fundamental organizing boundaries within landscapes. The extent to which the topologic form of divides, and thus river networks as a whole, are largely static (e.g., Bishop, 1995; Oberlander, 1985) or are dynamic features, changing rapidly through progressive divide migration and/or discrete capture events has recently become a topic of considerable interest and some debate (e.g. Whipple et al., 2017c; Willett et al., 2014). Assessing whether a drainage divide is potentially mobile is important, not only for quantifying how landscape evolution is affected by the resulting changes in drainage area, but also because many of the topographic metrics we use to interpret climatic or tectonic change (e.g., Wobus et al., 2006) assume that drainage area has not changed significantly over the response timescale of a catchment (e.g., Howard, 1988; Kooi and Beaumont, 1996; Whipple, 2001). Violation of this static drainage area assumption at best complicates the interpretation of topographic metrics and at worst invalidates the inferences drawn from them (e.g. Whipple et al., 2017a, 2017b; Willett, 2017; Yang et al., 2015). While recent work suggests that under normal circumstances the rate of divide motion is slow compared to the rate of channel adjustment to drainage area change (Whipple et al., 2017c), the potential importance of drainage divide mobility suggests that assessments of divide stability should be a routine part of topographic analyses.

Metrics of the relative stability of drainage divides are not new, indeed Gilbert (1877) first proposed a means of assessing divide stability with his ‘law of unequal declivities’, positing that if a divide was asymmetrical, this would imply different erosion rates on either side of the divide. The resulting across-divide erosion rate contrast would force the divide to move toward the side with lower slopes and erosion rates (Figure 1A). Recently, Willett et al (2014) proposed a new method of assessing divide stability through the use of χ-maps. χ, discussed in more detail in the following section, can be used as a proxy for steady-state channel elevation and thus this quantity should be nearly equal on either side of a stable divide. Maps of drainage networks colored by χ can reveal χ-anomalies across divides, where the χ value at channel heads are higher on one side of a divide, suggesting that this divide is unstable and should move from lower to higher χ. Barring complicating factors, divide migration would continue until the topology of the drainage network and drainage area distribution has changed such that the χ-anomaly is removed. In a limited number of locations, χ-anomalies appear coincident with an across-divide difference in average erosion rate, the underlying driver of divide motion (e.g., Beeson et al., 2017; Willett et al., 2014).

χ-maps are appealing as they are 1) relatively easy to calculate and 2) allow for a quick visual assessment of the stability of divides across a large area. There are, however, some challenges with their use and interpretation. Most significantly, the interpretation of χ-anomalies typically assumes uniform uplift, rock erodibility, and climate (Willett et al., 2014) and thus in situations where any of those parameters vary, as is often the case in natural systems, χ-anomalies can occur even when divides are stable (e.g. Whipple et al., 2017c). This led Whipple et al. (2017c) to propose a suite of alternative metrics of divide stability, largely an expansion of the ideas originally put forward by Gilbert (1877), including cross divide differences in channel elevation at a reference drainage area, mean headwater hillslope gradient, and mean headwater local relief. Whipple et al. (2017c) showed that for a simple synthetic landscape experiencing a non-uniform uplift rate, these alternative metrics were more consistent indicators of the current rate and direction of divide motion than across-divide differences in χ. Here we expand upon that work by 1) developing a set of user friendly Matlab based tools to produce maps of these alternative metrics along with χ-maps and to perform detailed analysis of multiple divide stability criteria, 2) applying these tools to two synthetic landscapes with non-uniform uplift and non-uniform lithology, 3) applying these metrics to three natural examples, and 4) comparing and contrasting the relative utility of these four different divide stability metrics.

2. Metrics of Divide Stability

2.1. Theory and Limitations of Metrics

Active motion of a drainage divide implies across-divide differences in erosion rates, thus many potential metrics of divide stability will essentially be topographic proxies for erosion rate. This was the basis for Gilbert's (1877) law of unequal declivities, which assumed that divides bounded by distinctly different gradients were unstable, with faster erosion on the steeper side progressively moving the divide towards the side with a gentler slope (Figure 1A). Since the time of Gilbert, empirical measures of erosion rate and comparison to various topographic metrics have suggested monotonic relationships at the catchment scale between erosion rates and normalized channel steepness (river slope normalized for drainage area) or local topographic relief (e.g., Harel et al., 2016; Kirby and Whipple, 2012; Lague, 2014) and at the hillslope scale between erosion rates and mean hillslope gradient, hillslope relief, and hilltop curvature (e.g., Hurst et al., 2013; Roering et al., 2007, 1999). Ultimately, divide motion is driven by differences in erosion rate at or in close proximity to the divide itself, so a metric like normalized channel steepness, which is only measurable away from the divide, may not be a viable proxy. Therefore, we choose to focus on gradient and relief. We do not consider hillslope curvature as accurate measurement of this quantity requires high resolution topographic data (e.g., Roering et al., 1999) and thus is not widely applicable to areas for which such data does not exist. Because mean gradients reach threshold values in steep landscapes and become insensitive to increases in erosion rate (e.g., Burbank et al., 1996), if gradients on both side of a divide are above ~0.7, then it is expected that the slope metric will no longer be sensitive to divide mobility. We also consider a third proxy, across-divide differences in channel elevation at a reference drainage area. Together we refer to these three metrics as the 'Gilbert metrics'. In detail, all three Gilbert metrics are intimately related because for a given divide, if a channel on one side has a steeper hillslope gradient, this generally implies both greater local relief and lower elevation of the channel at a reference drainage area as a simple geometrical consequence (Figure 1B).

We compare the Gilbert metrics to differences in the quantity 'χ' across a divide, (Willett et al., 2014). The derivation of and underlying rationale for the calculation of χ is discussed in detail in several recent publications (e.g., Harkins et al., 2007; Mudd et al., 2014; Perron and Royden, 2013; Royden and Perron, 2013) so we provide only a brief treatment here. In practice, χ is an integral quantity evaluated along a channel from the outlet (x_b) to the position of interest (x) with

$$\chi = \int_{x_b}^{x} \left(\frac{A_0}{A(x')}\right)^{\theta_{ref}} dx' \quad (1)$$

where A is upstream drainage area, A_0 is a reference scaling area, θ_{ref} is a reference concavity (Wobus et al., 2006), and x' is a dummy variable. A plot of channel elevation vs χ for a stream that is equilibrated to a spatially constant uplift rate and erosional efficiency should be a straight line and under these circumstances χ can be considered a proxy for steady-state channel elevation. If A_0 is set to unity then the slope of the chi-z plot will equal the normalized channel steepness (Wobus et al., 2006) but is dimensionless. As described by Willett et al. (2014), differences in χ at a reference drainage area across a drainage divide imply different steady-state channel elevations if uplift, climate, and rock properties are spatially uniform. Thus, the divide and drainage network topology are unstable if uplift, climate and rock properties are indeed uniform or will become unstable if current spatial differences in these properties are eliminated in future. This led to the proposition that maps of stream networks colored by χ and the identification of χ-anomalies across drainage divides could provide proxies for the stability of a drainage network.

In practice, interpretation of χ-maps and χ-anomalies has some challenges. When the assumption of spatially uniform rate of uplift (or base level fall) and erosional efficiency (set primarily by climate and rock properties) is violated, χ-anomalies can develop and persist at stable divides (e.g., Whipple et al., 2017c). In addition χ-values are sensitive to the choice of x_b and thus the elevation of the catchment outlet defined for computation of χ. Because χ is an integrated quantity and calculated from the outlet to the headwaters of a stream network, a χ-anomaly can result because of the choice of different outlet elevations for streams on either side of the divide. Many potential problems with this can be avoided with careful analysis and treatment of data (e.g., Willett et al., 2014), such as ensuring that stream networks are complete and all drain to the desired outlet elevation, but in some instances the choice of the 'correct' outlet elevation is non-trivial. As an example, we consider the case of the Greater Caucasus Mountains and two principle drainage divides within this range, one between rivers draining to the Black Sea or Caspian Sea and one between rivers draining into the northern or southern forelands of this range (Figure 2). We consider three options for selecting outlet elevations and calculate χ using (1) true base level, which varies between 0 m for rivers draining to the Black Sea and -27 m for rivers draining into the internally drained Caspian Sea, (2) a constant elevation of 550 m that roughly approximates the range-front of the Greater Caucasus in both the northern and southern forelands, or (3) a variable outlet elevation based on manual mapping of the apparent bedrock-alluvial transition at the range-front (Figure 2). If we choose to use true base level, this suggests the presence of a stark χ-anomaly around all streams draining into the Black Sea and through the southern foreland (Figure 2A). This χ-anomaly persists (but is more subtle) if we use the constant elevation of 550m, but the anomaly disappears when using the bedrock-alluvial transition as the outlet elevation (Figure 2B & C). Similarly, in the eastern Greater Caucasus, χ-anomalies suggest that the main divide between northern and southern drainages is unstable, but is predicted to move either south using true base-level (Figure 2A) or north using constant elevation or the bedrock-alluvial transition (Figure 2B & C). This highlights that care must be exercised when choosing outlet elevations for χ analysis, but also that there may be non-unique answers depending on different, but still reasonable, choices of outlet elevation.

2.2. Proposed Methodology for Use of Divide Metrics

While there are some potential problems with the use of χ-maps, they are appealing as a data exploration tool as they allow for quick assessment of the relative stability of a drainage divide and associated drainage network. Here we develop similar maps using the three "Gilbert" metrics described above. Mapping the elevation metric only requires coloring a drainage network by channel elevation. The elevation metric is interpreted the same as χ in χ-

maps: divides are expected to move from low to high values in the presence of an anomaly in channel elevations (Figure 1C & D).

For the local relief and gradient metrics, we are primarily concerned with average values of these properties near the divide, so a simple strategy of coloring stream networks by upstream running averages of either local relief or gradient is sufficient. These two metrics are more direct proxies for erosion and as such, divides are expected to move from high to low values (Figure 1C & D). For all four metrics, we are only concerned with the values at the channel heads, which are approximated by choosing a reference drainage area at which to evaluate the values, which we refer to as 'stream endpoints', so for all metrics (including χ) a full map of values along streams are not necessary, but provide for useful visuals.

Visual comparisons of contrasts in colors across a divide are useful for identifying potentially interesting patterns. However, the perception that a particular divide is unstable can be influenced by visual bias or choices of color scales. To interrogate this further one must assess the actual across-divide differences in the quantities of interest. Additionally, sometimes a single drainage divide may be heterogeneous so it is useful to segment a divide and analyze the stability of these sections individually. We visualize individual divide sections as histograms of values at all of the stream endpoints on either side of a divide (Figure 1D). In practice, this is useful to assess the degree of overlap or separation between values on either side of a divide. Along with the histograms, we calculate a mean, standard error of the mean, 95% bootstrap confidence interval, and standard deviation for the population of values on either side of a divide. In this study, we primarily use the conservative criteria that a divide is potentially stable according to a given metric if the mean of one side of the divide is within one standard deviation of the mean of the other side. These 'delta' values and their associated uncertainties can then be standardized so that positive and negative delta values of the different metrics indicate similar divide migration direction, providing an easy visual assessment of divide stability for individual divide segments (Figure 1E). The specific stability criteria we use is arbitrary, but it serves well to illustrate our main points. Ultimately determining the most suitable criteria requires comparisons of these types of data with empirical observations of divide motion. More generally, we emphasize the importance of looking at the populations of values across a divide and choosing some consistent criteria for stability or instability.

2.3. Tools for Evaluating Divide Stability

To ease assessing divide stability, we developed a series of Matlab functions based upon TopoToolbox (Schwanghart and Scherler, 2014). These functions are designed to produce visually appealing and readily assessed maps of the metrics described in the previous section (Figure 1). Beyond facilitating rapid qualitative assessment, a primary goal was also to allow users to interrogate individual sections of divides more deeply as will be illustrated in the examples below. These functions are available via github (http://github.com/amforte/DivideTools) and all of the base plots and data for the subsequent figures and maps were generated with these codes. In the supplement, we provide a brief summary of the primary functions included in this repository and where appropriate, the rationale behind the workings of these functions.

3. Principles of Metric Interpretation from Simulations

We present two landscape evolution models as simple examples of the expected behavior of the different divide metrics and to form a basic set of rules for interpreting these metrics in concert. These simulations are explicitly designed to explore cases that violate the underlying assumptions of χ-map analysis, specifically landscapes experiencing non-uniform uplift rate and/or spatially/temporally variable erosional efficiency. Both models were run in Fastscape (Braun and Willett, 2013) and were 10 km wide by 5 km long with a grid spacing of 25 meters. For both models, we track the average rate of divide motion at each time-step and compare that to across-divide differences in erosion rate, which is driving the divide motion, and the four proposed metrics, channel head elevation, mean upstream local relief, mean upstream gradient, and χ (computed using equation 1).

3.1. Asymmetric Uplift Simulation

The first simulation matches the scenario previously presented in Whipple et al. (2017c). In this simulation, we induce divide motion by first imposing an asymmetric uplift rate that increases toward the top of the model on an initially steady-state landscape, thus driving the divide towards the north (top) side of the model. This uplift-rate gradient is imposed for 20 Myr after which we force the model to return to a spatially uniform uplift rate for another 20 Myr to allow the divide to return to its original position at the center of the model. As expected, across-divide differences in erosion rate are linearly correlated with divide migration rates (Figure 3A). Across divide differences in all of the Gilbert metrics show similar linear correlations with divide migration rate (Figure 3B-D). In contrast, during the asymmetric uplift phase, χ is inversely correlated with divide migration rate, with the magnitude of the χ-anomaly increasing as the divide approaches a stable position. Conversely, when the uniform uplift phase begins, χ-anomalies correctly track divide migration rate (Figure 3E). Visualizing these across-divide differences as histograms of the values of the metrics at the reference drainage area provides an assessment of the variability even in this simple synthetic landscape and also highlights when the different metrics disagree (Figure 4).

3.2. Dipping Hard Layer Simulation

The second simulation has uniform uplift throughout the model run, but has a 500m thick layer, dipping at 35° to toward the top of the model that is more resistant to erosion than the rest of the landscape. The model is first run for a sufficient time to develop a steady state landscape with a single erosional efficiency. When the hard layer is first exposed, the divide begins to move south (e.g. 3.5 Myr in Figure 5). Once the hard layer reaches the divide, the divide begins to move north (e.g 6.0 & 8.0 Myr in Figure 5), until the hard layer is completely eroded at which time the divide again moves south toward the center of the model (e.g. 10.0 Myr in Figure 5). Like the asymmetric uplift model, divide migration rate is roughly linearly correlated with across-divide differences in erosion rate and all three Gilbert metrics (Figure 5A-D), whereas χ has a more complicated relationship to divide migration rate (Figure 5E). Also, like the asymmetric uplift model, this complicated relationship between across-divide differences in χ and divide migration rate results in times when χ-anomalies incorrectly predict the current direction of divide motion (Figure 6).

3.3. Proposed Usage of Metrics

Both simulations indicate that the Gilbert metrics are well correlated to both the current rate and direction of divide migration rate, and by extension the magnitude and sign of across-divide differences in erosion rates. However, it is important to note that the relationship between values of across-divide differences in any of these metrics and either the exact divide migration rate or across divide difference in erosion rate will depend on various factors including erosional efficiency, uplift rates, and the form of the erosion law (e.g. Whipple et al., 2017c). Thus, outside of application to models, the magnitudes of across divide differences in any of these metrics can only be reliably interpreted in terms of the direction of divide motion. With respect to χ, the model results highlight the expected outcome that χ only correctly predicts the current direction of divide motion when the uniform condition assumptions inherent in the interpretation of χ-maps are met. What the models also highlight is that χ-anomalies, and the divide motion implied by them, that exist or develop during non-uniform portions of the model runs indicate the predicted motion of the divide when and if the landscape returns to uniform conditions in the future. For example, at 2.0 Myr in the asymmetric uplift model, when the divide is moving north because of the gradient in uplift rate, the χ-anomaly that progressively develops indicates that the divide will eventually move south when (or if) that uplift gradient is relaxed (Figure 3 & 4).

Generally, the results of these two simulations suggests that using χ-maps in concert with one (or all) of the Gilbert metrics is ideal and further that if χ-maps are used exclusively, the current stability of a drainage divide may be interpreted incorrectly. If the different metrics agree, this should indicate both the direction of current divide motion and that the uniformity assumption within χ is met, or alternatively that the differences in uplift rate and erosional efficiency in the landscape either are small or counterbalance each other. If χ disagrees with the other metrics, this likely suggests that the Gilbert metrics are indicative of current divide behavior and that χ is (1) indicating potential future divide behavior should differences in uplift rate and/or erosional efficiency be eliminated, and (2) may suggest there is sufficient variability in uplift rate and/or erosional efficiency to cause divergence in the metrics. With this as a rubric for interpreting across divide differences in these metrics, we now apply them to three field examples.

4. Field Examples

4.1. Eastern Greater Caucasus Mountains

The Greater Caucasus Mountains are the main loci of active shortening within the central Arabia-Eurasia collision zone (e.g., Reilinger et al., 2006) and in the eastern Greater Caucasus (west of 45°E) are characterized by active thrust systems along both its northern and southern margins (Forte et al., 2014). This segment of the Greater Caucasus divide is notable as its location is consistently offset southward, sometimes by up to 40 km, with respect to the highest peaks of the range. Based on spatial patterns in normalized channel steepness and results of landscape evolution models, Forte et al., (2015) hypothesized that (1) the drainage divide location predates development of the topographic crest of the range, (2) the divide location is at least partially controlled by spatial gradients in uplift rate that reach a maximum near the divide, and (3) eventually the divide should move north as channels are generally steeper south of the divide.

For analysis purposes, we segment this drainage divide into 8 sections based on visual inspection of the four metrics and choose break points between portions of the divide that appear to display transitions in at least one of the criteria. Results for all metrics and associated river profiles for the eight divide segments are available in the supplement (Supplemental Figures 1-16). In practice, while the elevation metric was useful in the model results (e.g. Figure 4 & 6), the results of the elevation metric are typically equivocal in natural settings we have examined due to large standard deviations (Figure 7). The elevation metric, and indeed all of the metrics, tend to indicate more divide mobility if the standard error of the mean is used to estimate uncertainty. Unsurprisingly, the mean upstream slope and mean upstream relief metrics are very similar, though the similarity of these metrics will depend on the chosen relief radius (e.g., DiBiase et al., 2010). Thus, in comparing divide metrics along the length of the divide for this and subsequent examples, we focus our discussion on χ and relief.

With the exception of two segments (GC7 & GC8, Figure 7C), χ always predicts northward movement of the divide (using the 550m outlet elevation) whereas the relief metric suggests the divide is stable within uncertainty (using the standard deviation) except for two segments (GC3 and GC5, Figure 7C). The means of all metrics (except for GC7) agree in the direction of divide motion and applying a less restrictive uncertainty (e.g. standard error) shows more agreement between all metrics. As discussed earlier, the choice of outlet elevation for χ in the eastern Greater Caucasus (e.g. Figure 2) significantly influences predicted divide behavior, with χ suggesting southward motion of the divide if 'true base level' is used for the outlet elevation (Figure 7D). There are no quantitative estimates of erosion rates on either side of the divide so we do not have a way to evaluate the 'right' answer in this setting, but depending on the uncertainty criteria used, this result is consistent with previous suggestions by Forte et al. (2015) that the divide is currently fixed but may eventually move northward depending on future circumstances or may already be moving northward. There are isolated south flowing drainages showing characteristic 'area-gain' signatures in χ-normalized profiles (Willett et al., 2014) indicating past divide motion to the north (Figure 8), though these signatures are rare (Supplemental Figures 2, 4, 6, 8, 10, 12, 14, & 16).

In terms of diagnosing contributions to divide stability, there are no significant differences in either rock type (Forte et al., 2014) or mean annual precipitation (Forte et al., 2016) directly across the divide, suggesting that a change in erosional efficiency is unlikely as a driver. Thus, the simplest interpretation of these results is similar to that posited by Forte et al. (2015, 2014), that this indicates the presence of an uplift rate gradient that is 'holding' the divide in place and that the χ metric is sensitive to this and indicating the expected reaction of the divide if or when this uplift rate gradient dissipates.

4.2. Kars Volcanic Plateau

The Kars Volcanic Plateau is also part of the Arabia-Eurasia collision zone, but the tectonics and local geology are decidedly different than that of the Greater Caucasus to the north. This portion of the collision zone has relatively low rates of active internal deformation (Reilinger et al., 2006), which occur primarily on normal and strike slip faults with some portions of the deformation related to local volcanic features (e.g., Dhont and Chorowicz, 2006; Koçyiğit et al., 2001). The Kars Plateau is part of the broader East Anatolian Plateau which lacks mantle lithosphere (Zor, 2008) after a slab detachment or delamination event at ~7-8 Ma (Keskin, 2003; Şengör et al., 2003). The average ~2 km high, roughly dome shaped plateau (e.g., Şengör et al., 2003) Is thought to have been produced by this delamination event through mantle upwelling (e.g., Göğüş and Pysklywec, 2008). The delamination is also thought to have driven extensive melting and the eruption of a package of nearly horizontal volcanic rocks ranging in composition from basalts to rhyolites with thicknesses of 100-1000 m that blanket much of the plateau region (Keskin et al., 1998; Pearce et al., 1990, Figure 8B).

We selected two distinct drainage divides within the Kars Volcanic Plateau, both of which lie near the edges of the volcanic deposits (Figure 9B). We segment the western drainage divide into 4 sections based again on visual inspection of divide metrics, but also to separate areas where there are major differences in the outlet locations on at least one side of the divide. Streams west of the KV1 & KV2 divides are part of the Choruh watershed and flow into the Black Sea and streams east of the KV1 & KV2 divides form the headwaters of the Kura river, the main axial drainage within the Kura Basin and which flows eastward between the Greater and Lesser Caucasus and eventually into the Caspian Sea. Streams east of KV3 are also part of the Choruh watershed, but streams west of KV3 flow southeast into the Ararat Basin and are tributaries of the Arax River that merges with the Kura River shortly before it empties into the Caspian. KV4 divides two different tributaries of the Arax river and KV5, on the eastern edge of the Kars Plateau, separates branches and tributaries of the Kura river (Figure 9).

For all the analyzed divides, the relief metric suggests they are stable using the standard deviation criterion and close to stable using the standard error whereas χ consistently suggests that divides should move toward the center of the Kars Plateau (Figure 9D). Using the model results as a basis for interpretation suggests this is likely a case in which a contrast in either erosional efficiency or rock uplift perturbs the χ metric (e.g., Figure 5 & 6). Specifically, in all cases, rivers within the plateau flow through significant portions of volcanic rocks, whereas rivers more external to the plateau flow through less of the young volcanic sequence (Figure 9B). This interpretation depends on the hypothesis that key volcanic units are more resistant to erosion, which has not been quantified in this region, but is consistent with the form of the topography (e.g. river profiles in Supplemental Figures 18, 20, 22, 24, & 26). It is also possible that differential uplift, specifically from dynamic topography, influences this pattern. For the case of the western divide separating the Kars Plateau from the Choruh watershed (KV1, KV2, & KV3), Forte et al. (2016) suggested that the topography of this region was primarily controlled by response to mantle upwelling (Zor, 2008) producing a gradient in uplift rate between the outlet and headwaters of the Choruh watershed. Ultimately, because we do not have quantitative estimates of divide mobility from catchment averaged or in-situ erosion rates, it is difficult to (1) independently know the stability of these divides or (2) link the stability of these divides to a particular cause, but it does suggest that environments such as this where the Gilbert and χ metrics are in consistent disagreement represent important opportunities for empirically testing these metrics.

4.3. San Bernadino Mountains

The San Bernadino Mountains are part of the Transverse Ranges in southern California and are bounded to the south by several strands of the San Andreas Fault (e.g., Spotila et al., 1998). The western portion of the range primarily consists of the Big Bear Plateau which is a high-elevation, low-relief region interpreted as a relict landscape developed in deeply weathered granite that is surrounded by steep escarpments on nearly every side (e.g., Blythe et al., 2000; Spotila et al., 2002, 1998). Thermochronologic data indicate that the Big Bear Plateau has been uplifted with respect to both the Mojave Desert to the north and Los Angeles Basin to the south. Prior work suggests that the escarpments surrounding the Big Bear Plateau are retreating inwards, gradually consuming the plateau (e.g., Binnie et al., 2008; Spotila et al., 2002).

We investigate a portion of the drainage divide that roughly defines much of the Big Bear Plateau and includes portions of both the southern and northern Big Bear escarpments as defined by Binnie et al. (2008) and segment this divide into 10 sections (Figure 10). We use available cosmogenic erosion rates for this region (Binnie et al., 2008, 2007) and a relation between mean local relief within a 2.5 km radius and these catchment averaged erosion rates (Supplemental Figure 27) to produce a continuous map of erosion rate to compare to the various divide metrics (Figure 10). This result is broadly consistent with a similar map produced by Spotila et al (2002) based on low-temperature thermochronology and geologic constraints. In this region, we use a constant outlet elevation of 1100 m to calculate χ. We choose this outlet elevation as this is approximately the effective base level to which drainages on the northern side of the San Bernadino Mountains grade, though this means a portion of drainages on the southern flank are excluded as the effective base level for these southern drainages is significantly lower in elevation.

Across all 10 divide segments, χ and Gilbert metrics are both largely consistent with each other and what is predicted from the erosion rate map (Figure 10D). If we accept the erosion rate map as accurate and that contrasts in erosion rate across a divide from this map are unequivocal evidence of current or future divide motion, then despite agreement overall, there are examples of both χ and relief failing to correctly identify divide instability given uncertainty in cross-divide differences (Figure 10D). In detail, SB2 and SB8 are cases where χ agrees with erosion rates (but not relief) and SB6 is a case where relief agrees with erosion rates (but not χ). There are possible interpretations of these deviations, but importantly, these are all cases where (1) a relatively small number of values are used to determine potential divide motion and (2) the determination of divide stability or mobility is dictated by how much overlap or separation in means and standard deviations are required to deem a divide stable or mobile, respectively. This highlights the utility of viewing divide metrics in forms like the histograms used here for evaluating confidence in a given determination and also suggests that there is likely a minimum segmentation length of divides below which the data is simply too noisy to make a clear determination (Figure 10D). In this case all of the divide metrics are broadly consistent with prior interpretations (e.g., Binnie et al., 2008; Spotila et al., 2002) of this region suggesting that portions of the divide along the southern and northern Big Bear escarpments are mobile and actively consuming the Big Bear Plateau (Figure 10). The only stable portion of the divide appears to be between internal plateau streams and streams draining into Big Bear Lake (SB5 & SB6, Figure 10).

Using the model results as a means to interpret the divide metrics would suggest that all other divides are currently moving and that any spatial differences in erosional efficiency or uplift rate are absent or sufficiently small such that χ is still a viable metric in this setting. This is consistent with known constraints from this region, specifically uniform uplift, simple bedrock geology, and unique relationships between erosion rate and mean channel steepness and erosion rate and mean hillslope gradient (e.g., Binnie et al., 2007; DiBiase et al., 2010).

5. Discussion and Conclusions

The results of both the simulations and field examples highlight differences in the utility of the considered metrics for assessing drainage network stability and further demonstrate that relying on any one metric is limiting. The Gilbert metrics are the best choice to assess the current status of the drainage network (i.e. are divides currently moving), whereas χ-maps may be the best choice to assess whether a drainage network may reorganize in the future, though (1) the lack of a clear timescale that emerges from these measurements and (2) the reliance on a future and uncertain change in uplift and/or erosional efficiency gradients complicates this assessment. Among the Gilbert metrics, relief is likely the most reliable. Gradient also works well in the natural examples, but there are challenges related to the development of threshold slopes (e.g., Burbank et al., 1996) so care must be exercised when using mean gradients, and by extension local relief with small radii which mirror gradients (e.g., DiBiase et al., 2010), especially in high-relief landscapes. The elevation metric works well in model results, but in most natural cases always suggests stable divides within uncertainty using the standard deviation. We believe that there is value in considering all of the Gilbert metrics, but emphasize the importance of interrogating the results of the divide stability analysis.

Ultimately, using the Gilbert and χ metrics in concert maximizes the information one can extract from the landscape with regard to drainage network stability. The strengths of the two classes of metric are not necessarily surprising. The top-down method of calculation for the Gilbert metrics means that they are largely only sensitive to changes in the hillslopes directly near divides and thus represent a more 'instantaneous' view of the behavior of the divides. In contrast, the bottom-up method of calculation of χ-values at divides means that they are sensitive to spatial variability in rock strength, climate, and tectonics throughout a catchment and thus represent a more integrated, 'long-term' view of possible influences on divide stability. These differences in scale also present different challenges in calculation. The Gilbert metrics, at least the mean upstream gradient and to a lesser extent, mean upstream local relief, have the potential to be sensitive to data resolution (e.g., Finlayson and Montgomery, 2003), where as because χ-values only require drainage area measurements, these should be relatively insensitive to data resolution as long as flow routing algorithms are reasonably accurate. In contrast, the divide-scale of the Gilbert metrics make them entirely insensitive to any of the choice of outlet elevation issues that can potentially plague χ-maps (e.g. Figure 2). It is also worth noting that none of the metrics are useful for explicitly illuminating past divide motion. All metrics in certain scenarios may be useful in this regard to the extent that current divide motion implies some prior history of divide motion, but because none of these metrics contain any time information, this assumption is hard to validate without independent evidence of past divide motion.

In addition to considering multiple metrics, more detailed analyses of differences in values across divides are necessary to fully assess divide stability. In many cases, visual differences in maps of either χ or the Gilbert metrics seem to suggest a robust 'anomaly' across a divide, but the histogram of values or the uncertainty on delta values actually show significant amounts of overlap in values, e.g. divide GC2 which in map view seems to highlight an across divide difference in local relief (Figure 7A), but in detail has relatively similar values in local relief near channel heads (Figure 7D). A lingering issue is what constitutes suitable amounts of overlap in values across a divide to suggest that said divide is stable or unstable. We do not have any basis for suggesting that the criteria we primarily use (i.e. neither mean value is within one standard deviation of the other for a stable divide) is correct. Comparing predictions using the standard deviation and standard error highlights the importance of the stability criteria, as for example in the Greater Caucasus examples, using the standard deviation with the Gilbert metrics suggested mostly stable divides where as using the standard error suggests more mobile divides. Generally, because standard deviations are larger than bootstrap confidence intervals which are in turn larger than standard errors, using standard deviations bias results towards stable divides (more possibility of overlap) and standard errors bias results towards mobile divides (less possibility of overlap) with bootstrap confidence intervals representing a middle ground. Choosing any estimation of uncertainty is reasonable, but we emphasize that at minimum workers should specify what criteria they are using to judge relative stability or mobility.

The software tools provided along with this work allow for relatively easy analysis of drainage divide stability and hopefully will aid the addition of this analysis to routine characterization of landscapes. However, this should always be done in concert with traditional landscape analyses. As described above, the presence of a χ-anomaly along with absence of a Gilbert-anomaly at a divide indicates a spatial gradient in uplift rate, erosional efficiency, or both may exist in one or both sets of the catchments that define the divide, but it doesn't provide any information as to the nature of these gradients or their location. For this, maps of streams colored by normalized channel steepness or examining traditional longitudinal or χ-transformed river profiles would provide more information. Thus, we primarily view these types of metrics as cursory data analysis tools to illuminate areas that necessitate deeper investigation.

Finally, fully testing the accuracy of different metrics of divide stability fundamentally requires comparing them to areas for which we have some constraints on erosion rates on either side of divides and thus direct information on the degree of divide mobility. Special attention should be paid to areas where the Gilbert and χ metrics disagree, as understanding erosion rate contrasts (or the lack of contrasts) in these settings have the greatest potential to provide more general information on the utility of these metrics in different situations and thus contribute to determining the most reliable topographic expression of divide mobility.

Acknowledgments

The most up to date version of the tools described in this paper are available on github (http://github.com/amforte/DivideTools). This work and development of these tools was supported by EAR-1450970 awarded to AMF and KXW. The implementation of the method to control outlet elevation and check of stream completeness was adapted from methods suggested by Wolfgang Schwanghart via his blog (https://topotoolbox.wordpress.com/). We thank Nicole Gasparini for helpful discussions regarding implementation of the tools.

Figure Captions

Figure 1 – A) Schematic of Gilbert's (1877) 'Law of Unequal Declivities', predicated on the idea that divides will move when erosion rates are not equal on either side of the divide and that this difference in erosion rate will likely be driven by differences in topographic gradient on either side of the divide. B) Reference drainage area used in all metrics for calculating across divide differences. C) Idealized form of maps of the four different divide metrics discussed in the main text in the case that they are all consistent and all indicative of divide motion to the left (Side 2). D) Corresponding plots of the distributions of values at minimum reference drainage areas. All metrics are predicated on the idea that the stable condition is nearly equal quantities on either side of the divide, however the prediction of motion direction based on across divide differences is different for the different metrics. For χ and elevation metrics, the divide should move towards the side with higher values, whereas for relief and gradient, the divide should move towards the side with lower values. E) Comparison of delta values for all four metrics with propagated uncertainties normalized such that positive and negative delta values indicate the same direction of divide motion across all metrics. If any portion of the mean or its uncertainty overlaps with the stable divide line, then we assume the divide is stable. Bars are considering standard deviation as the uncertainty, shaded boxes the standard error. Though not shown, bootstrap confidence intervals would be intermediate.

Figure 2 – Example from the Greater Caucasus Mountains of the complications of the sensitivity of χ values to the choice of outlet elevation. Extent of maps are all the same, heavy black line is

divide between rivers flowing to the Caspian (base level -27m ASL) and Black (base level 0m ASL) Seas, thin black line is divide between rivers flowing north and south. Solid black arrows indicate general flow direction for streams on either side of divides, hollow arrows indicate interpreted direction of divide motion from χ-anomalies. Maps show χ calculated as a continuous grid with base level defined as A) true base level, i.e. calculated from river mouths at either the Black or Caspian Seas, B) a constant elevation of 550m ASL, which approximates the range-front for most of the Greater Caucasus, and C) an estimate of the bedrock-alluvial transition based on manual clipping of the DEM. All three outlet elevations are equally valid, but suggest markedly different stability for the main divides.

Figure 3 – Selected results from the asymmetric uplift model. Left side are plots of average delta values of divide migration rate compared to A) erosion rate, B) channel head elevation, C) local 250m relief, D) gradient and E) χ. Points are colored by the model time step with open circles during the asymmetric uplift phase and filled circles during the uniform uplift phase. Right side are maps of selected portions of the landscape during 5 key time frames and from top to bottom, colored by A) erosion rate, B) channel elevation, C) upstream mean relief, D) upstream mean gradient, and E) χ. In top erosion rate panels, the rate and direction of divide motion is displayed as a vector, with divide motion towards the top of the page defined as positive.

Figure 4 – Divide metric histograms for three key timesteps during the asymmetric uplift model: A) near peak divide migration rate during the tilt phase (2.0 Myr); B) stable divide near the end of the tilt phase (19.8 Myr); and C) near peak divide migration rate during the return phase (21.4 Myr).

Figure 5 – Selected results from the dipping hard layer model, plot setup is nearly identical to Figure 3, except the top map panel is split between erosion rate on the left and rock strength on the right. The erosional efficiency, K, of the hard layer is 0.25 times the rest of the landscape.

Figure 6 – Divide metric histograms for two key timesteps during the dipping hard layer model: A) near peak divide migration rate before the hard layer reaches the divide (3.5 Myr) and B) when the divide and the hard – soft contact are coincident (6.0 Myr).

Figure 7 – Divide stability analysis of the southeastern Greater Caucasus drainage divide. For this analysis, we use a constant outlet elevation of 550m for calculating χ (e.g. Figure 2B). A) Stream network colored by mean upstream relief superimposed on a continuous χ grid draped over a hillshade. White line is the divide, black squares mark boundaries between divide segments and small inset shows nomenclature for the divide segments. Black box shows outline of Figure 8A. B) Hillshade colored by elevation of the same area for context. C) Standardized delta plot for the 8 segments along the divide. Bars are considering standard deviation as the uncertainty, shaded boxes the standard error.

Figure 8 – Evidence of northward divide motion in the eastern Greater Caucasus. A) Topography near the divide with a possible capture highlighted, see Figure 7 for location within context. When identifying potential former captures from ‘area-gain’ signatures in χ-normalized profiles, a viable former connection such as this is an essential observation given the extremely short time-scale of preservation for such signatures within topography (Whipple et al., 2017c). B) χ-transformed profiles of the two drainages highlighted in 8A. Section of the south flowing drainage shows characteristic ‘area-gain’ signature below a possible captured reach. C) Longitudinal profile of the two drainages highlighted in 8A.

Figure 9– Kars volcanic plateau. For this analysis, we use a constant outlet elevation of 550m for calculating χ. A) Stream network colored by mean upstream relief on top of continuous χ grid and hillshade. While lines indicate divides, black squares are boundaries between divide segments. Inset in top left shows labels for the divide segments. B) Simplified geologic map from Forte et al. (2016), area is same as in A, divides shown for reference. C) Hillshade colored by elevation for the Kars area with labels of features discussed in the main text. D) Standardized

delta plot for the 5 segments along the divide. Bars are considering standard deviation as the uncertainty, shaded boxes the standard error.

Figure 10 – Western San Bernadino Mountains. A) Streams colored by mean upstream relief on top of a continuous χ grid draped over a hillshade. White lines mark divides of interest, black squares show boundaries between divide segments. Inset in top left show names for divide segments. B) Interpolated erosion rate map based on cosmogenic erosion rate data from Binnie et al. (2008, 2007), see text and supplement for additional discussion. C) Hillshade colored by elevation of the western San Bernadino Mountains with labels for important features discussed in text. D) Standardized delta plot for the 10 segments along the divide. Bars are considering standard deviation as the uncertainty, shaded boxes the standard error.

References

Beeson, H.W., McCoy, S.W., Keen-Zebert, A., 2017. Geometric disequilibrium of river basins produces long-lived transient landscapes. Earth Planet. Sci. Lett. 475, 34–43. doi:10.1016/j.epsl.2017.07.010

Binnie, S.A., Phillips, W.M., Summerfield, M.A., Fifield, L.K., 2007. Tectonic uplift, theshold hillslopes, and denudation rates in a developing mountain range. Geology 35, 743–746. doi:10.1130/G23641A.1

Binnie, S.A., Phillips, W.M., Summerfield, M.A., Fifield, L.K., Spotila, J.A., 2008. Patterns of denudation through time in the San Bernardino Mountains , California : Implications for early-stage orogenesis. Earth Planet. Sci. Lett. 276, 62–72. doi:10.1016/j.epsl.2008.09.008

Bishop, P., 1995. Drainage rearrangement by river catpure, beheading and diversion. Prog. Phys. Geogr. 19, 449–473. doi:10.1177/030913339501900402

Blythe, A.E., Burbank, D., Farley, K.A., Fielding, E.J., 2000. Structural and topographic evolution of the central Transverse Ranges, California, from apatite fission-track, (U-Th/He) and digital elevation model analyses. Basin Res. 12, 97–114.

Braun, J., Willett, S.D., 2013. A very efficient 0(n), implicit and parallel method to solve the stream power equation governing fluvial incision and landscape evolution. Geomorphology 180–181, 170–179. doi:10.1016/j.geomorph.2012.10.008

Burbank, D., Leland, J., Fielding, E., Anderson, R.S., Brozovic, N., Reid, M.R., Duncan, C., 1996. Bedrock incision, rock uplift and threshold hillslopes in the northwestern Himalaya. Nature 379, 505–510.

Dhont, D., Chorowicz, J., 2006. Review of the neotectonics of the Eastern Turkish-Armenian Plateau by geomorphic analysis of digital elevation model imagery. Int. J. Earth Sci. 95, 34–49.

DiBiase, R.A., Whipple, K.X., Heimsath, A.M., Ouimet, W.B., 2010. Landscape form and millenial erosion rates in the San Gabriel Mountains, CA. Earth Planet. Sci. Lett. 289, 134–144.

Finlayson, D.P., Montgomery, D.R., 2003. Modeling large-scale fluvial erosion in geographic information systems. Geomorphology 53, 147–164. doi:10.1016/S0169-555X(02)00351-3

Forte, A.M., Cowgill, E., Whipple, K.X., 2014. Transition from a singly vergent to doubly vergent wedge in a young orogen: The Greater Caucasus. Tectonics 33, 2077–2101. doi:10.1002/2014TC003651

Forte, A.M., Whipple, K.X., Bookhagen, B., Rossi, M.W., 2016. Decoupling of modern shortening rates, climate, and topography in the Caucasus. Earth Planet. Sci. Lett. 449, 282–294. doi:10.1016/j.epsl.2016.06.013

Forte, A.M., Whipple, K.X., Cowgill, E., 2015. Drainage network reveals patterns and history of active deformation in the eastern Greater Caucasus. Geosphere 11. doi:10.1130/GES01121.1

Gilbert, G.K., 1877. Geology of the Henry Mountains, USGS Report. Government Printing Office, Washington, D.C.

Göğüş, O.H., Pysklywec, R.N., 2008. Mantle lithopshere delamination driving plateau uplift and synconvergent extension in eastern Anatolia. Geology 36, 723–726.

Harel, M.A., Mudd, S.M., Attal, M., 2016. Global analysis of the stream power law parameters based on worldwide 10Be denudation rates. Geomorphology 268, 184–196. doi:10.1016/j.geomorph.2016.05.035

Harkins, N., Kirby, E., Heimsath, A.M., Robinson, R., Reiser, U., 2007. Transient fluvial incision in the headwaters of the Yellow River, northeastern Tibet, China. J. Geophys. Res. 112, F03S04.

Howard, A.D., 1988. Equilibrium models in geomorphology, in: Anderson, M.G. (Ed.), Modelling Geomorphological Systems. John Wiley & Sons, pp. 49–70.

Hurst, M.D., Mudd, S.M., Yoo, K., Attal, M., Walcott, R., 2013. Influence of lithology on hillslope morphology and response to tectonic forcing in the northern Sierra Nevada of California. J. Geophys. Res. 118, 832–851. doi:10.1002/jgrf.20049

Keskin, M., 2003. Magma generation by slab steepening and breakoff beneath a subduction-accretion complex: An alternative model for collision-related volcanism in Eastern Anatolia, Turkey. Geophys. Res. Lett. 30, doi:10.1029/2003GL018019.

Keskin, M., Pearce, J.A., Mitchell, J.G., 1998. Volcano-stratigraphy and geochemistry of collision-related volcanism on the Erzurum-Kars Plateau, northeastern Turkey. J. Volcanol. Geotherm. Res. 85, 355–404.

Kirby, E., Whipple, K.X., 2012. Expression of active tectonics in erosional landscapes. J. Struct. Geol. 44, 54–75.

Koçyiğit, A., Yılmaz, A., Adamia, S., Kuloshvili, S., 2001. Neotectonics of East Anatolia Plateau (Turkey) and Lesser Caucasus: implication for transition from thrusting to strike-slip faulting. Geodin. Acta 14, 177–195.

Kooi, H., Beaumont, C., 1996. Large-scale geomorphology: Classical concepts reconciled and integrated with contemporary ideas via a surface processes model. J. Geophys. Res. 101, 3361–3386.

Lague, D., 2014. The stream power river incision model: evidence, theory and beyond. Earth Surf. Process. Landforms 39, 38–61. doi:10.1002/esp.3462

Mudd, S.M., Attal, M., Mildowski, D.T., Grieve, S.W.D., Valters, D.A., 2014. A statistical framework to quantify spatial variation in channel gradients using the integral method of channel profile analysis. J. Geophys. Res. 119, 138–152. doi:10.1002/2013JF002981

Oberlander, T.M., 1985. Origin of drainage transverse to structures in orogens, in: Morisawa, M., Hacker, J.T. (Eds.), 15th Annual Binghamton Geomorphology Symposium. pp. 155–182.

Pearce, J.A., Bender, J.F., De Long, S.E., Kidd, W.S.F., Low, P.J., Guner, Y., Saroglu, F., Yılmaz, Y., Moorbath, S., Mitchell, J.G., 1990. Genesis of collision volcanism in eastern Anatolia, Turkey. J. Volcanol. Geotherm. Res. 44, 189–229.

Perron, J.T., Royden, L.H., 2013. An intergral approach to bedrock river profile analysis. Earth Surf. Process. Landforms 38, 570–576. doi:10.1002/esp.3302

Reilinger, R., McClusky, S., Vernant, P., Lawrence, S., Ergintav, S., Cakmak, R., Ozener, H., Kadirov, F., Guliev, I., Stepanyan, R., Nadariya, M., Hahubia, G., Mahmoud, S., Sakr, K., ArRajehi, A., Paradissis, D., Al-Aydrus, A., Prilepin, M., Guseva, T., Evren, E., Dmitrotsa, A., Filikov, S. V, Gomez, F., Al-Ghazzi, R., Karam, G., 2006. GPS constraints on continental deformation in the Africa-Arabia-Eurasia continental collision zone and implications for the dynamics of plate interactions. J. Geophys. Res. 111, doi:10.1029/2005JB004051.

Roering, J.J., Kirchner, J.W., Dietrich, D., 1999. Evidence for nonlinear, diffusive sediment transport on hillslopes and implications for landscape morphology. Water Resour. Res. 35, 853–870.

Roering, J.J., Perron, J.T., Kirchner, J.W., 2007. Functional relatoniships between denudation and hillslope form and relief. Earth Planet. Sci. Lett. 264, 245–258.

Royden, L.H., Perron, J.T., 2013. Solutions of the stream power equation and application to the evolution of river longitudinal profiles. J. Geophys. Res. 118, 497–518. doi:10.1002/jgrf.20031

Schwanghart, W., Scherler, D., 2014. Short Communication: TopoToolbox 2 - MATLAB based software for topographic analysis and modeling in Earth surface sciences. Earth Surf. Dyn. 2, 1–7. doi:10.5194/esurf-2-1-2014

Şengör, A.M.C., Özeren, S., Genç, T., Zor, E., 2003. East Anatolian high plateau as a mantle-supported, north-south shortened domal structure. Geophys. Res. Lett. 30, doi:10.1029/2003GL017858.

Spotila, J.A., Farley, K.A., Sieh, K., 1998. Uplift and erosion of the San Bernardino Mountains associated with transpression along the San Andreas fault , California , as constrained by radiogenic helium thermochronometry. Tectonics 17, 360–378.

Spotila, J., House, M.A., Blythe, A.E., Niemi, N.A., Bank, G.C., 2002. Controls on the erosion and geomorphic evolution of the San Bernardino and San Gabriel Mountains, southern

California. pp. 205–230.
Whipple, K.X., 2001. Fluvial landscape response time: How plausible is steady-state denudation? Am. J. Sci. 301, 313–325.
Whipple, K.X., Dibiase, R.A., Ouimet, W.B., Forte, A.M., 2017a. Preservation or piracy: Diagnosing low-relief, high-elevation surface formation mechanisms REPLY. Geology 45. doi:10.1130/G39252Y.1
Whipple, K.X., DiBiase, R.A., Ouimet, W.B., Forte, A.M., 2017b. Preservation or piracy: Diagnosing low-relief, high-elevation surface formation mechanisms. Geology 45, 91–94. doi:10.1130/G38490.1
Whipple, K.X., Forte, A.M., DiBiase, R.A., Gasparini, N.M., Ouimet, W.B., 2017c. Timescales of landscape response to divide migration and drainage capture: Implications for the role of divide mobility in landscape evolution. J. Geophys. Res. Earth Surf. doi:10.1002/2016JF003973
Willett, S., 2017. Preservation or piracy: Diagnosing low-relief, high-elevation surface formation mechanism COMMENT. Geology 45. doi:10.1130/G3829C.1
Willett, S.D., McCoy, S.W., Perron, J.T., Goren, L., Chen, C.-Y., 2014. Dynamic reorganization of river basins. Science (80-.). 343, 1248765. doi:10.1126/science.1248765
Wobus, C.W., Whipple, K.X., Kirby, E., Snyder, N.P., Johnson, J., Spyropolou, K., Crosby, B.T., Sheehan, D., 2006. Tectonics from topography: Procedures, promise, and pitfalls, in: Willett, S.D., Hovius, N., Brandon, M.T., Fisher, D. (Eds.), Tectonics, Climate, and Landscape Evolution. The Geological Society of America, Boulder, CO, pp. 55–74.
Yang, R., Willett, S.D., Goren, L., 2015. In situ low-relief landscape formation as a result of river network disruption. Nature 520, 526–529.
Zor, E., 2008. Tomographic evidence of slab detachment beneath eastern Turkey and the Caucasus. Geophys. J. Int. 175, 1273–1282.

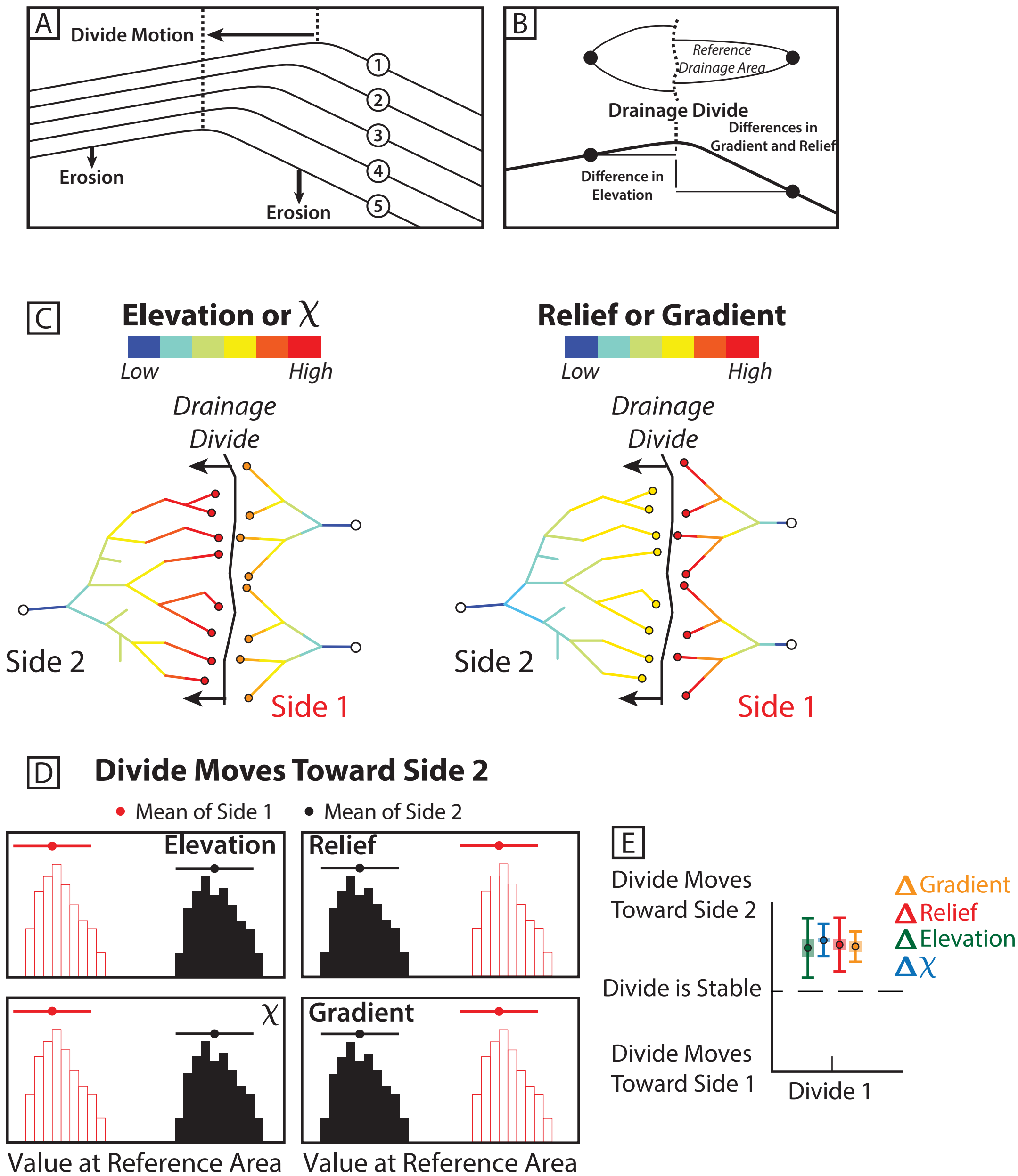
A
Divide Motion
1
2
3
4
5
Erosion
Erosion
B
Reference
Drainage Area
Drainage Divide
Differences in
Gradient and Relief
Difference in
Elevation
C
Elevation or χ
Low
High
Drainage
Divide
Side 2
Side 1
Relief or Gradient
Low
High
Drainage
Divide
Side 2
Side 1
D
Divide Moves Toward Side 2
Mean of Side 1
Mean of Side 2
Elevation
Relief
χ
Gradient
Value at Reference Area
Value at Reference Area
E
Divide Moves
Toward Side 2
Divide is Stable
Divide Moves
Toward Side 1
Divide 1
Δ Gradient
Δ Relief
Δ Elevation
Δ χ

Figure 1

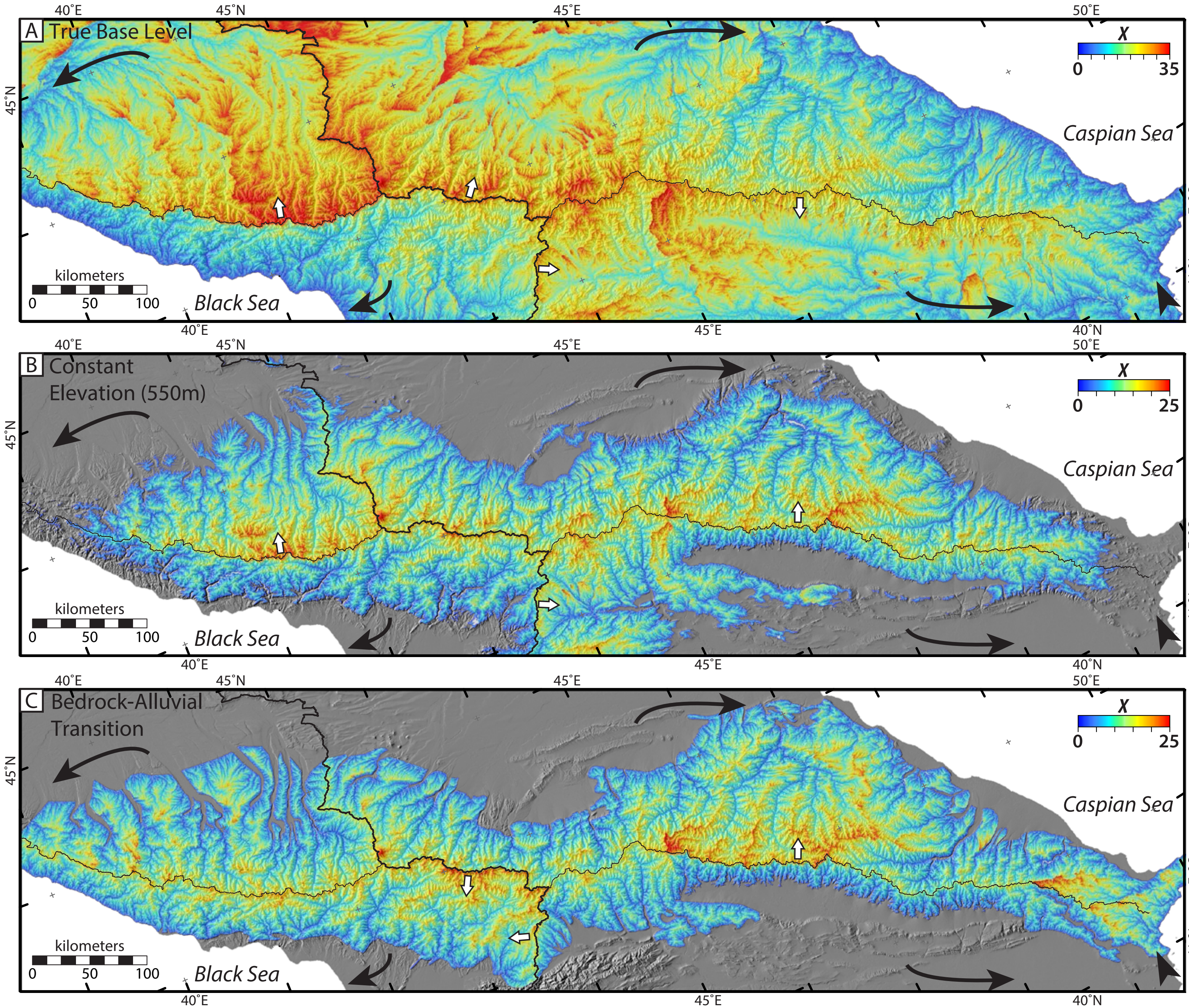
A True Base Level
B Constant
Elevation (550m)
C Bedrock-Alluvial
Transition
Caspian Sea
Black Sea
kilometers
0
50
100
χ
0
35
25
40˚E
45˚E
50˚E
45˚N
40˚N

Figure 2

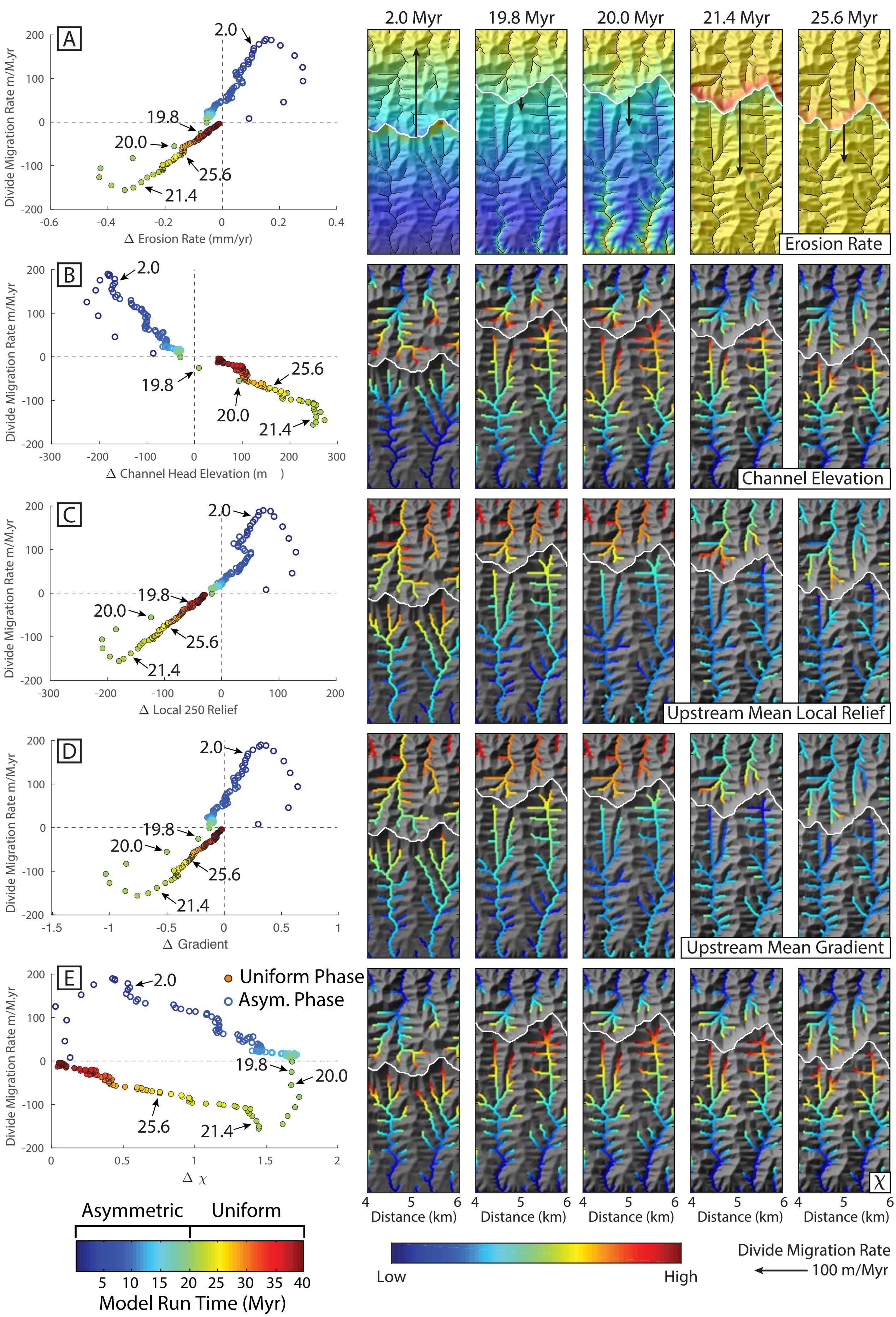

2.0 Myr
19.8 Myr
20.0 Myr
21.4 Myr
25.6 Myr
A
B
C
D
E
Divide Migration Rate m/M.yr
Δ Erosion Rate (mm/yr)
Δ Channel Head Elevation (m)
Δ Local 250 Relief
Δ Gradient
Δ χ
Erosion Rate
Channel Elevation
Upstream Mean Local Relief
Upstream Mean Gradient
χ
Distance (km)
Uniform Phase
Asym. Phase
Asymmetric
Uniform
Model Run Time (Myr)
Low
High
Divide Migration Rate
100 m/Myr

Figure 3

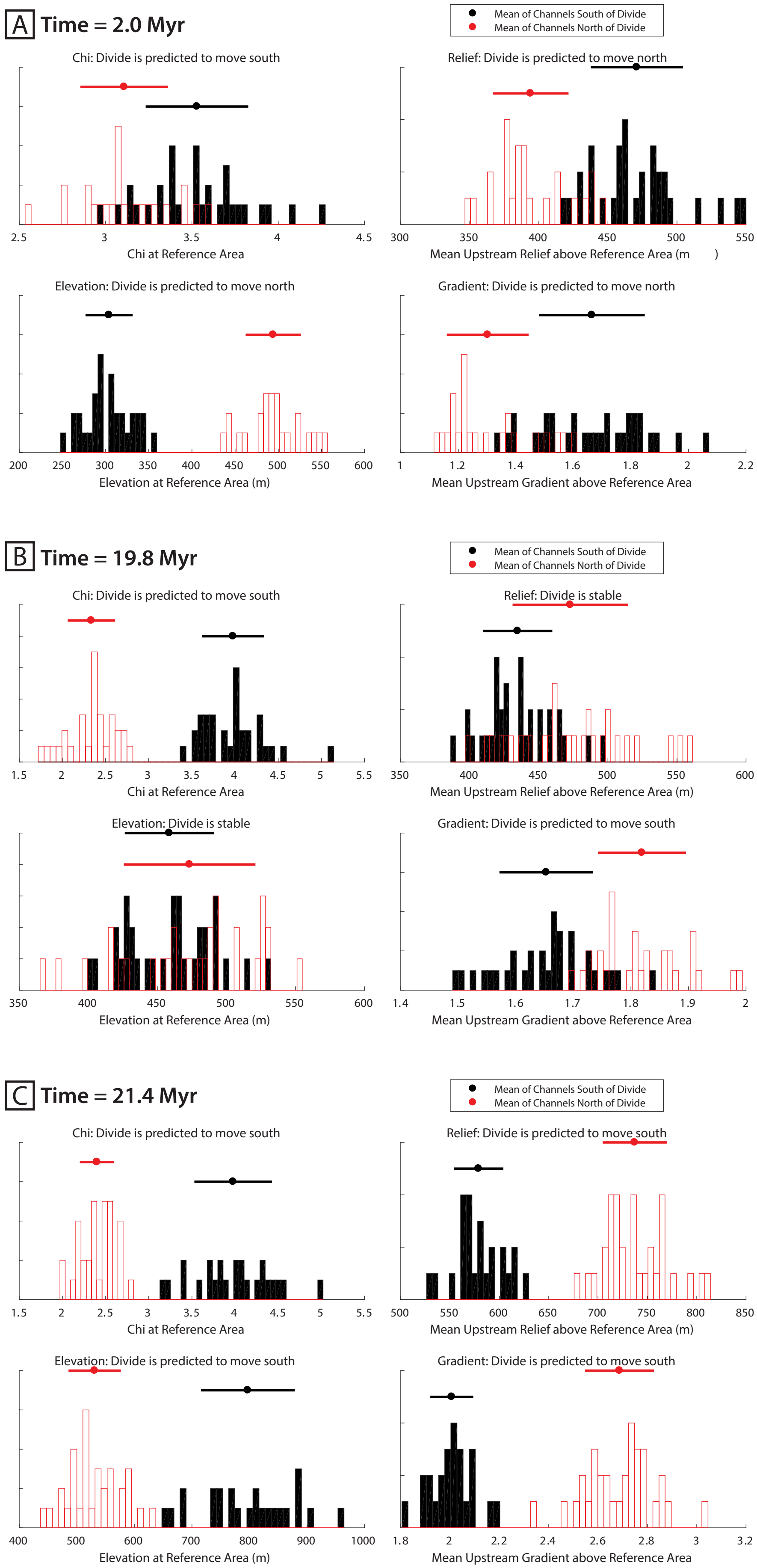

A Time = 2.0 Myr
Mean of Channels South of Divide
Mean of Channels North of Divide
Chi: Divide is predicted to move south
Chi at Reference Area
Relief: Divide is predicted to move north
Mean Upstream Relief above Reference Area (m)
Elevation: Divide is predicted to move north
Elevation at Reference Area (m)
Gradient: Divide is predicted to move north
Mean Upstream Gradient above Reference Area
B Time = 19.8 Myr
Mean of Channels South of Divide
Mean of Channels North of Divide
Chi: Divide is predicted to move south
Chi at Reference Area
Relief: Divide is stable
Mean Upstream Relief above Reference Area (m)
Elevation: Divide is stable
Elevation at Reference Area (m)
Gradient: Divide is predicted to move south
Mean Upstream Gradient above Reference Area
C Time = 21.4 Myr
Mean of Channels South of Divide
Mean of Channels North of Divide
Chi: Divide is predicted to move south
Chi at Reference Area
Relief: Divide is predicted to move south
Mean Upstream Relief above Reference Area (m)
Elevation: Divide is predicted to move south
Elevation at Reference Area (m)
Gradient: Divide is predicted to move south
Mean Upstream Gradient above Reference Area

Figure 4

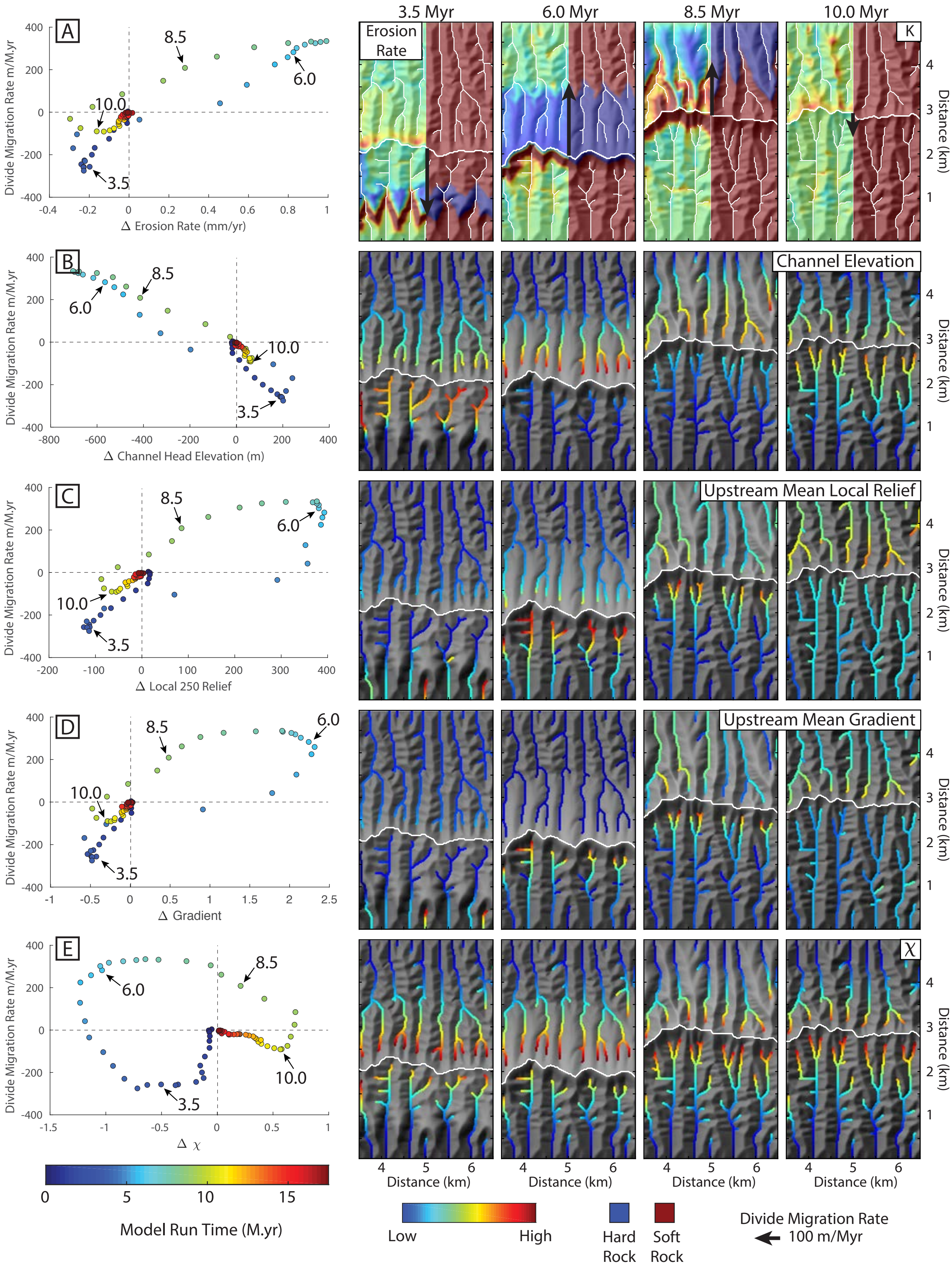

A
B
C
D
E
K
Divide Migration Rate m/M.yr
Δ Erosion Rate (mm/yr)
Δ Channel Head Elevation (m)
Δ Local 250 Relief
Δ Gradient
Δ χ
3.5 Myr
6.0 Myr
8.5 Myr
10.0 Myr
Erosion Rate
Channel Elevation
Upstream Mean Local Relief
Upstream Mean Gradient
χ
Distance (km)
Model Run Time (M.yr)
Low
High
Hard Rock
Soft Rock
Divide Migration Rate
100 m/Myr

Figure 5

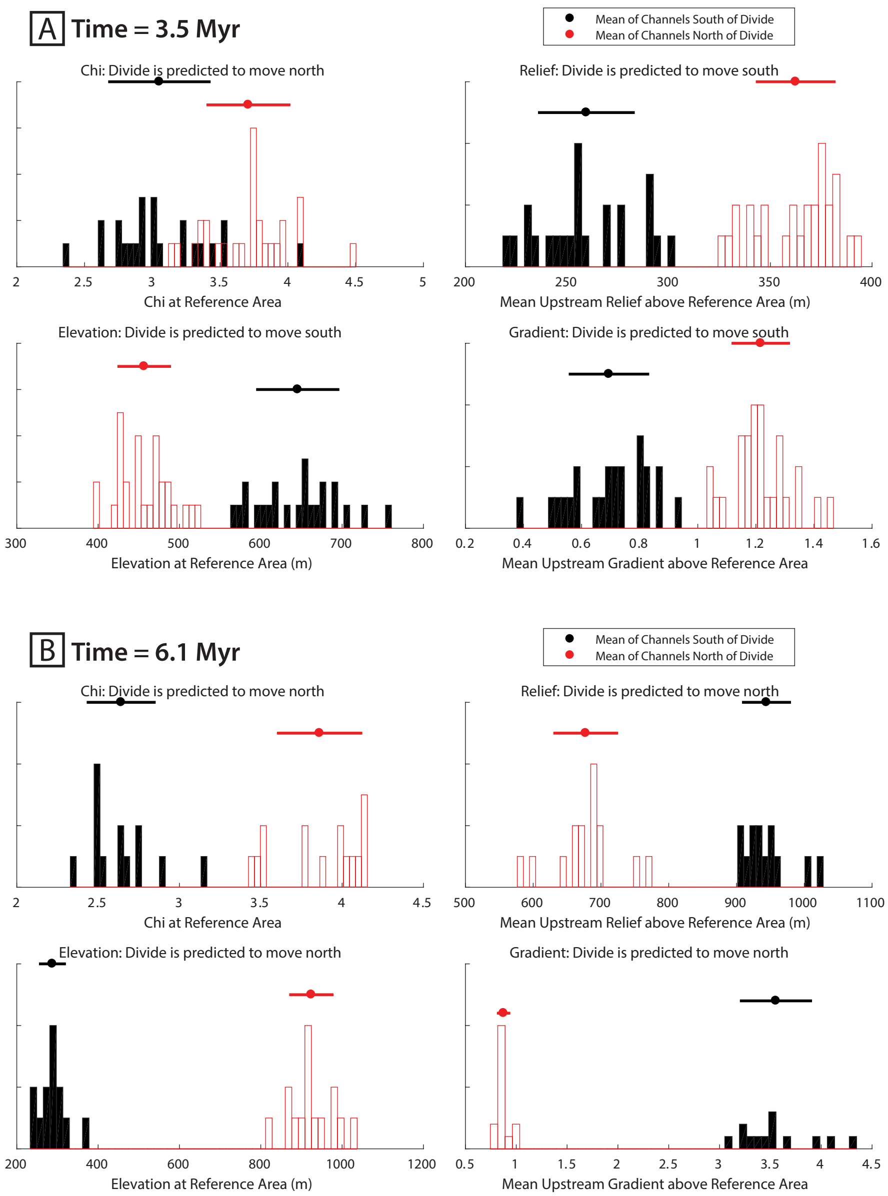
A
Time = 3.5 Myr
Mean of Channels South of Divide
Mean of Channels North of Divide
Chi: Divide is predicted to move north
Chi at Reference Area
Relief: Divide is predicted to move south
Mean Upstream Relief above Reference Area (m)
Elevation: Divide is predicted to move south
Elevation at Reference Area (m)
Gradient: Divide is predicted to move south
Mean Upstream Gradient above Reference Area
B
Time = 6.1 Myr
Mean of Channels South of Divide
Mean of Channels North of Divide
Chi: Divide is predicted to move north
Chi at Reference Area
Relief: Divide is predicted to move north
Mean Upstream Relief above Reference Area (m)
Elevation: Divide is predicted to move north
Elevation at Reference Area (m)
Gradient: Divide is predicted to move north
Mean Upstream Gradient above Reference Area

Figure 6

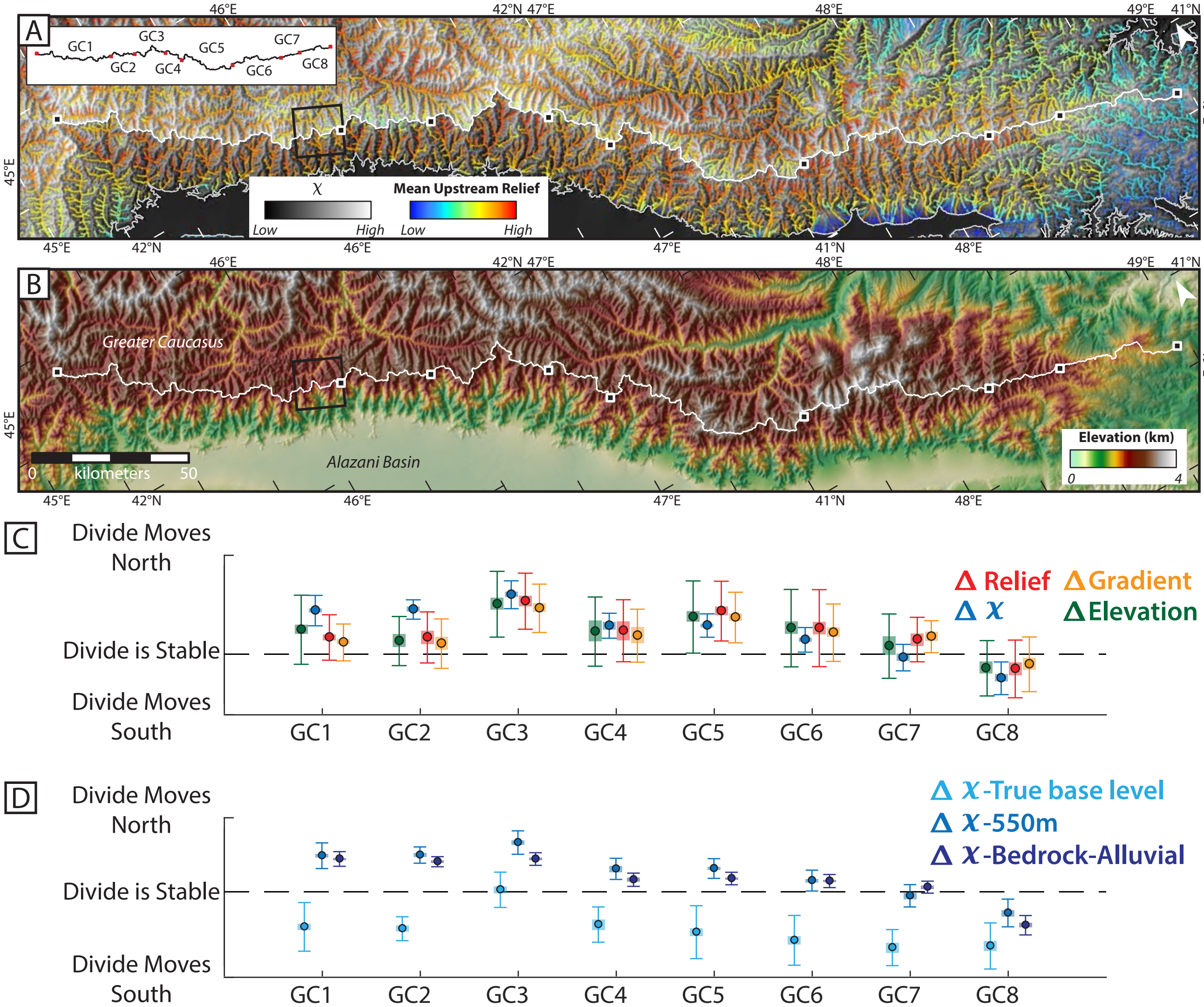

A
GC1
GC3
GC5
GC7
GC2
GC4
GC6
GC8
χ
Low
High
Mean Upstream Relief
Low
High
B
Greater Caucasus
Alazani Basin
0
kilometers
50
Elevation (km)
0
4
46°E
42°N 47°E
48°E
49°E
41°N
45°E
42°N
46°E
47°E
41°N
48°E
C
Divide Moves North
Divide is Stable
Divide Moves South
Δ Relief
Δ Gradient
Δ χ
Δ Elevation
D
Divide Moves North
Divide is Stable
Divide Moves South
Δ χ-True base level
Δ χ-550m
Δ χ-Bedrock-Alluvial

Figure 7

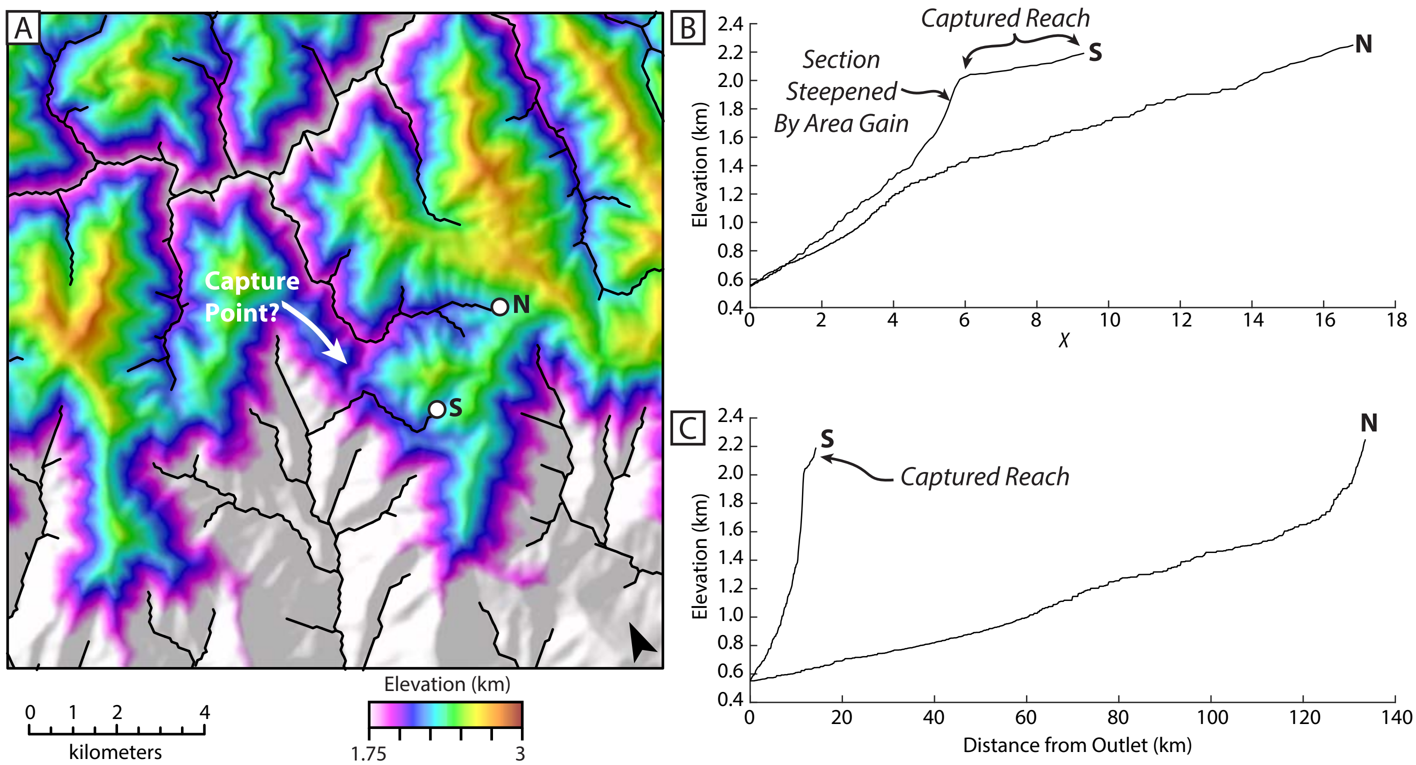
A
Capture Point?
N
S
0 1 2 4
kilometers
Elevation (km)
1.75
3
B
Captured Reach
Section Steepened By Area Gain
S
N
Elevation (km)
X
C
S
Captured Reach
N
Elevation (km)
Distance from Outlet (km)

Figure 8

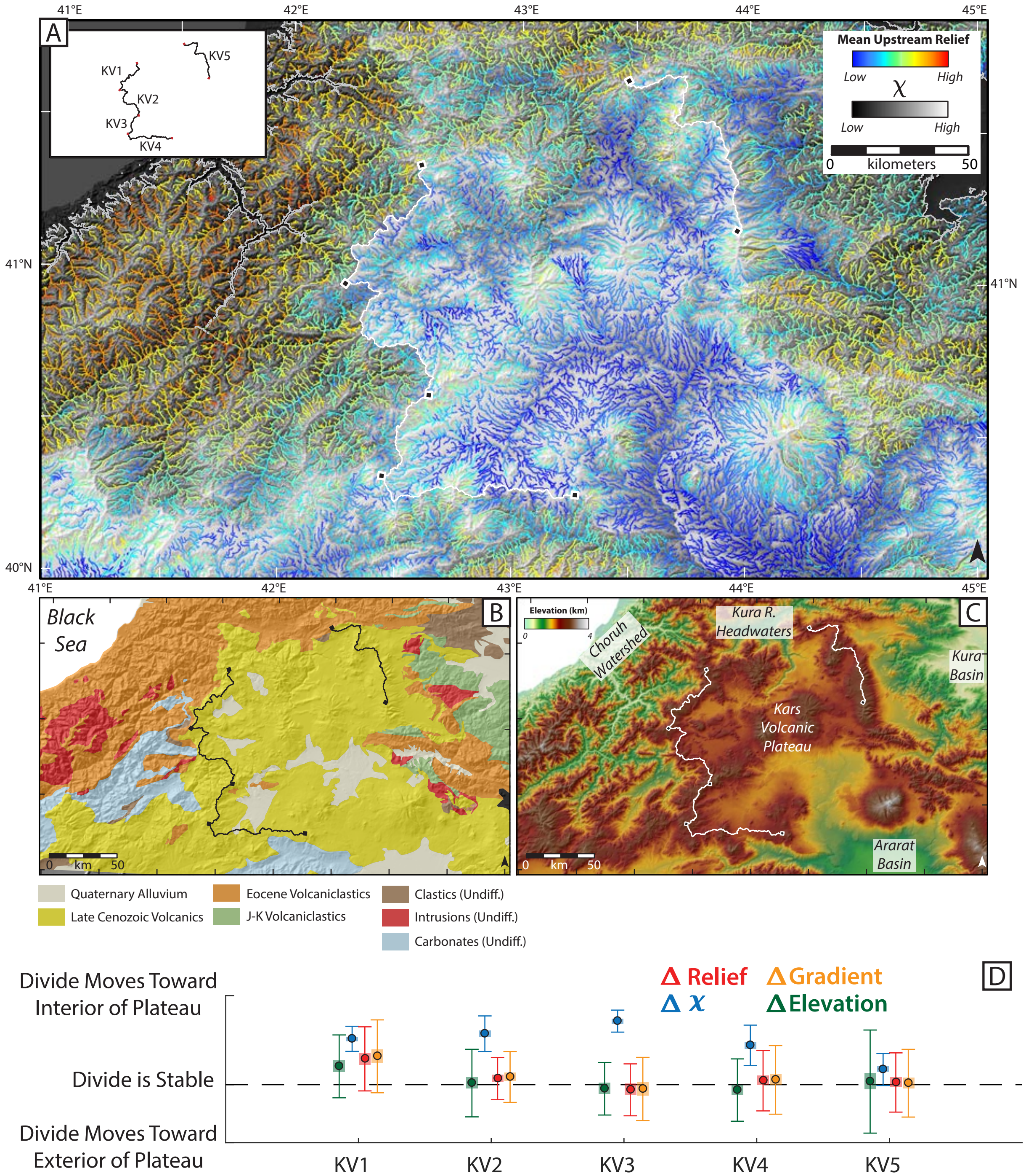
41°E
42°E
43°E
44°E
45°E
41°N
40°N
A
KV1
KV2
KV3
KV4
KV5
Mean Upstream Relief
Low
High
χ
Low
High
0
kilometers
50
B
Black Sea
0
km
50
C
Elevation (km)
0
4
Choruh Watershed
Kura R. Headwaters
Kura Basin
Kars Volcanic Plateau
Ararat Basin
0
km
50
Quaternary Alluvium
Late Cenozoic Volcanics
Eocene Volcaniclastics
J-K Volcaniclastics
Clastics (Undiff.)
Intrusions (Undiff.)
Carbonates (Undiff.)
D
Δ Relief
Δ Gradient
Δ χ
Δ Elevation
Divide Moves Toward Interior of Plateau
Divide is Stable
Divide Moves Toward Exterior of Plateau
KV1
KV2
KV3
KV4
KV5

Figure 9

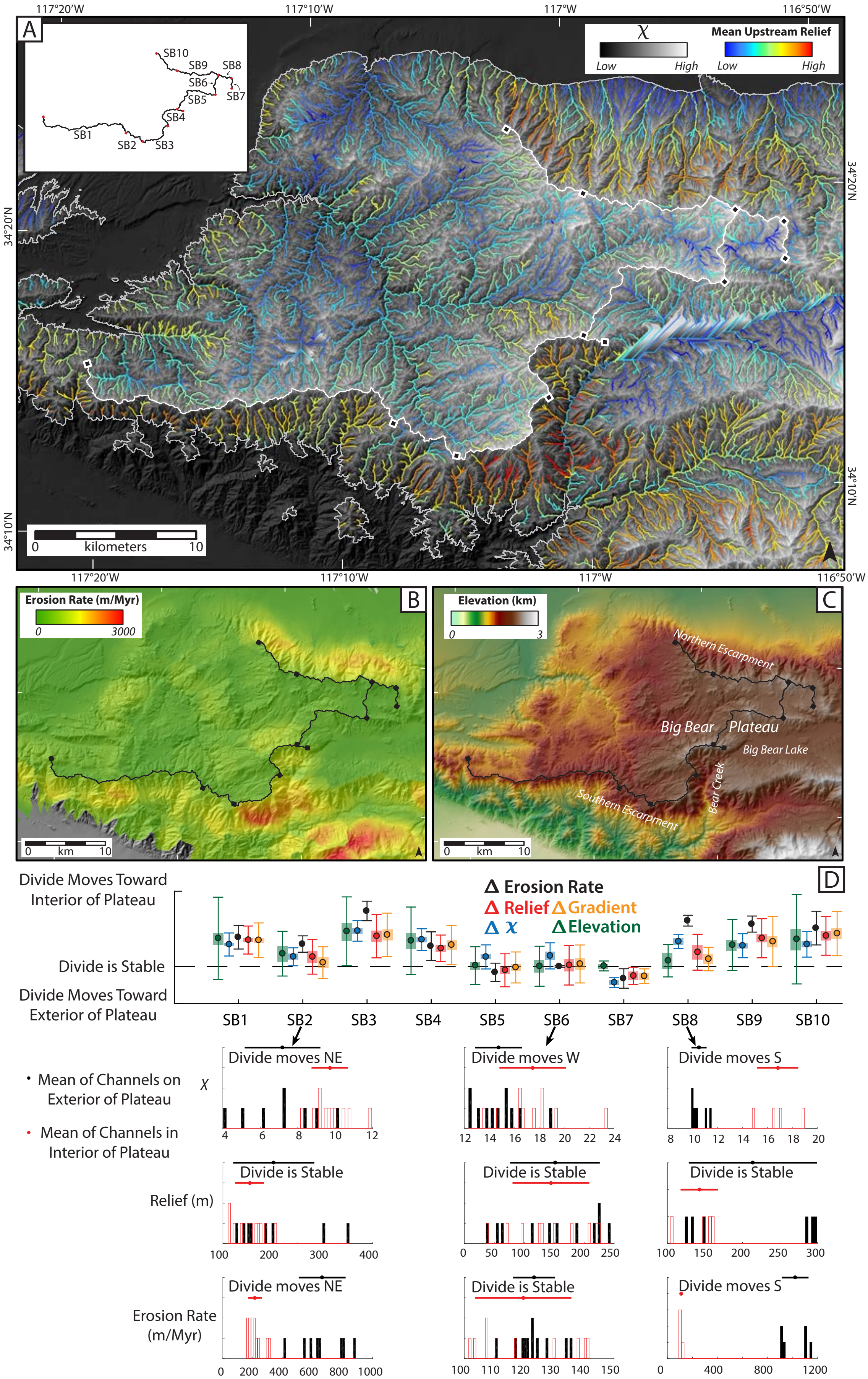
A
B
C
D
117°20'W
117°10'W
117°W
116°50'W
34°20'N
34°10'N
χ
Low
High
Mean Upstream Relief
SB1
SB2
SB3
SB4
SB5
SB6
SB7
SB8
SB9
SB10
0
kilometers
10
Erosion Rate (m/Myr)
3000
km
Elevation (km)
Northern Escarpment
Big Bear Plateau
Big Bear Lake
Bear Creek
Southern Escarpment
Divide Moves Toward Interior of Plateau
Divide is Stable
Divide Moves Toward Exterior of Plateau
Δ Erosion Rate
Δ Relief
Δ Gradient
Δ χ
Δ Elevation
Mean of Channels on Exterior of Plateau
Mean of Channels in Interior of Plateau
Relief (m)
Erosion Rate (m/Myr)
Divide moves NE
Divide moves W
Divide moves S
Divide is Stable

Figure 10

Supplemental Text for 'Criteria and Tools for Determining Drainage Divide Stability' by Adam M. Forte & Kelin X. Whipple

S1. Description of codes included in Github repository

S1.1. DivideStability – For a given area, this routine produces shapefiles (or alternatively rasters convertible to shapefiles within a GIS program) that includes a stream network with values for all four metrics (χ, channel elevation, upstream mean relief, and upstream mean gradient) so that the user can produce maps of stream networks colored by these quantities (e.g. Figure 1). To aid in sensible color scaling, values for the 'Gilbert metrics' are normalized to vary between 0 and 1. Because the calculation of χ is sensitive to the choice of outlet elevation (e.g. Figure 2), careful control of outlet elevation is essential for meaningful interpretations of χ-anomalies. For this reason, this function allows the user to modify a stream network to remove portions of streams below a minimum elevation. This function also checks to make sure that stream outlets along the edge of the DEM meet the criteria defined and that all drainage basins are 'complete', i.e. that the summation of drainage area is accurate and is not influenced by tributaries that are cut off. Either of these cases could result in artificial χ-anomalies, but generally should have no effect on the Gilbert metrics.

S1.2. ChiGrid – The *DivideStability* code calculates χ along the stream network, but we find it useful to be able to visualize χ and an additional metric simultaneously. This code calculates χ at every pixel in the DEM so that colored stream networks can overlay this χ raster. Similar to *DivideStability*, a minimum elevation can be specified for calculating the χ raster and a check is performed to ensure included drainage basins are complete.

S1.3. AcrossDivide – Tool uses the output of *DivideStability* and allows users to select sections of a divide of interest to perform detailed analysis of divide sections (e.g. Figure 1D). This function provides users multiple ways of defining a divide of interest, but all of them generally function on the idea that the user (or the function itself in the case of automated detection schemes) defines divides of interest by selecting the drainages that define this divide. End results are plots of the distribution and means of the values at the reference drainage area of all four metrics on either side of the divide of interest (e.g. Figure 1) along with a prediction from each metric independently regarding whether and in which direction the divide should move. The prediction of a divide stability or mobility is made on the basis of a user selected assessment of uncertainty and whether the uncertainty of the distributions overlap with the means of the opposing side of the divide. If there is overlap, the divide is considered stable, and if there is no overlap, the divide is considered mobile. This is not meant as an absolute criteria, simply a quick first order assessment. The user can choose to use the standard deviation of the population (default), the standard error on the mean, or the 95% bootstrap confidence interval determined from a 1000 iteration resampling scheme. This function also produces a list of channel head coordinates and their respective values for the four metrics that define the divide of interest.

S1.4. PlotDivideProfiles – To understand the predicted behavior of a divide, it is often necessary to consider the longitudinal profiles of the rivers in question. This functions plots χ-elevation and distance-elevation plots for the streams used to define the divide. Various plotting options exist to allow the user to plot only specific channels and to color drainages by either gradient or relief to compare predictions of individual metrics.

S1.5. AlongDividePlot – If the user has defined multiple divide segments, this allows them to produce a plot similar to what is shown in the text (e.g. Figures 7C, 9D, or 10D). In detail, this function will produce three plots for each divide (made up of multiple segments), (1) a plot of divide segment means with uncertainties, (2) a plot of across-divide delta values with propagated uncertainties with true values (i.e. relief and gradient will have opposite signs from elevation and chi delta values if they are all consistent), and (3) a standardized plot of delta values to that 'positive' values indicate the same direction of divide motion for all metrics. Similar to *AcrossDivide*, the user can choose to use the standard deviation of the populations, standard error on the mean, or 95% bootstrap confidence interval as the uncertainty value.

S2. Captions for supplemental figures

Supplemental Figure 1 – Divide stability histograms for divide GC1.

Supplemental Figure 2 – Longitudinal and χ-normalized profiles for rivers that define divide GC1.

Supplemental Figure 3 – Divide stability histograms for divide GC2.

Supplemental Figure 4 – Longitudinal and χ-normalized profiles for rivers that define divide GC2.

Supplemental Figure 5 – Divide stability histograms for divide GC3.

Supplemental Figure 6 – Longitudinal and χ-normalized profiles for rivers that define divide GC3.

Supplemental Figure 7 – Divide stability histograms for divide GC4.

Supplemental Figure 8 – Longitudinal and χ-normalized profiles for rivers that define divide GC4.

Supplemental Figure 9 – Divide stability histograms for divide GC5.

Supplemental Figure 10 – Longitudinal and χ-normalized profiles for rivers that define divide GC5.

Supplemental Figure 11 – Divide stability histograms for divide GC6.

Supplemental Figure 12 – Longitudinal and χ-normalized profiles for rivers that define divide GC6.

Supplemental Figure 13 – Divide stability histograms for divide GC7.

Supplemental Figure 14 – Longitudinal and χ-normalized profiles for rivers that define divide GC7.

Supplemental Figure 15 – Divide stability histograms for divide GC8.

Supplemental Figure 16 – Longitudinal and χ-normalized profiles for rivers that define divide GC8.

Supplemental Figure 17 – Divide stability histograms for divide KV1.

Supplemental Figure 18 – Longitudinal and χ-normalized profiles for rivers that define divide KV1.

Supplemental Figure 19 – Divide stability histograms for divide KV2.

Supplemental Figure 20 – Longitudinal and χ-normalized profiles for rivers that define divide KV2.

Supplemental Figure 21 – Divide stability histograms for divide KV3.

Supplemental Figure 22 – Longitudinal and χ-normalized profiles for rivers that define divide KV3.

Supplemental Figure 23 – Divide stability histograms for divide KV4.

Supplemental Figure 24 – Longitudinal and χ-normalized profiles for rivers that define divide KV4.

Supplemental Figure 25 – Divide stability histograms for divide KV5.

Supplemental Figure 26 – Longitudinal and χ-normalized profiles for rivers that define divide KV5.

Supplemental Figure 27 – Empirical relationship between Be10 erosion rate data and local 2.5 km relief in the San Bernadino Mountains used to produce the erosion rate map in Figure 10B.

Supplemental Figure 28 – Divide stability histograms for divide SB1.

Supplemental Figure 29 – Longitudinal and χ-normalized profiles for rivers that define divide SB1.

Supplemental Figure 30 – Divide stability histograms for divide SB2.

Supplemental Figure 31 – Longitudinal and χ-normalized profiles for rivers that define divide SB2.

Supplemental Figure 32 – Divide stability histograms for divide SB3.

Supplemental Figure 33 – Longitudinal and χ-normalized profiles for rivers that define divide SB3.

Supplemental Figure 34 – Divide stability histograms for divide SB4.

Supplemental Figure 35 – Longitudinal and χ-normalized profiles for rivers that define divide SB4.

Supplemental Figure 36 – Divide stability histograms for divide SB5.

Supplemental Figure 37 – Longitudinal and χ-normalized profiles for rivers that define divide SB5.

Supplemental Figure 38 – Divide stability histograms for divide SB6.

Supplemental Figure 39 – Longitudinal and χ-normalized profiles for rivers that define divide SB6.

Supplemental Figure 40 – Divide stability histograms for divide SB7.

Supplemental Figure 41 – Longitudinal and χ-normalized profiles for rivers that define divide SB7.

Supplemental Figure 42 – Divide stability histograms for divide SB8.

Supplemental Figure 43 – Longitudinal and χ-normalized profiles for rivers that define divide SB8.

Supplemental Figure 44 – Divide stability histograms for divide SB9.

Supplemental Figure 45 – Longitudinal and χ-normalized profiles for rivers that define divide SB9.

Supplemental Figure 46 – Divide stability histograms for divide SB10.

Supplemental Figure 47 – Longitudinal and χ-normalized profiles for rivers that define divide SB10.

Divide GC1

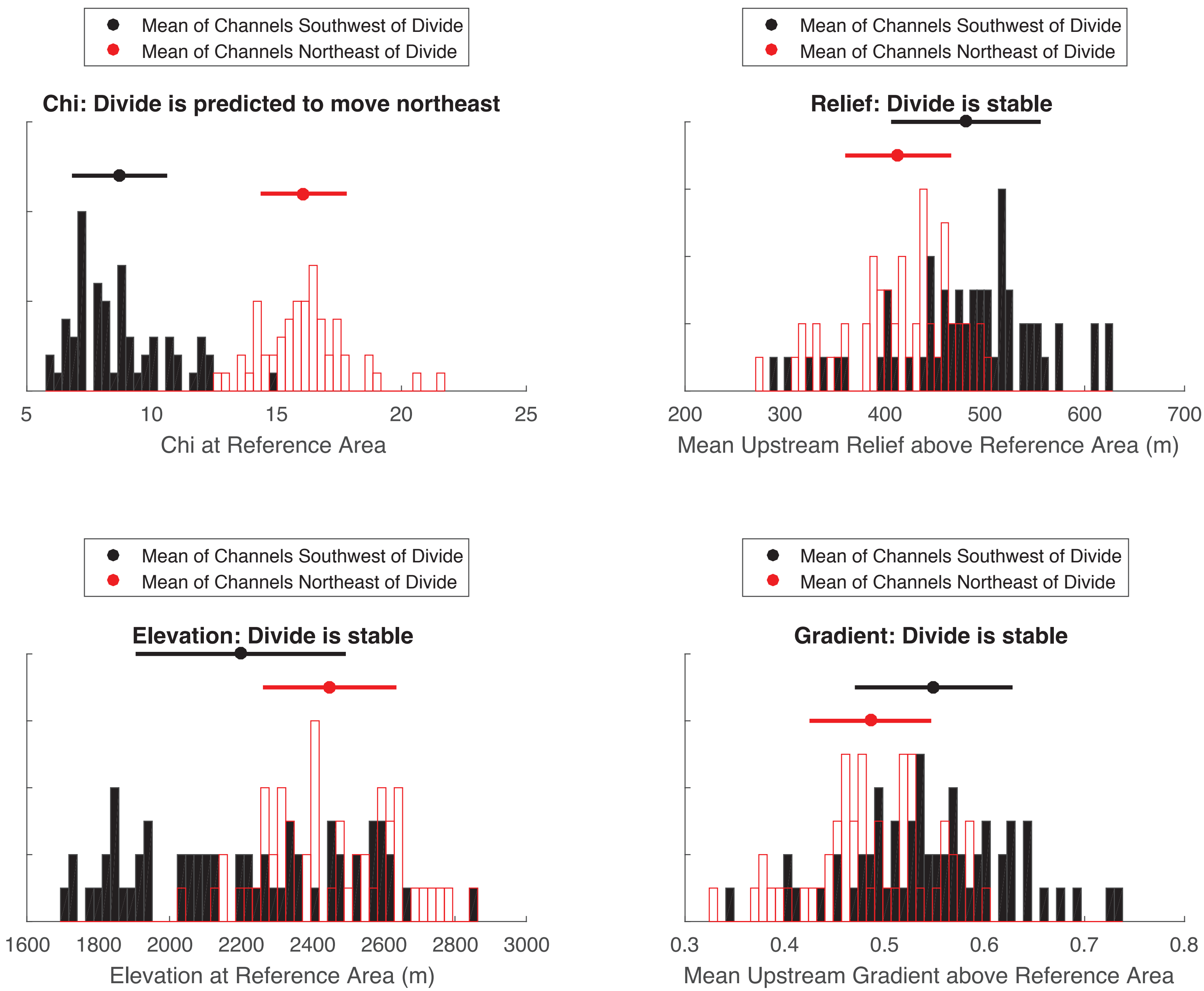

Supplemental Figure 1

Divide GC1

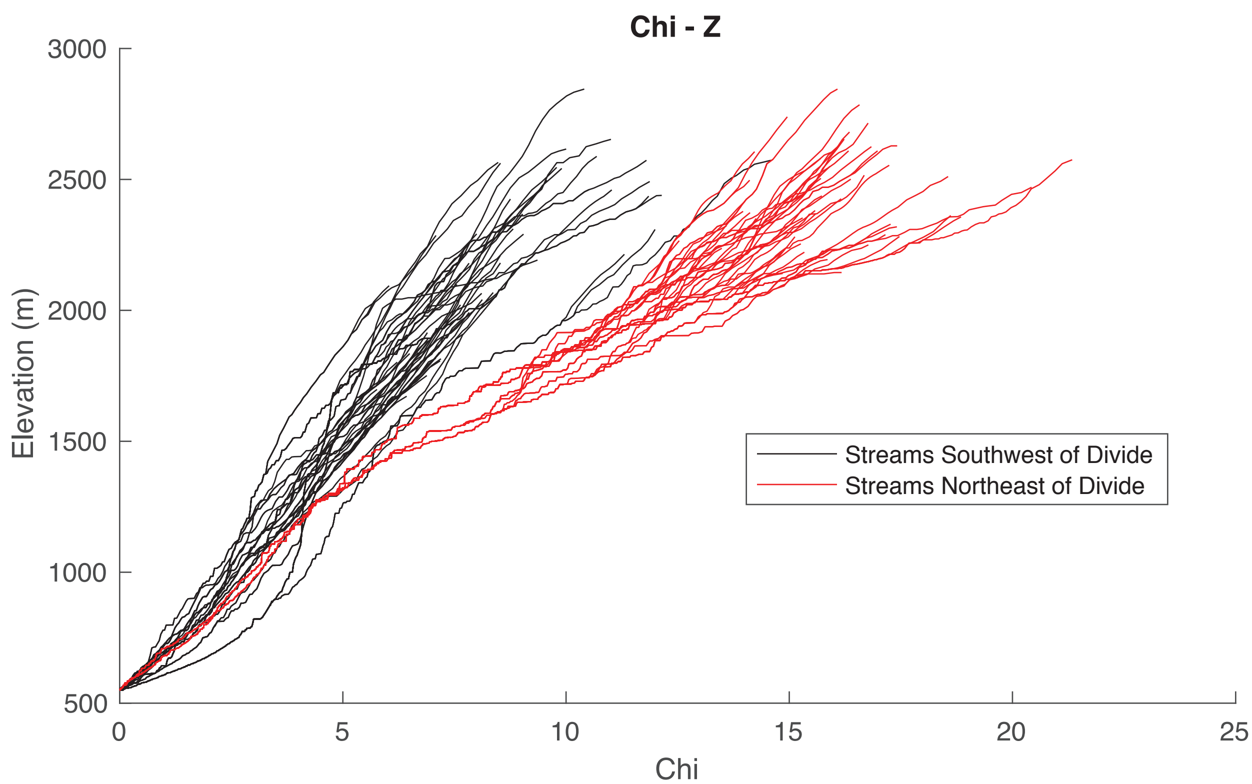

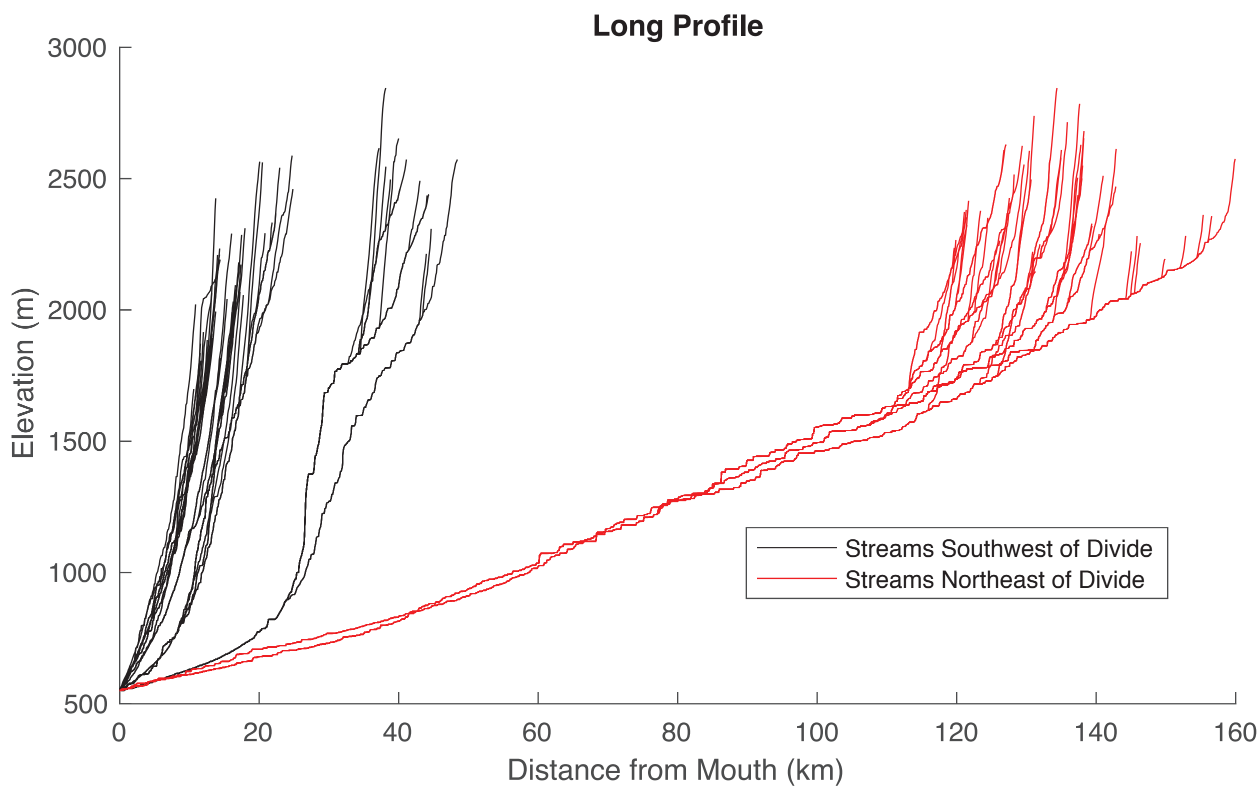

Supplemental Figure 2

Divide GC2

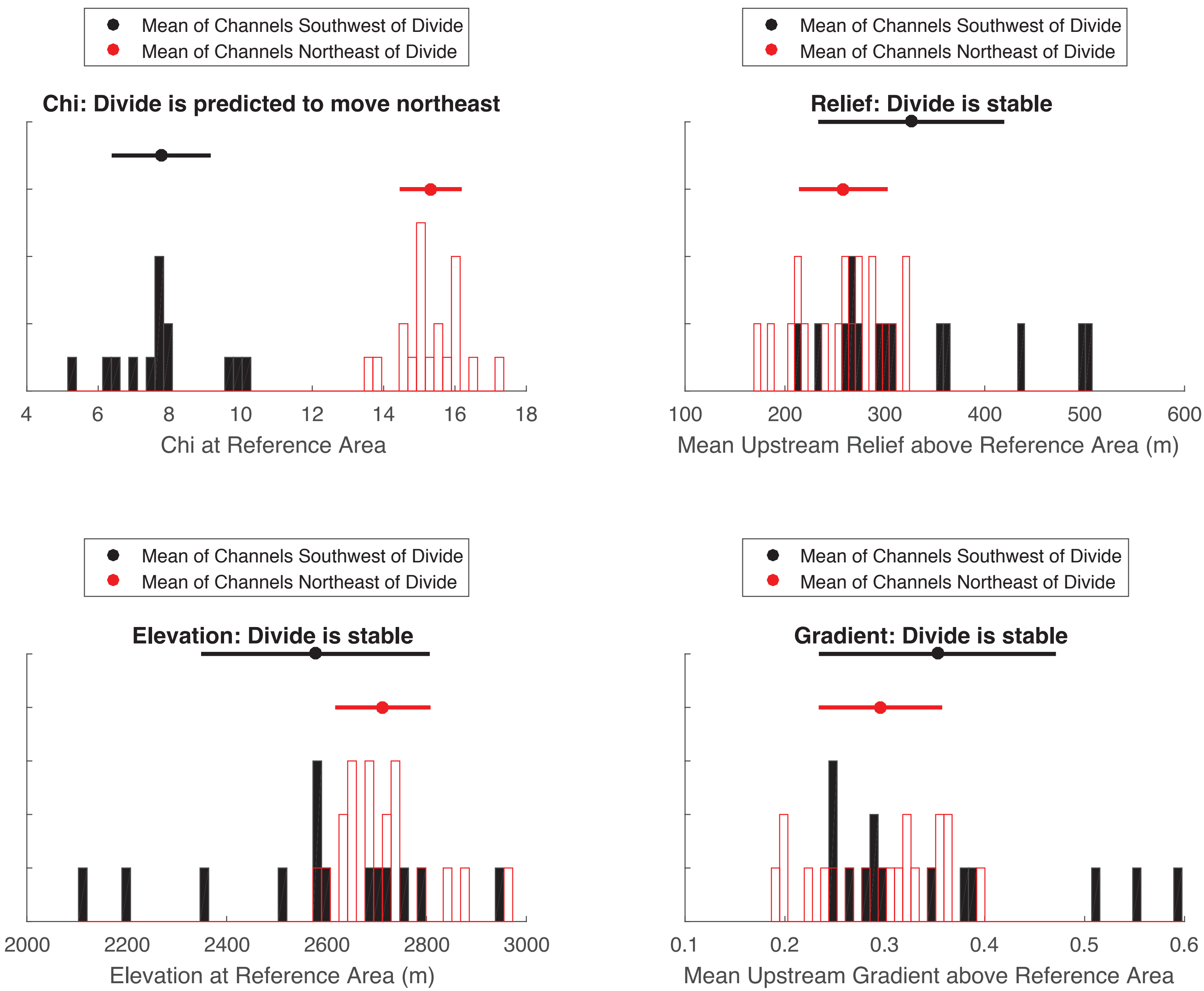

Supplemental Figure 3

Divide GC2

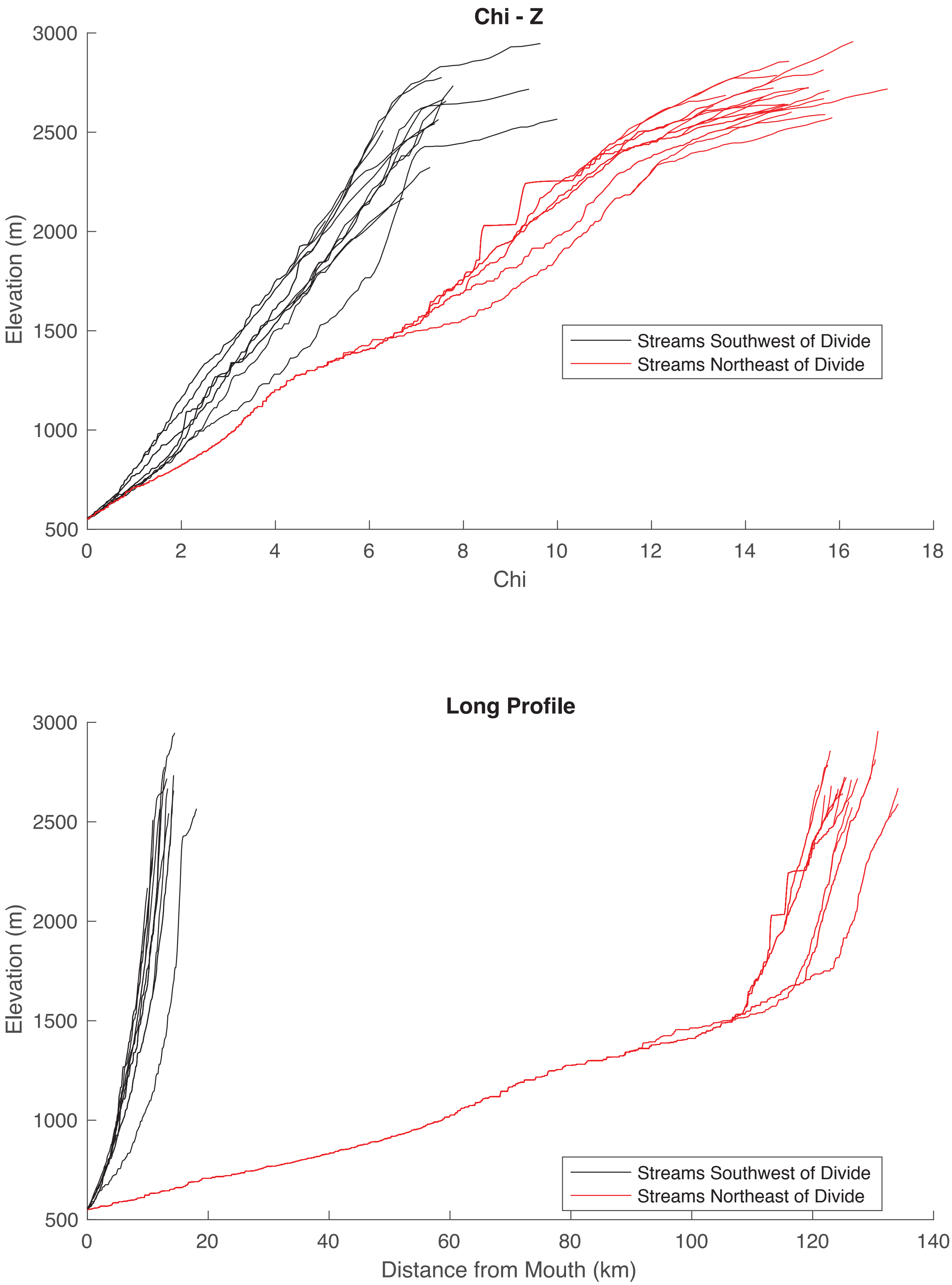

Supplemental Figure 4

Divide GC3

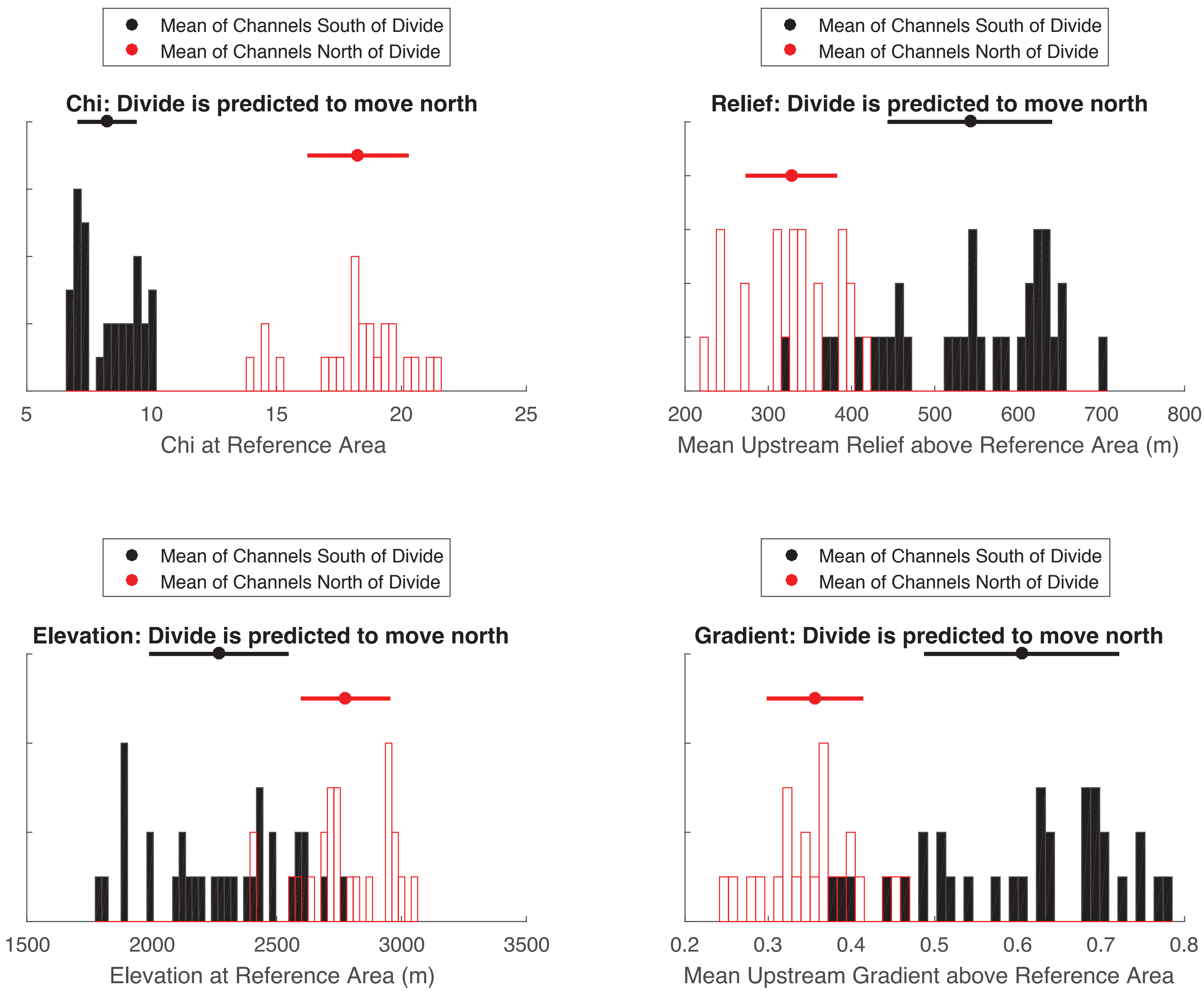

Supplemental Figure 5

Divide GC3

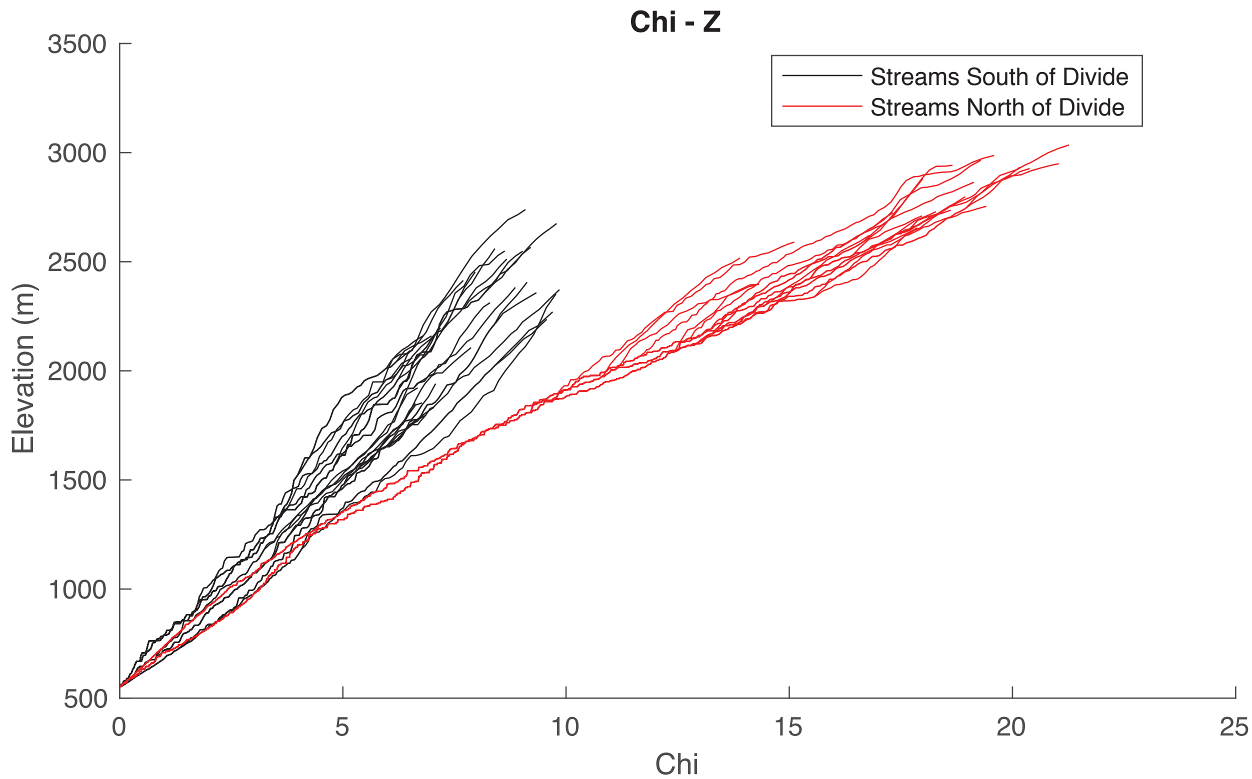

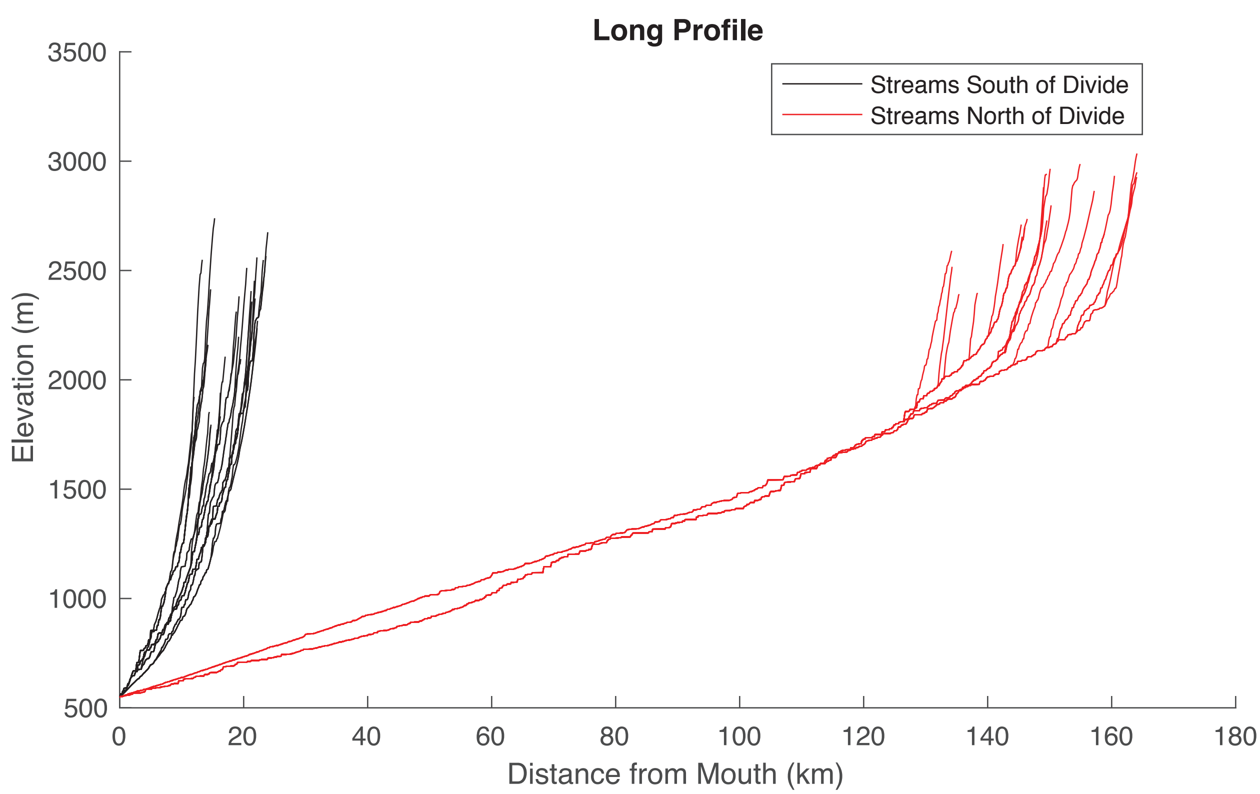

Supplemental Figure 6

Divide GC4

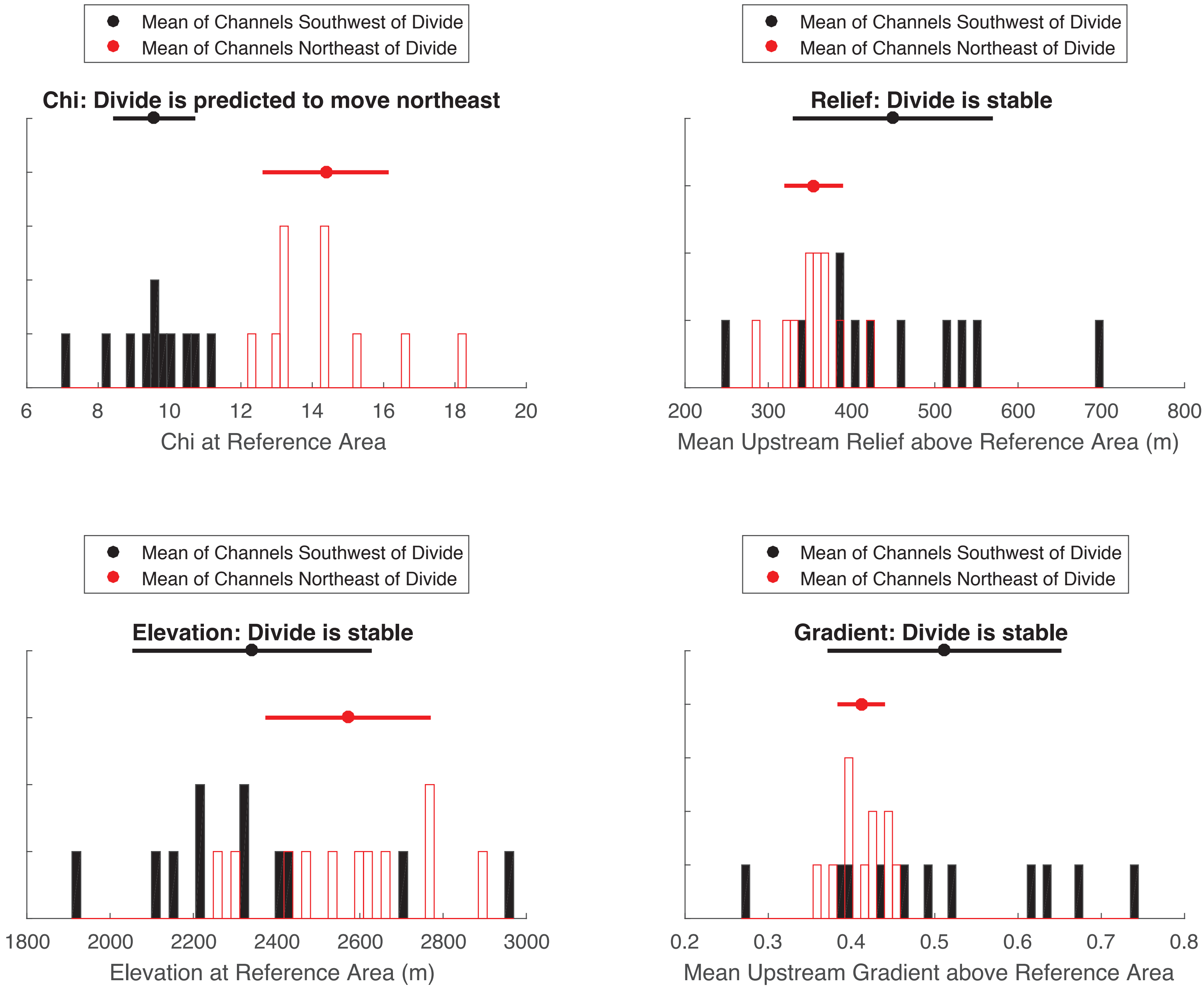

Supplemental Figure 7

Divide GC4

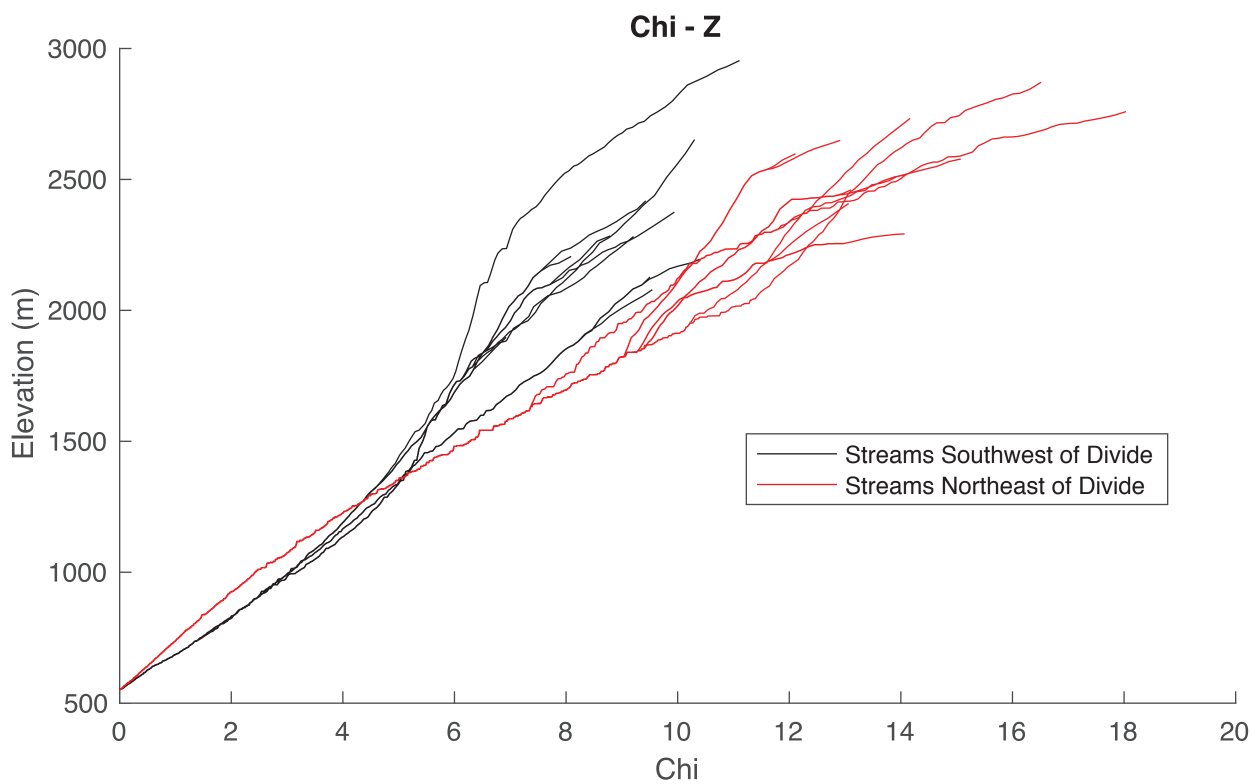

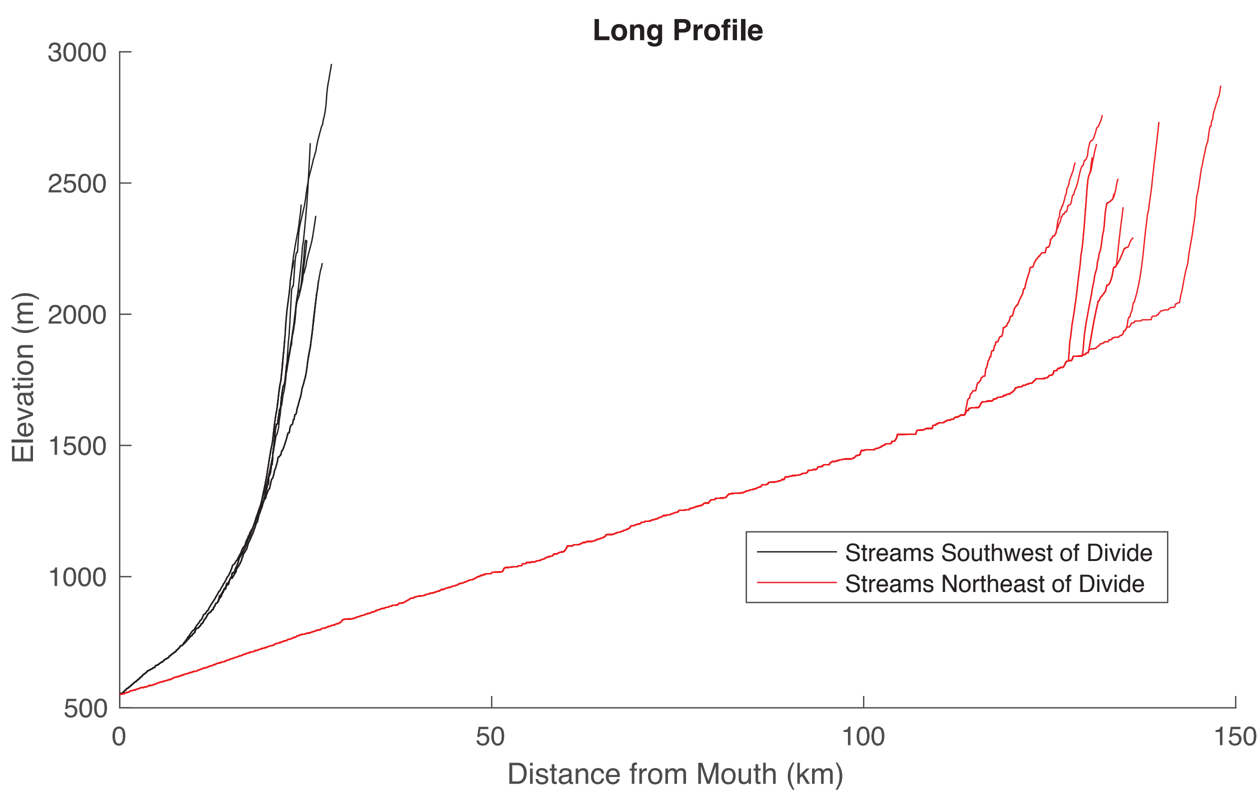

Supplemental Figure 8

Divide GC5

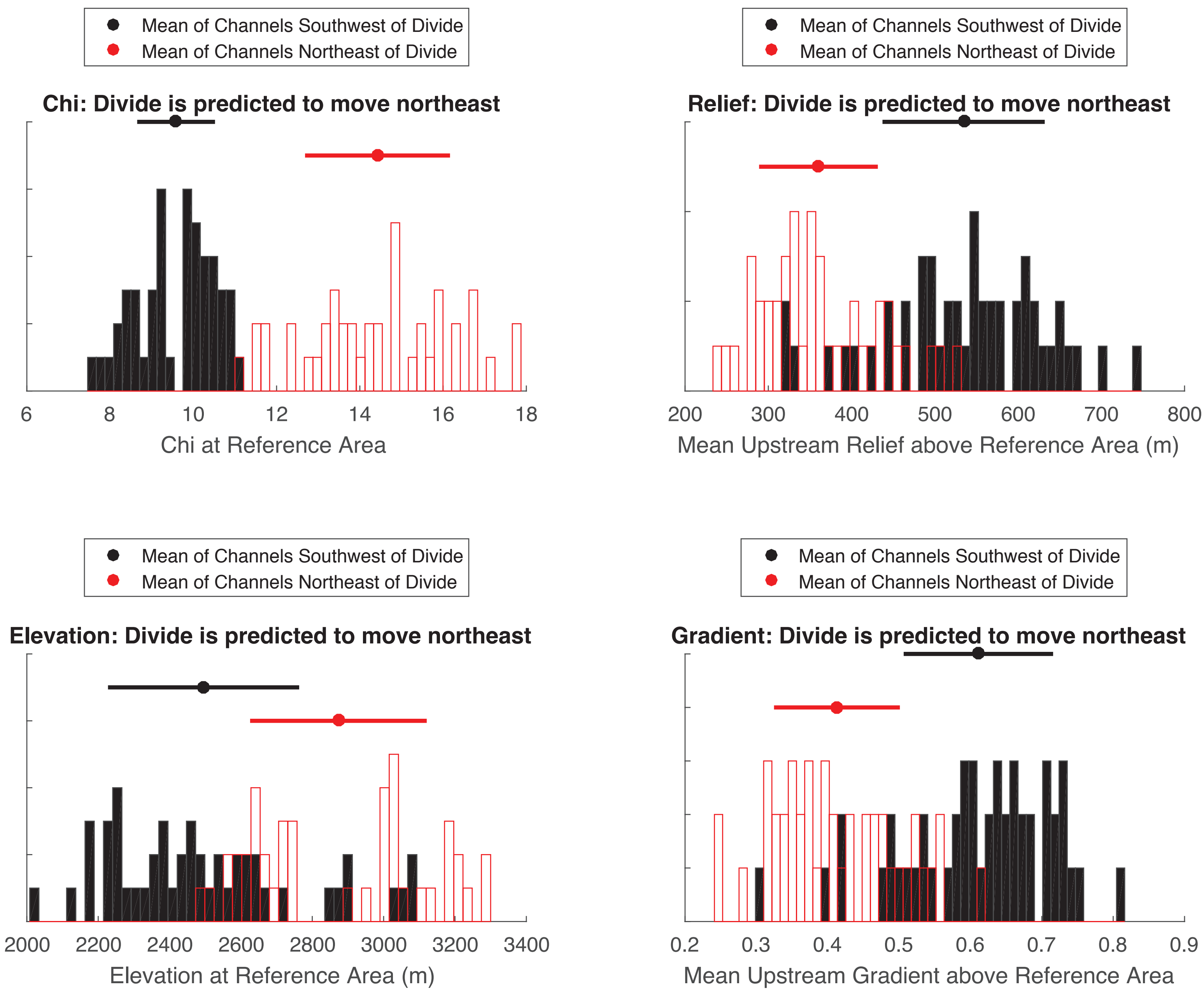

Supplemental Figure 9

Divide GC5

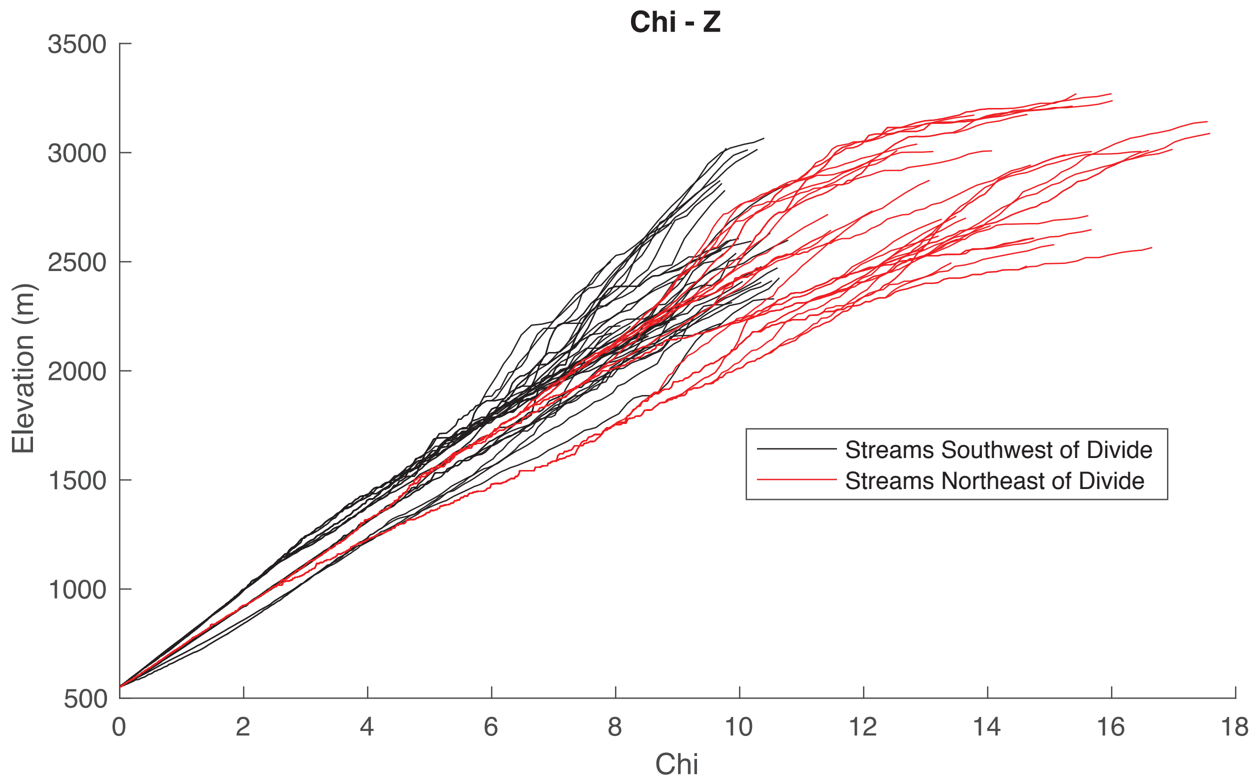

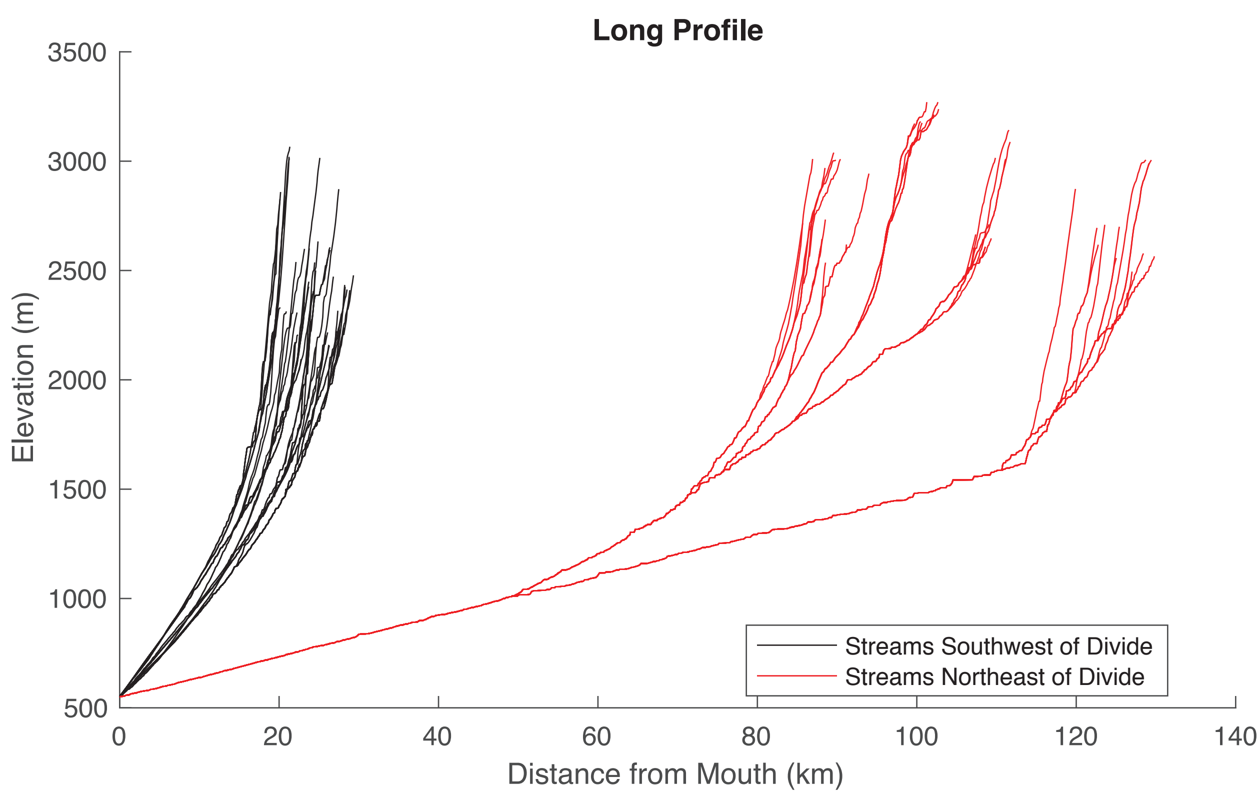

Supplemental Figure 10

Divide GC6

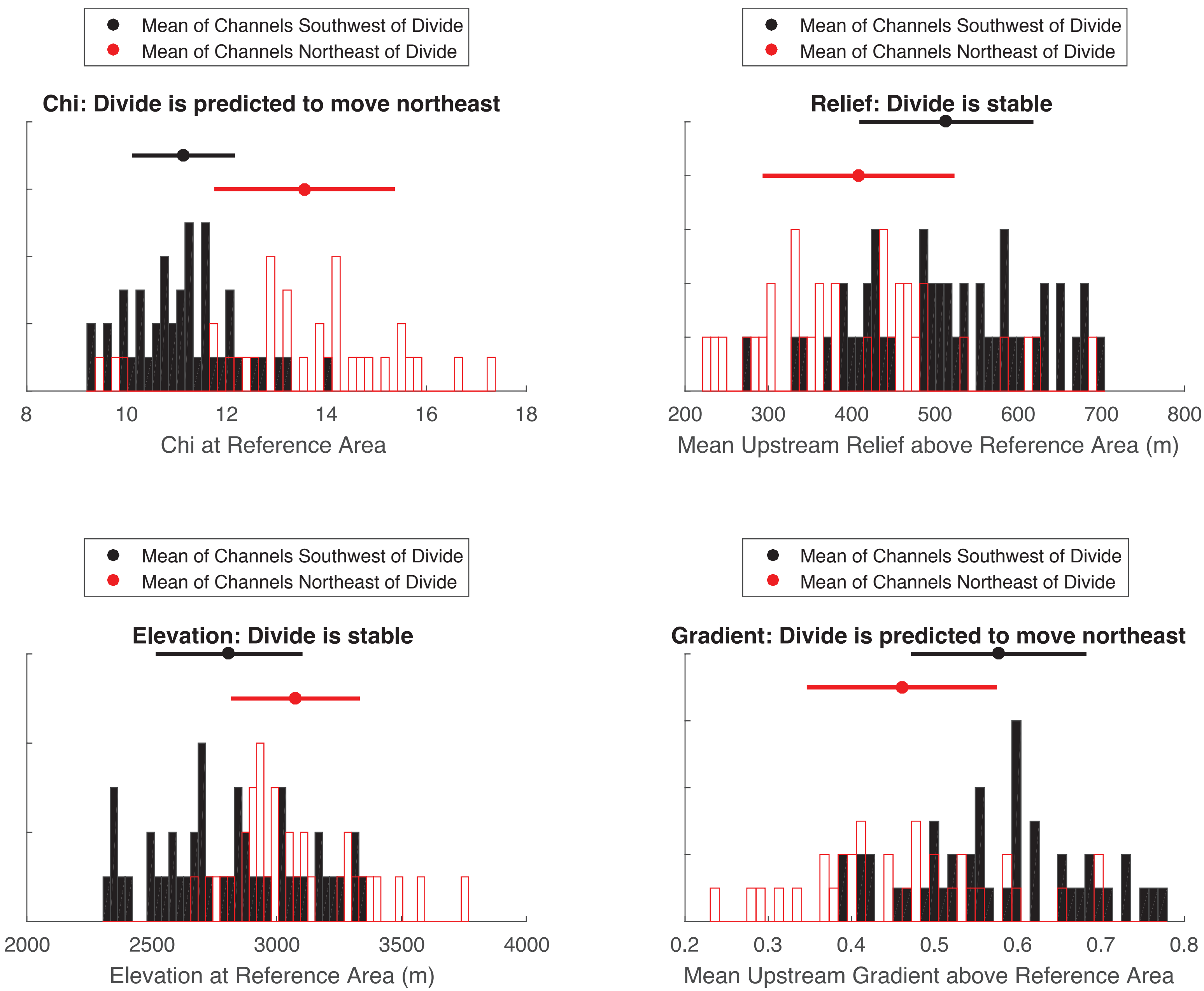

Supplemental Figure 11

Divide GC6

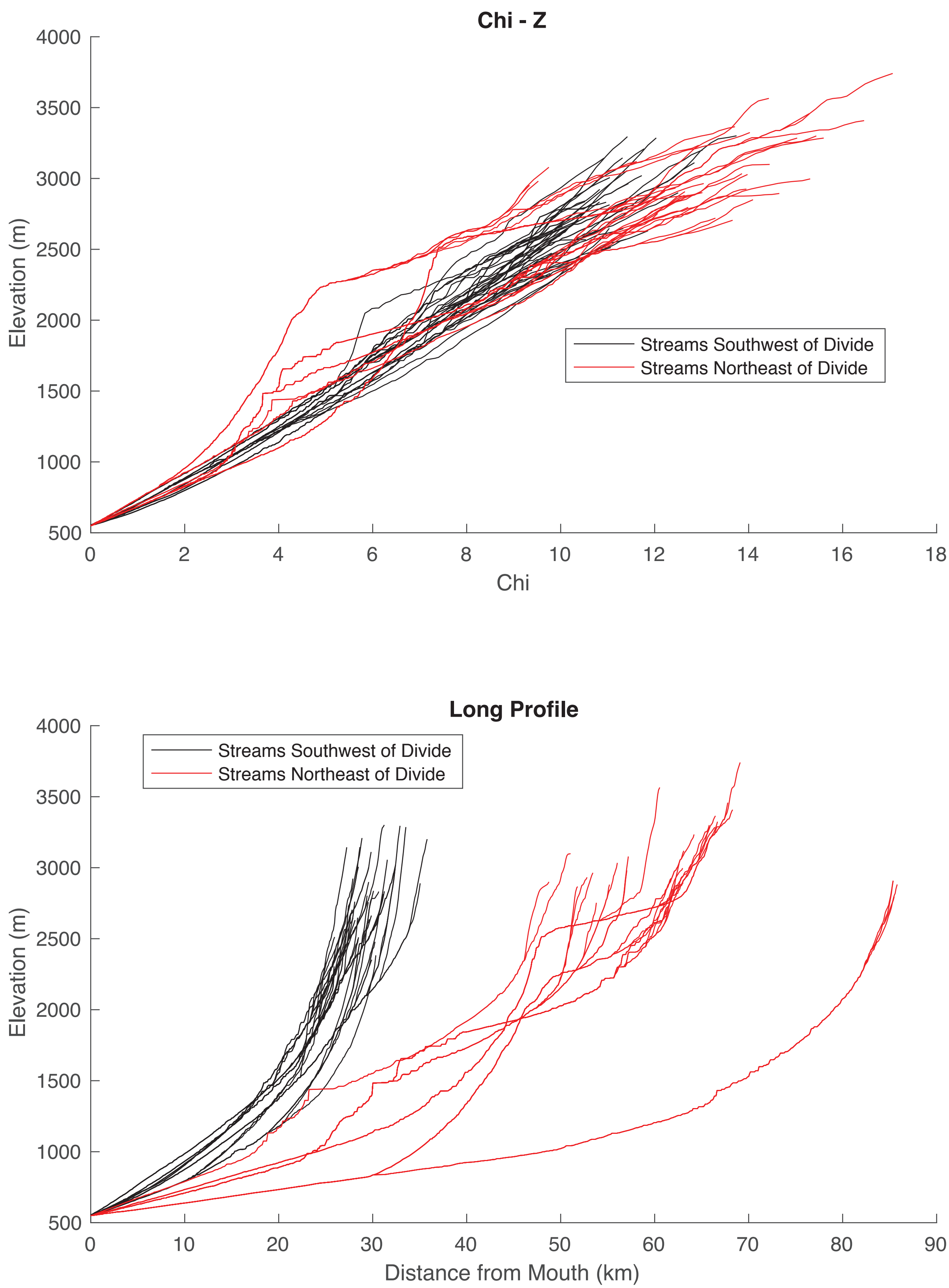

Supplemental Figure 12

Divide GC7

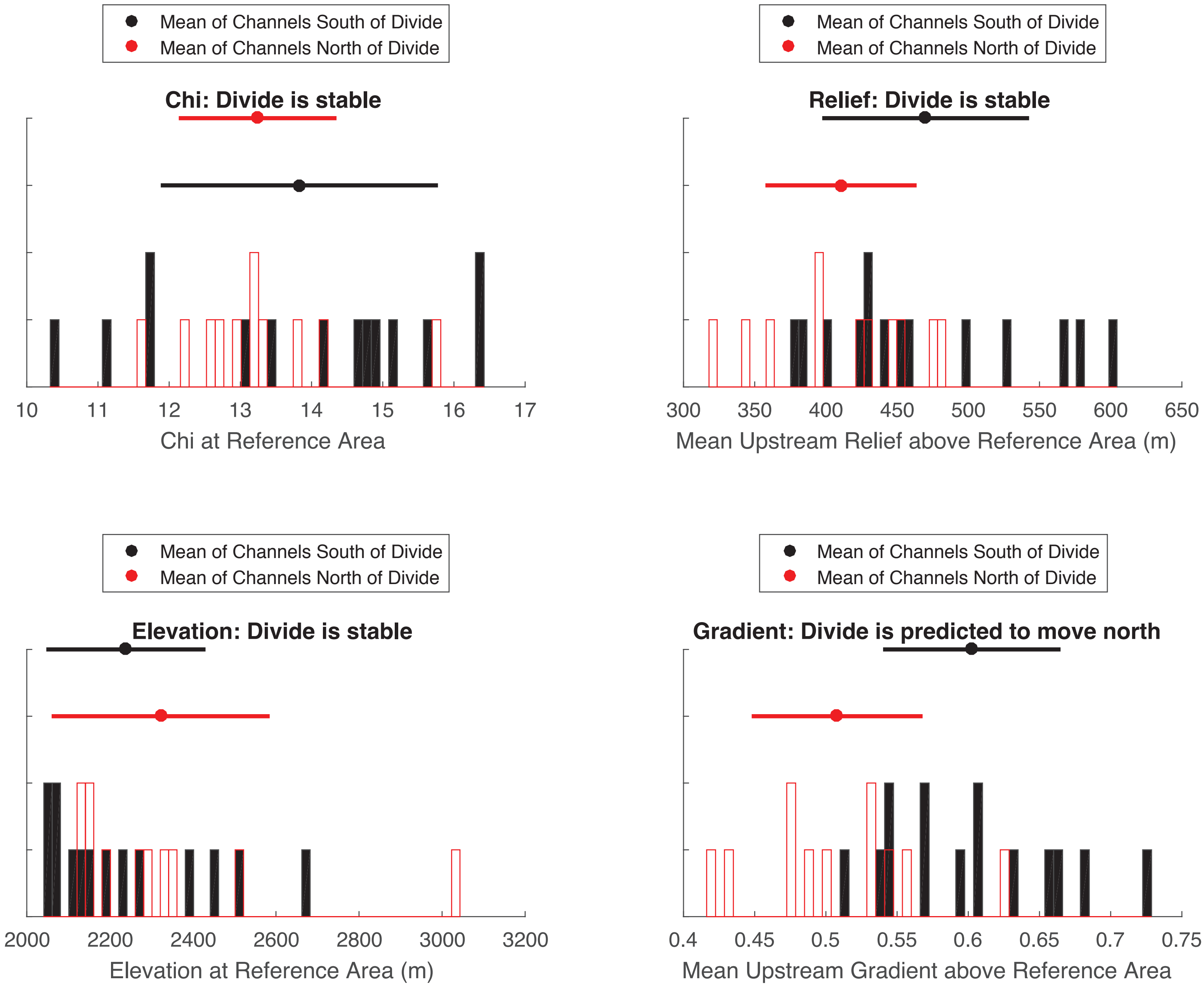

Supplemental Figure 13

Divide GC7

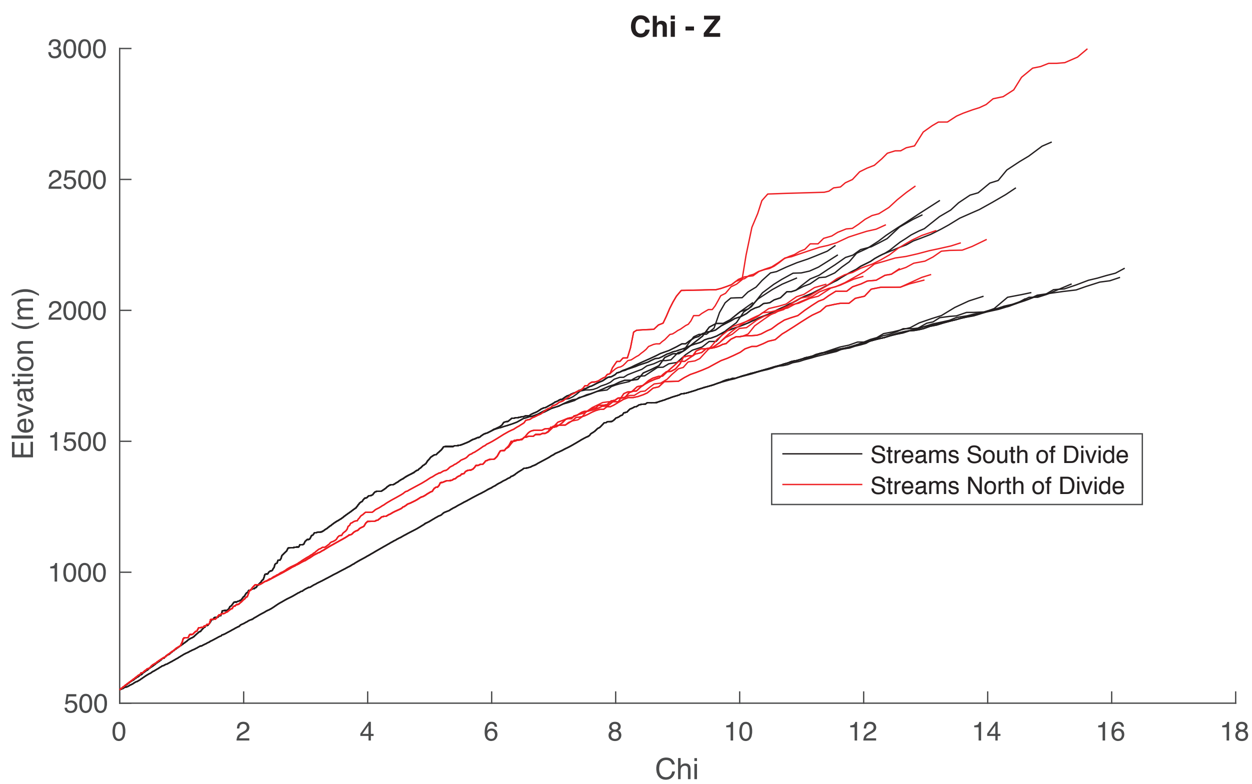

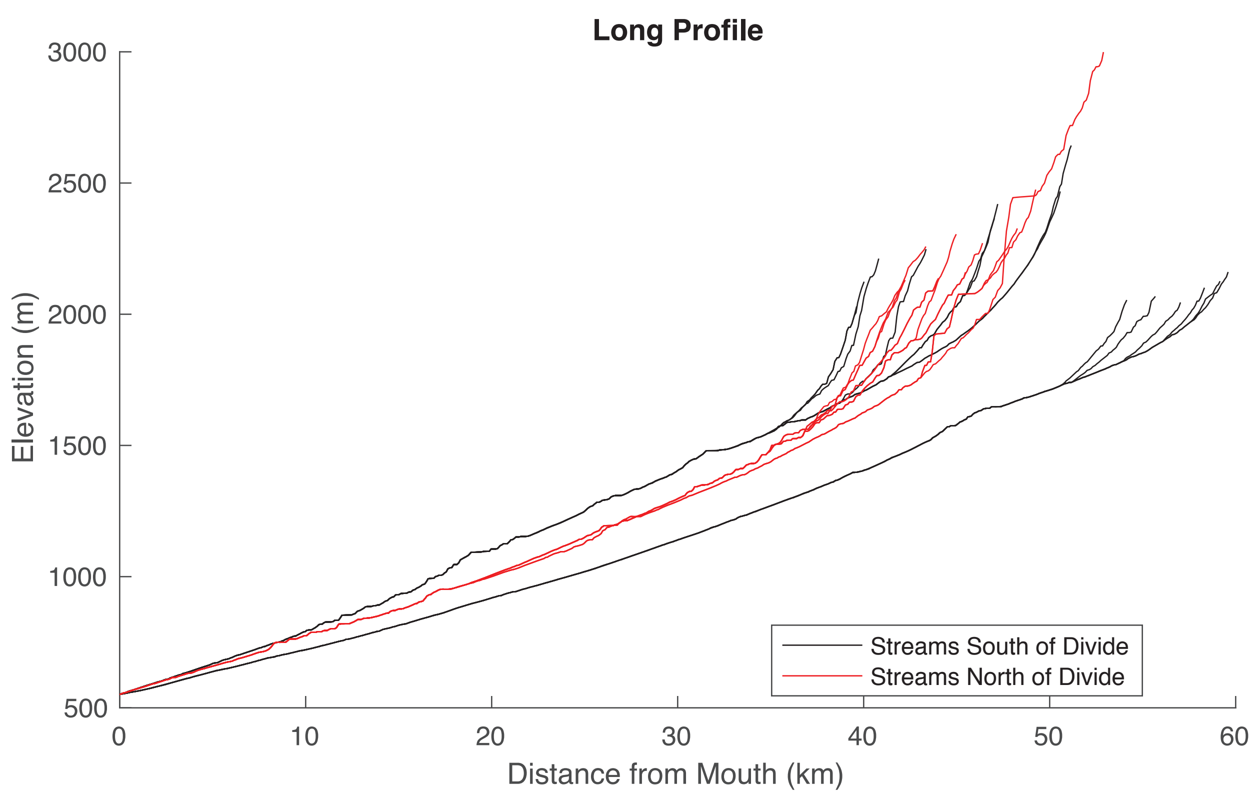

Supplemental Figure 14

Divide GC8

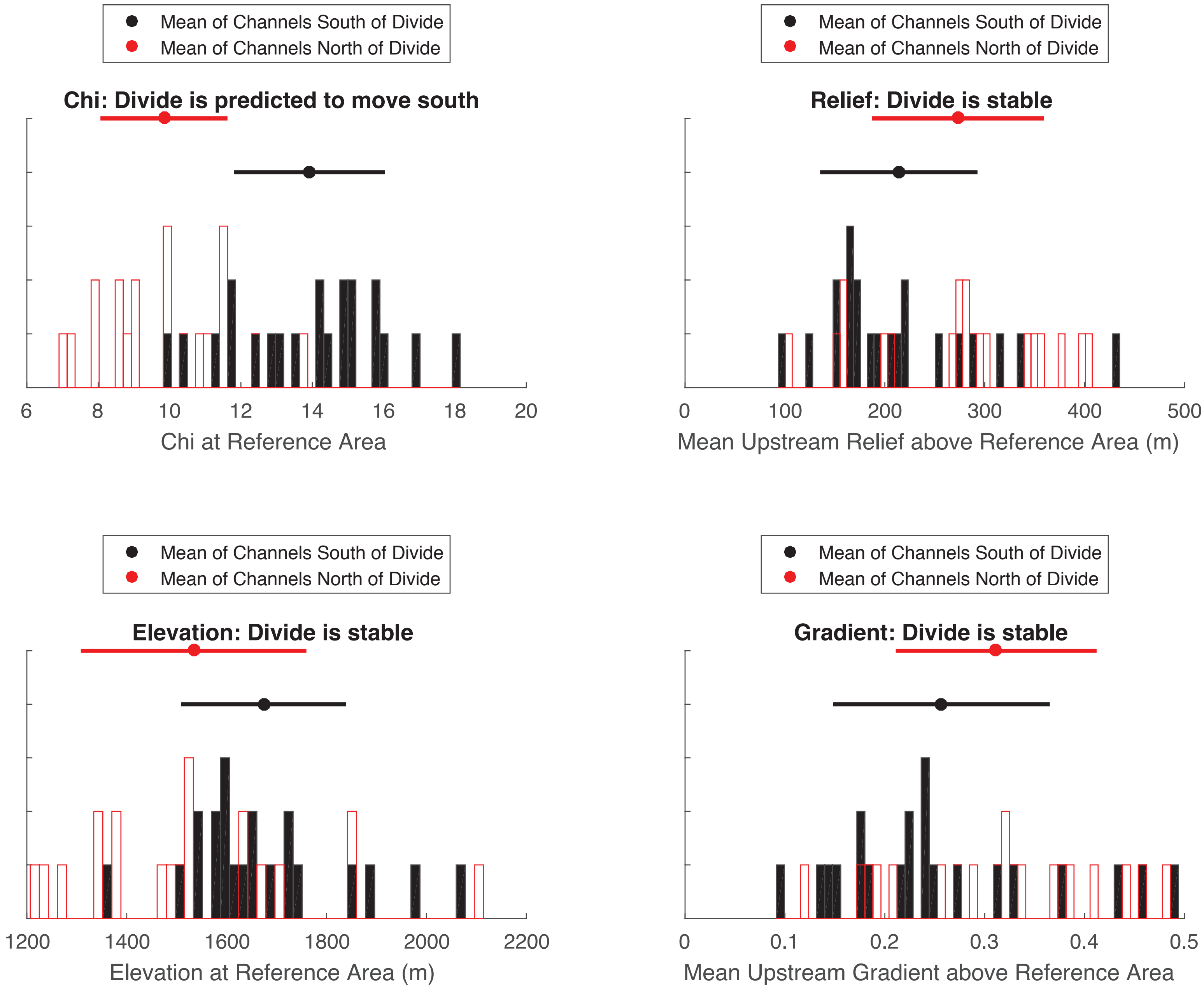

Supplemental Figure 15

Divide GC8

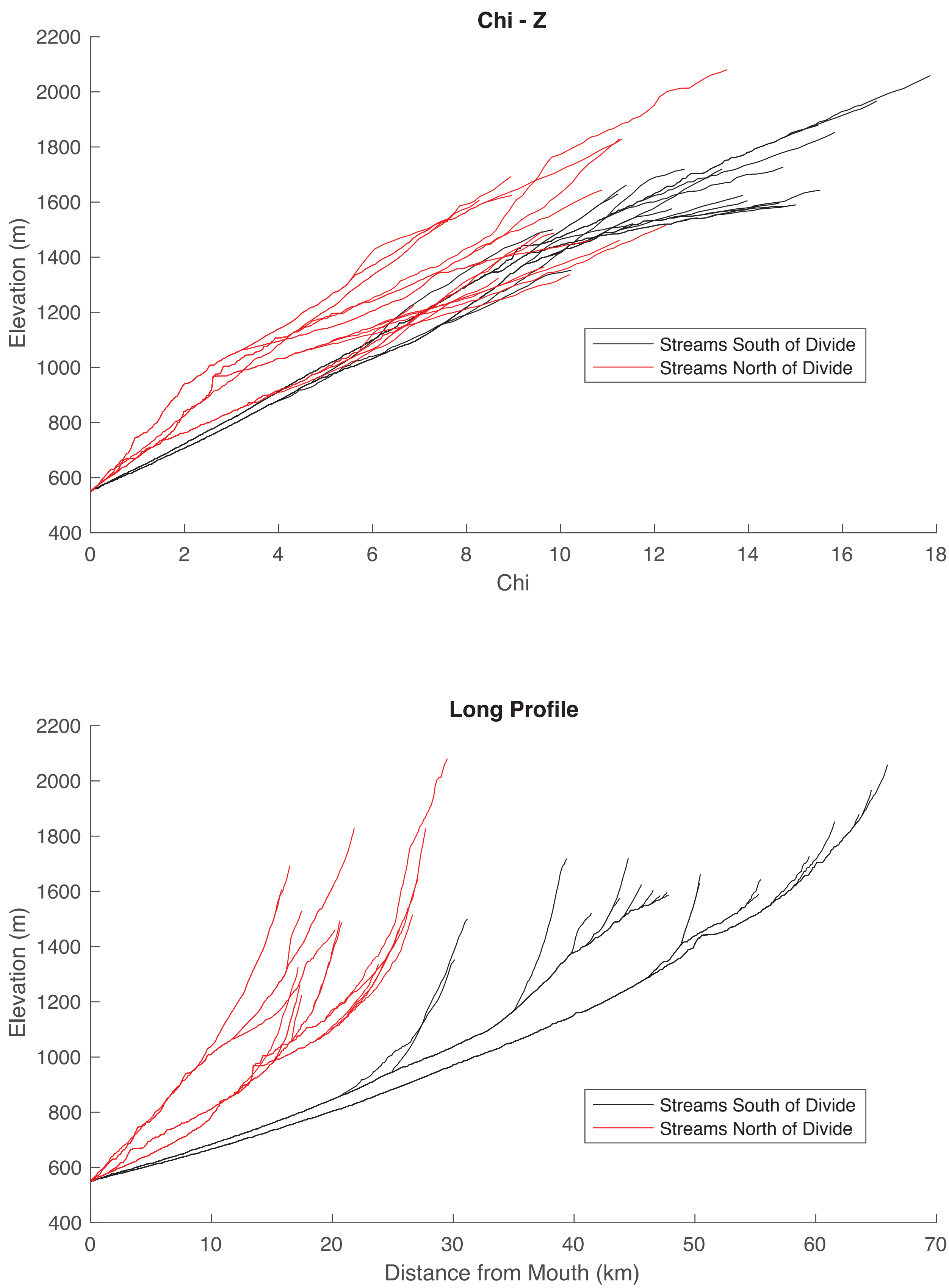

Supplemental Figure 16

Divide KV1

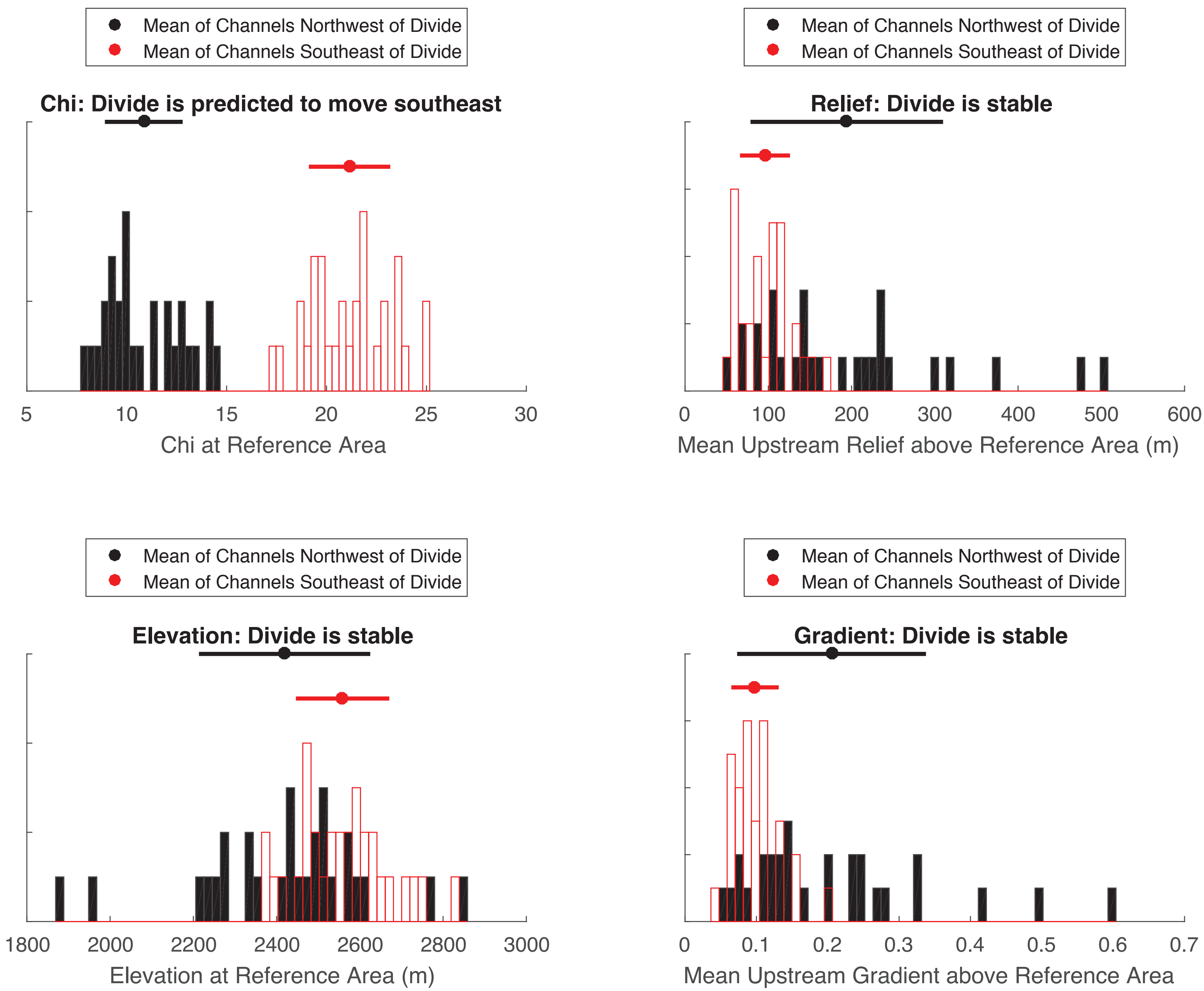

Supplemental Figure 17

Divide KV1

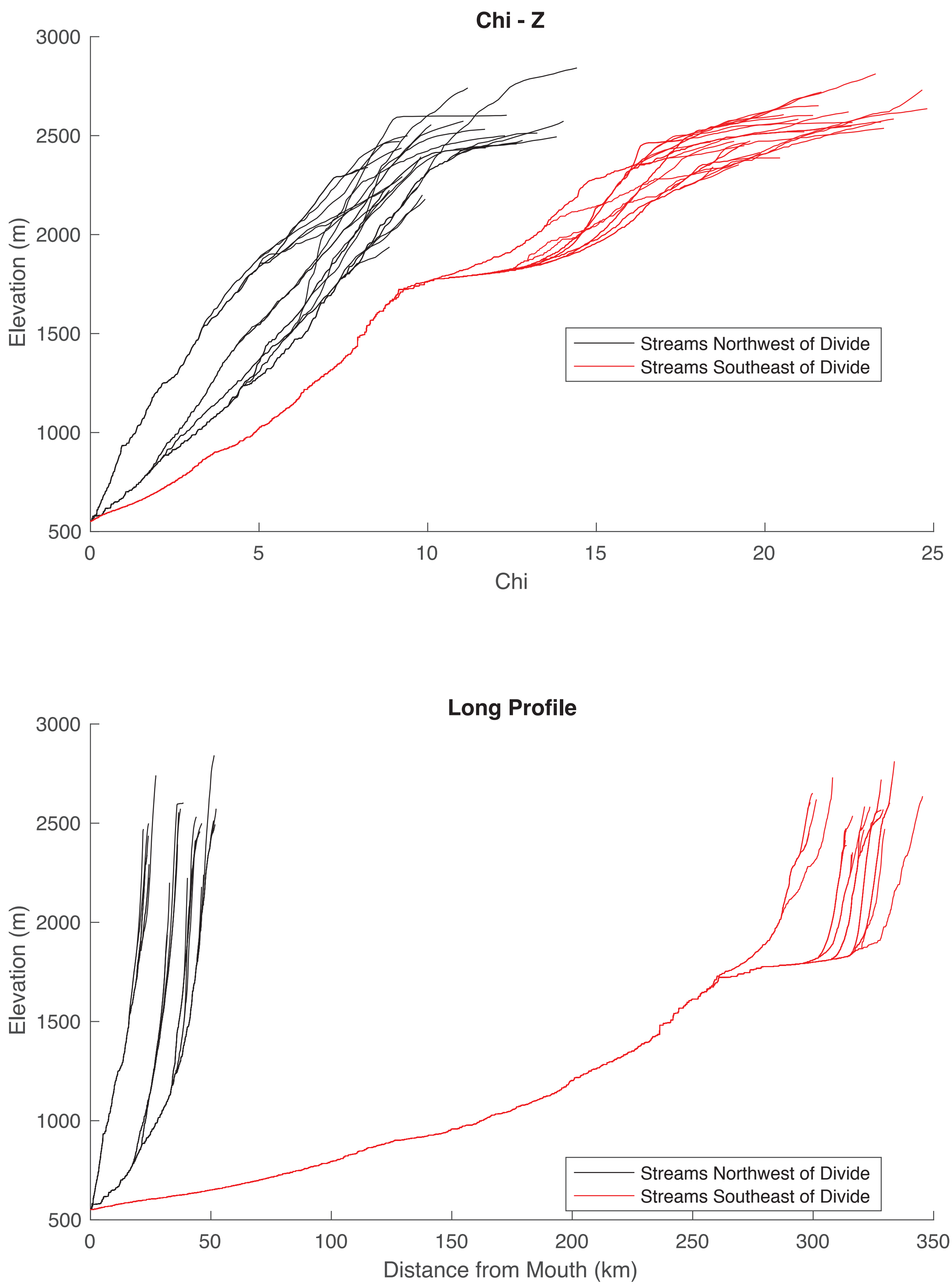

Supplemental Figure 18

Divide KV2

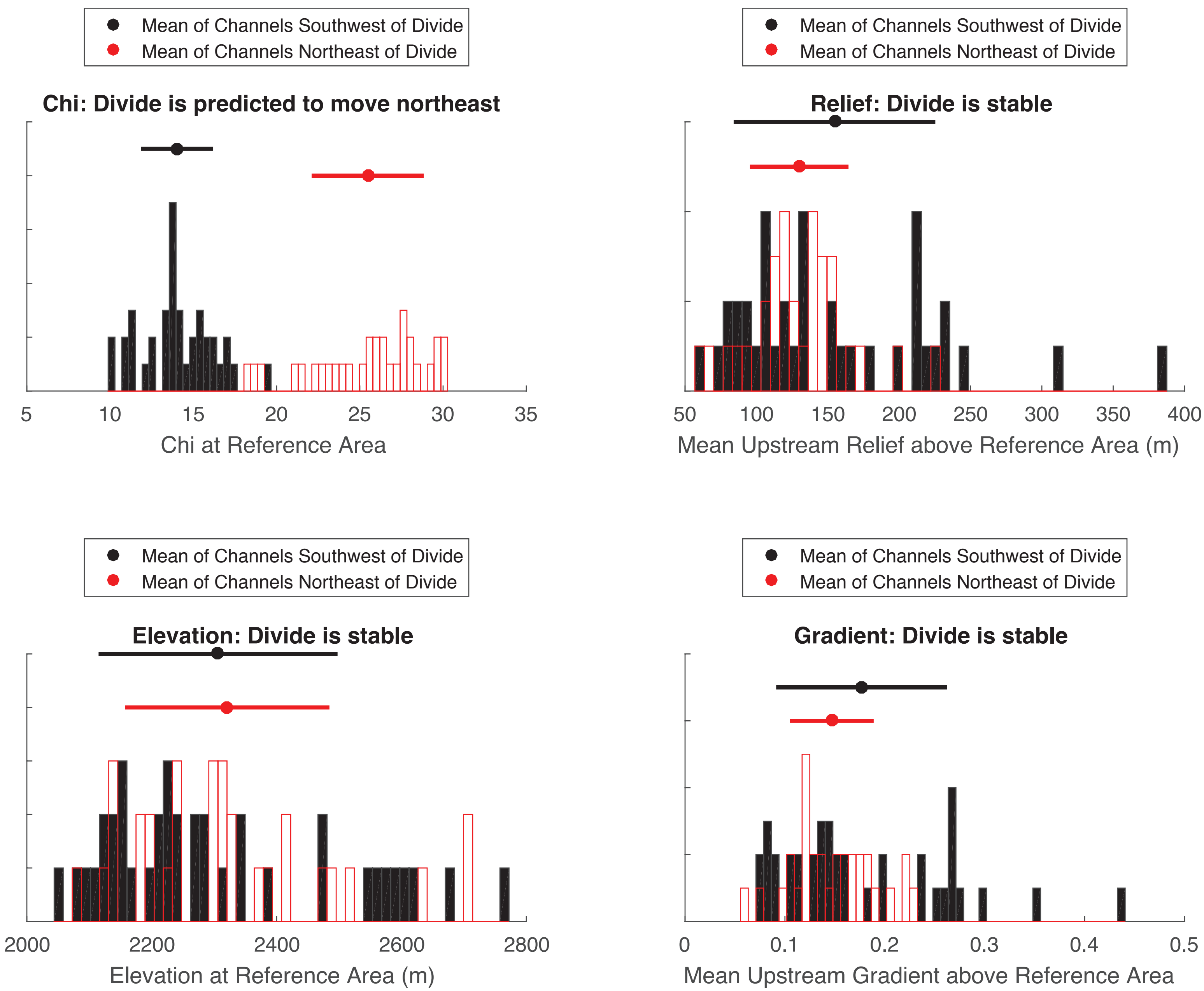

Supplemental Figure 19

Divide KV2

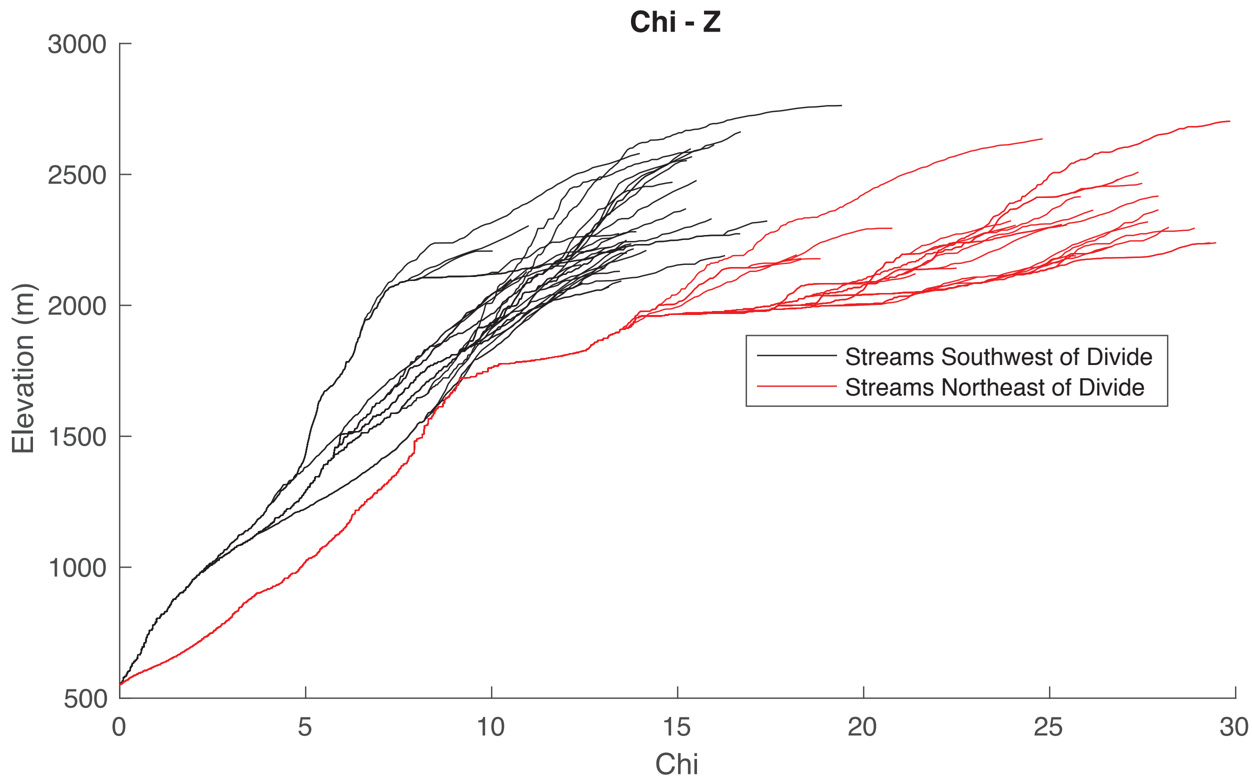

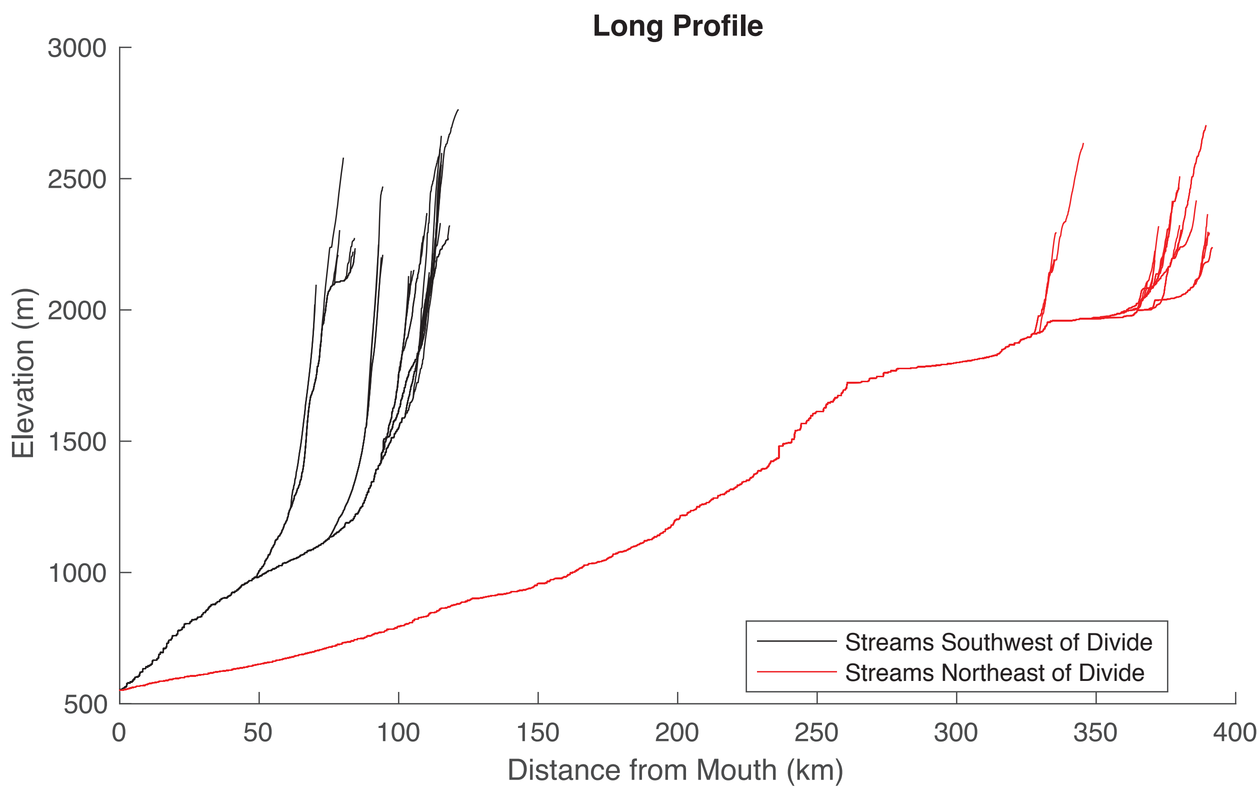

Supplemental Figure 20

Divide KV3

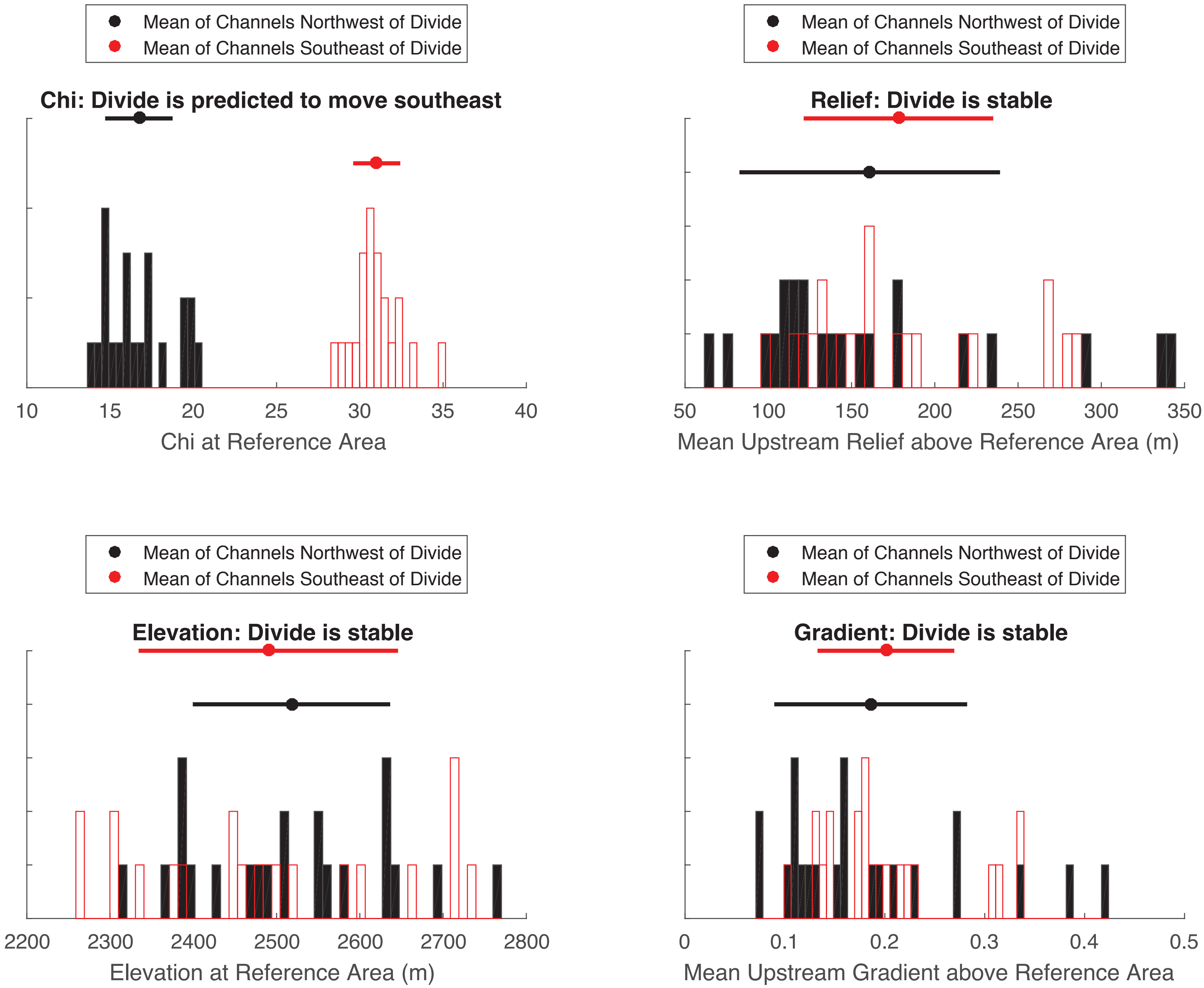

Supplemental Figure 21

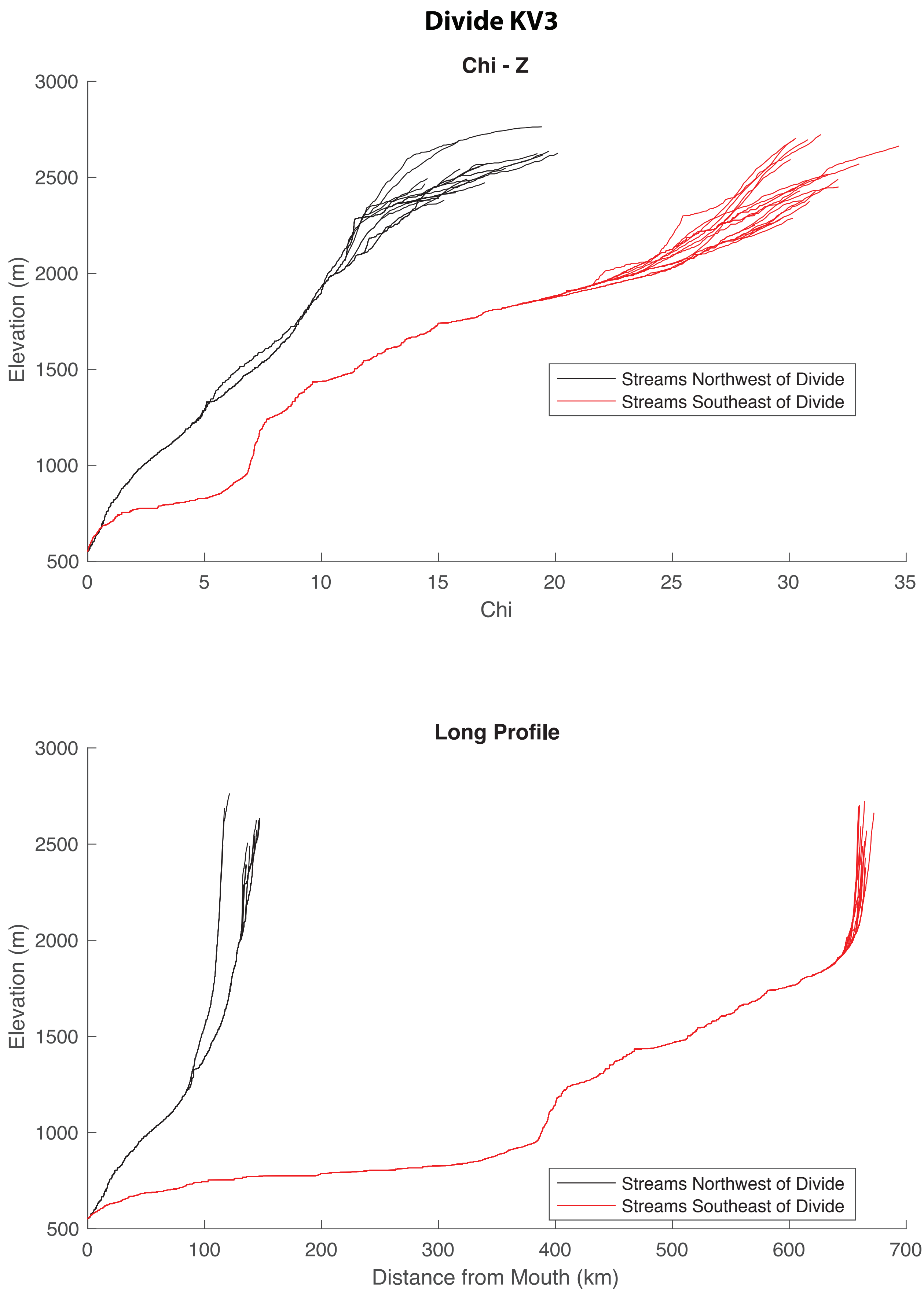

Supplemental Figure 22

Divide KV4

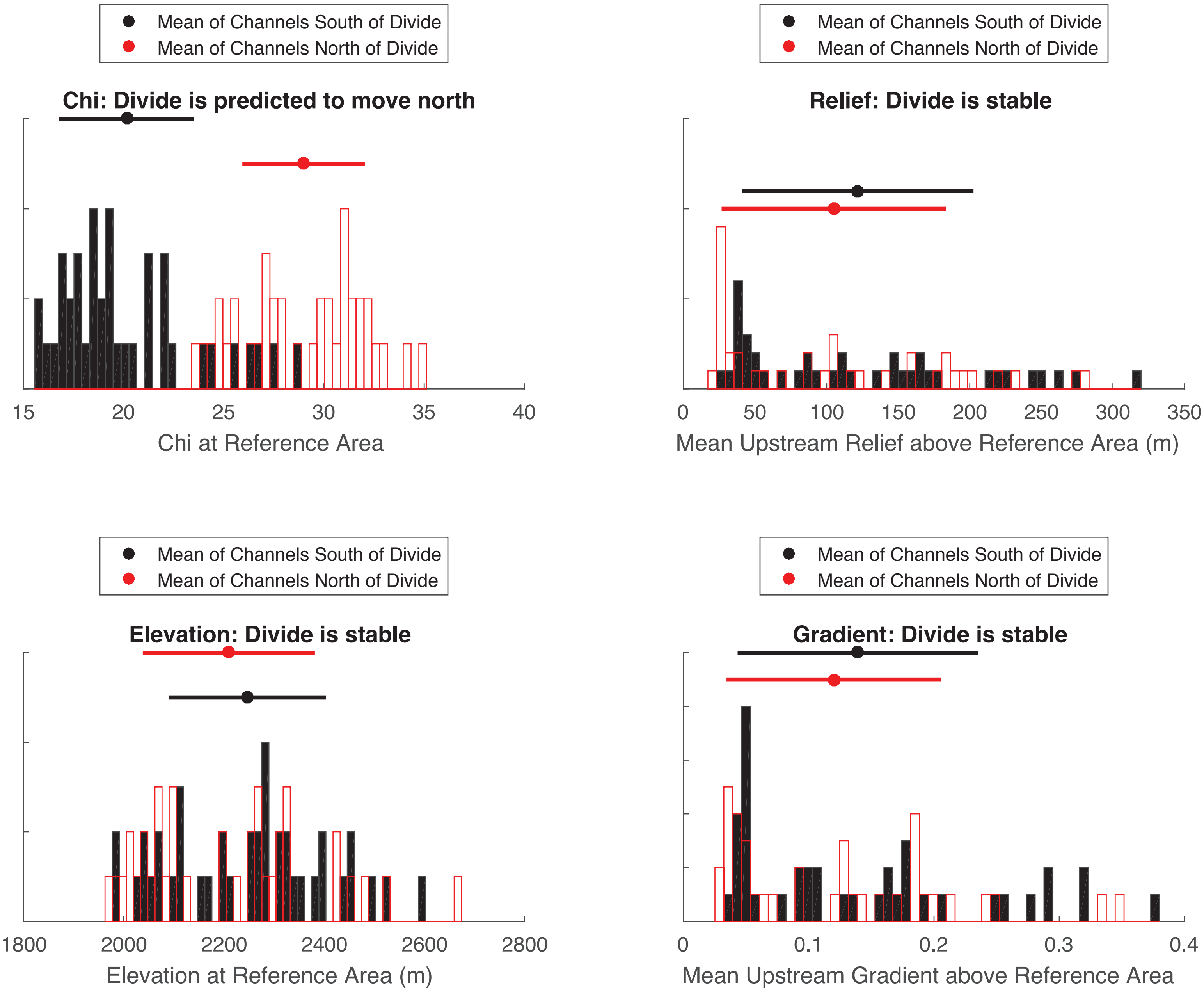

Supplemental Figure 23

Divide KV4

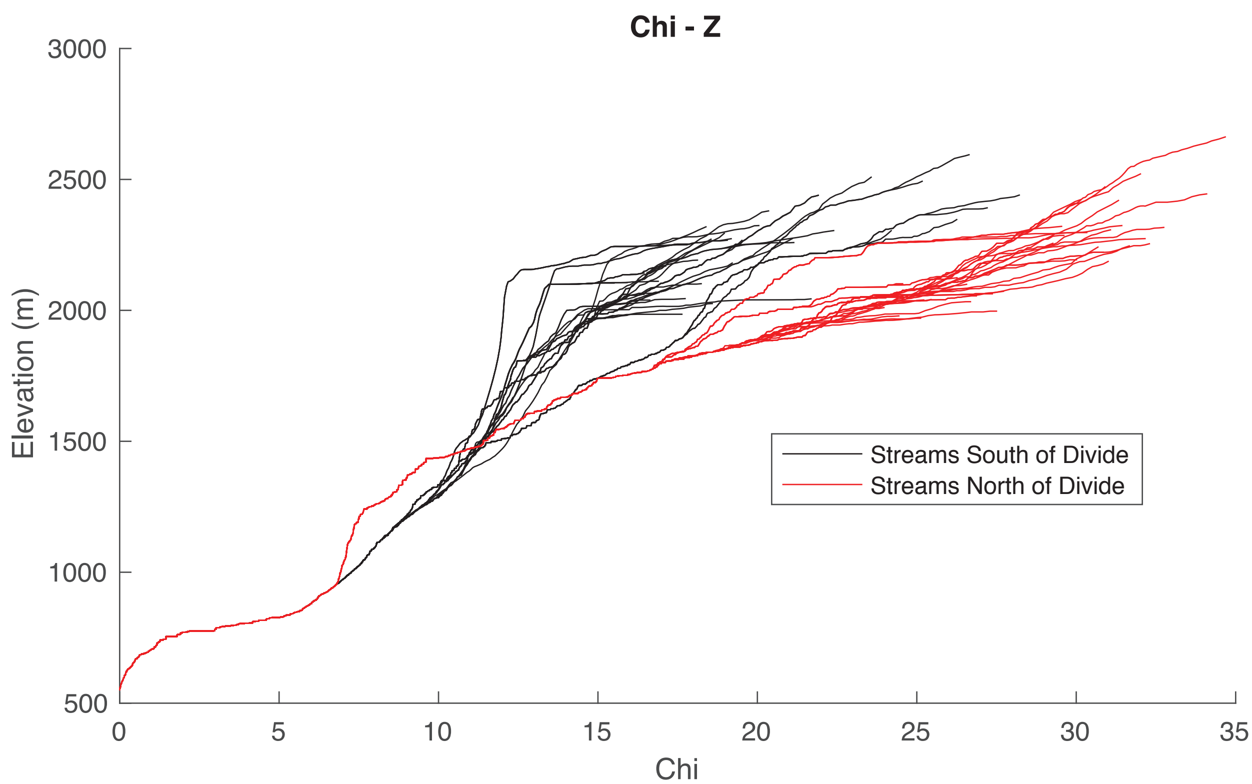

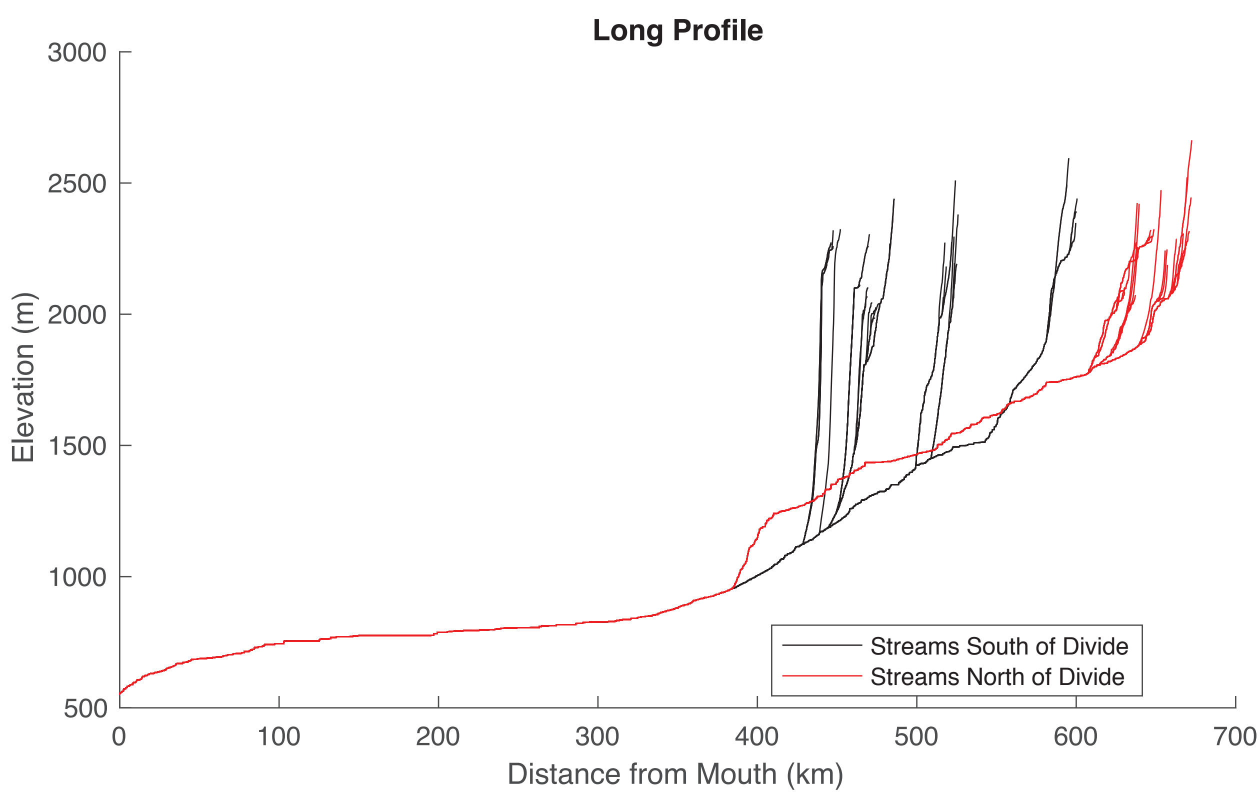

Supplemental Figure 24

Divide KV5

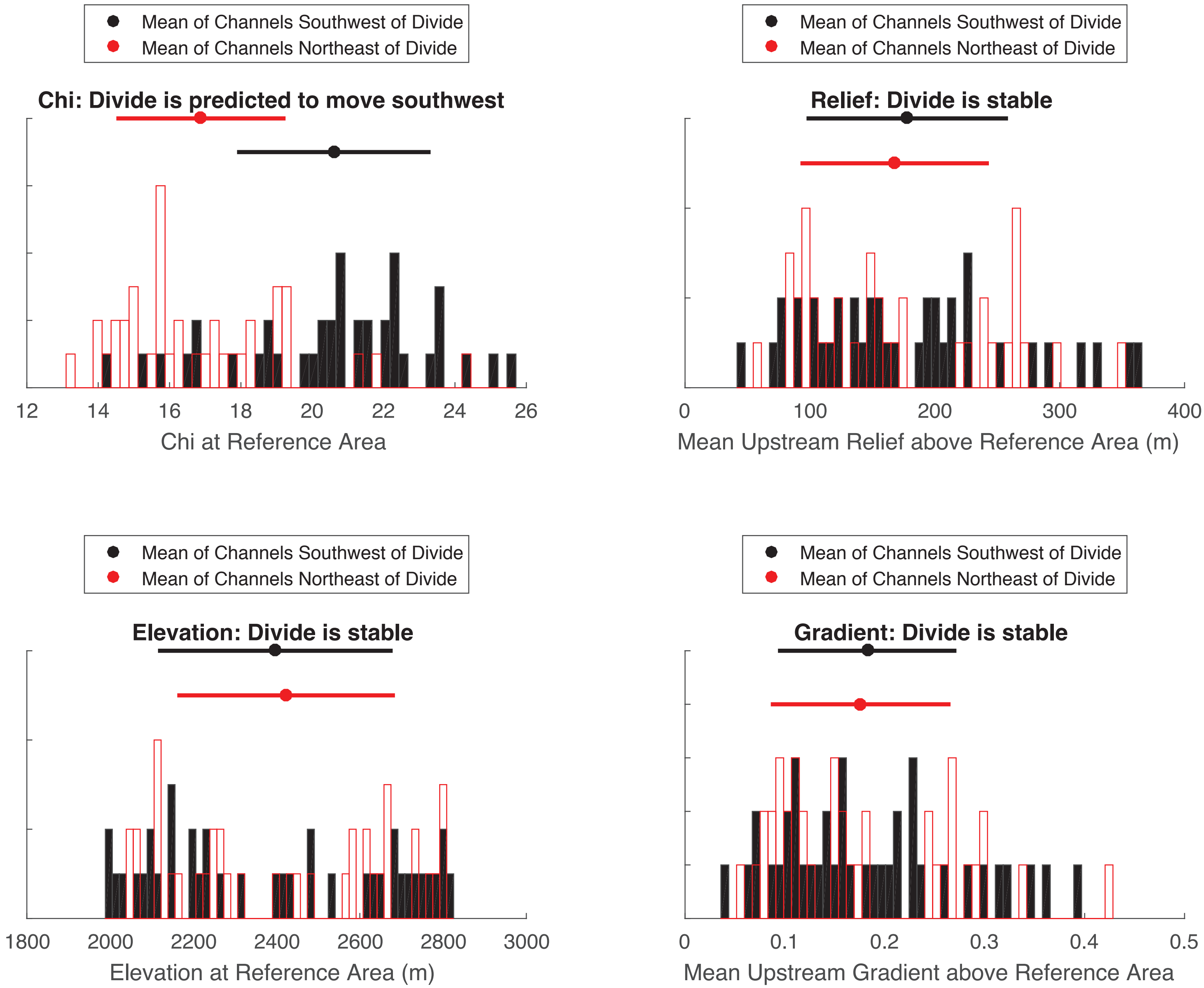

Supplemental Figure 25

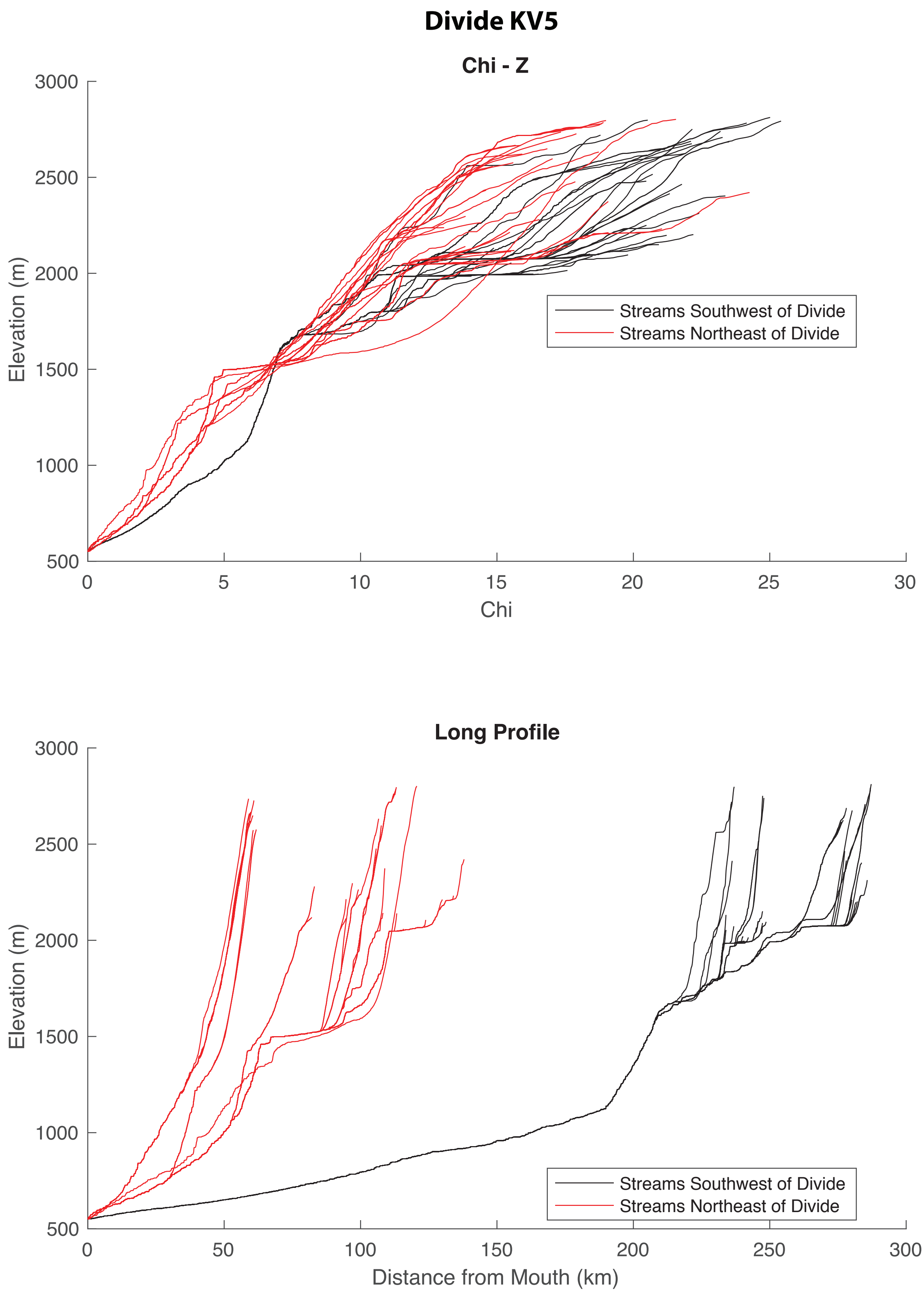

Supplemental Figure 26

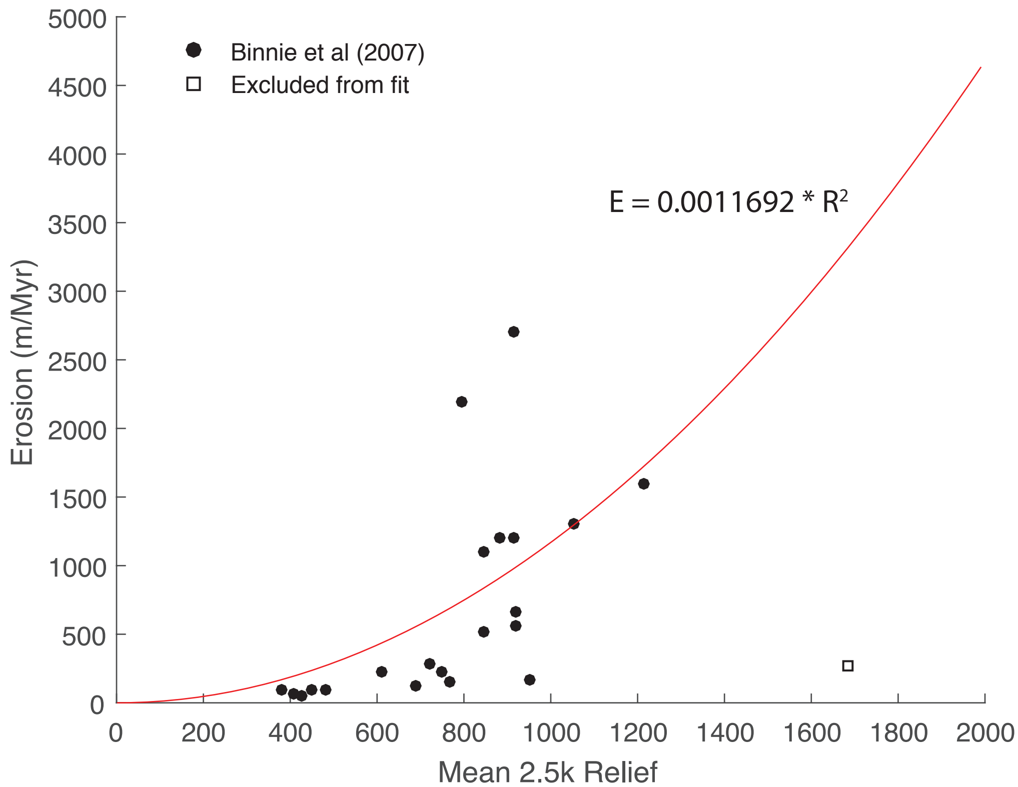

Supplemental Figure 27

Divide SB1

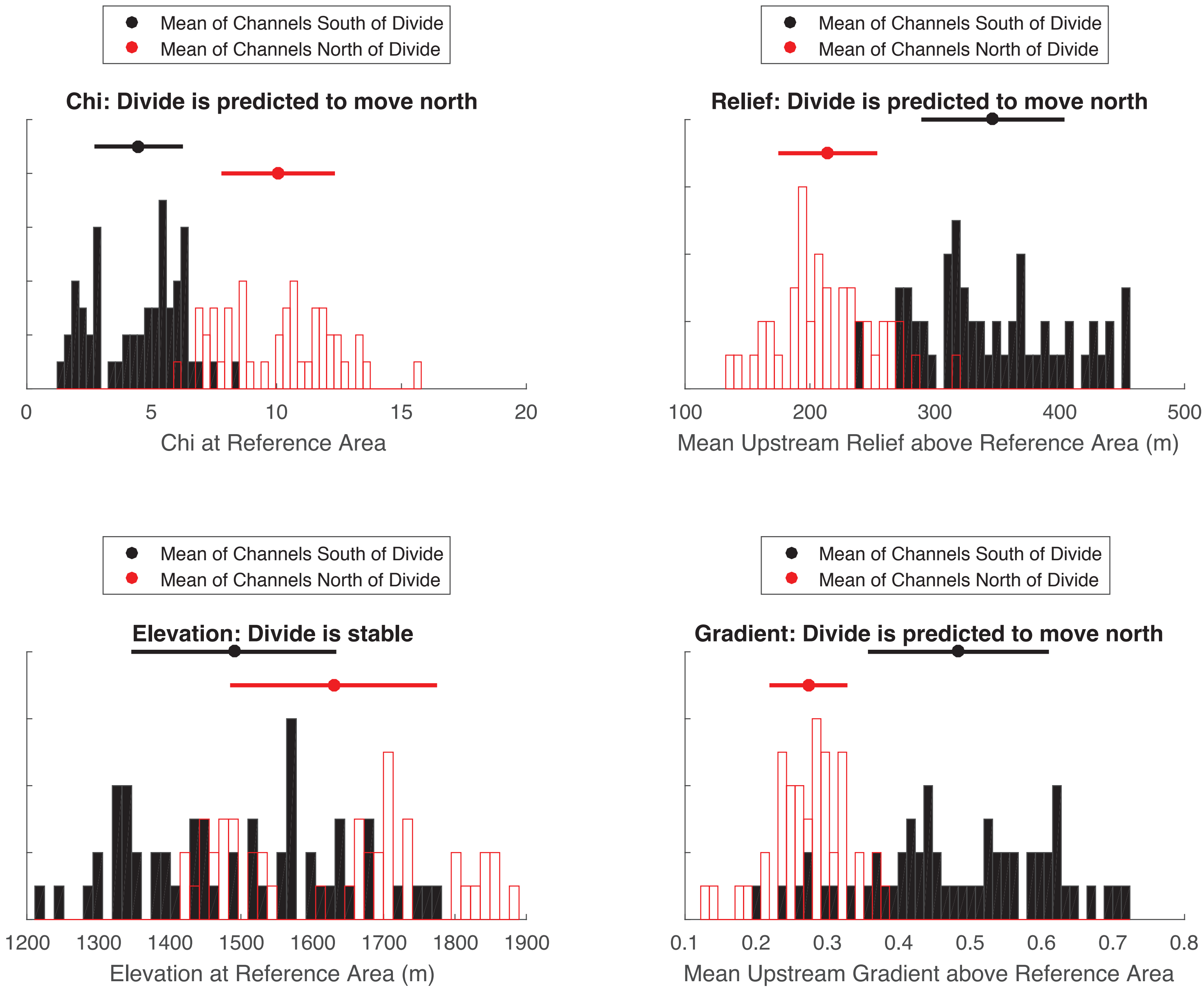

Supplemental Figure 28

Divide SB1

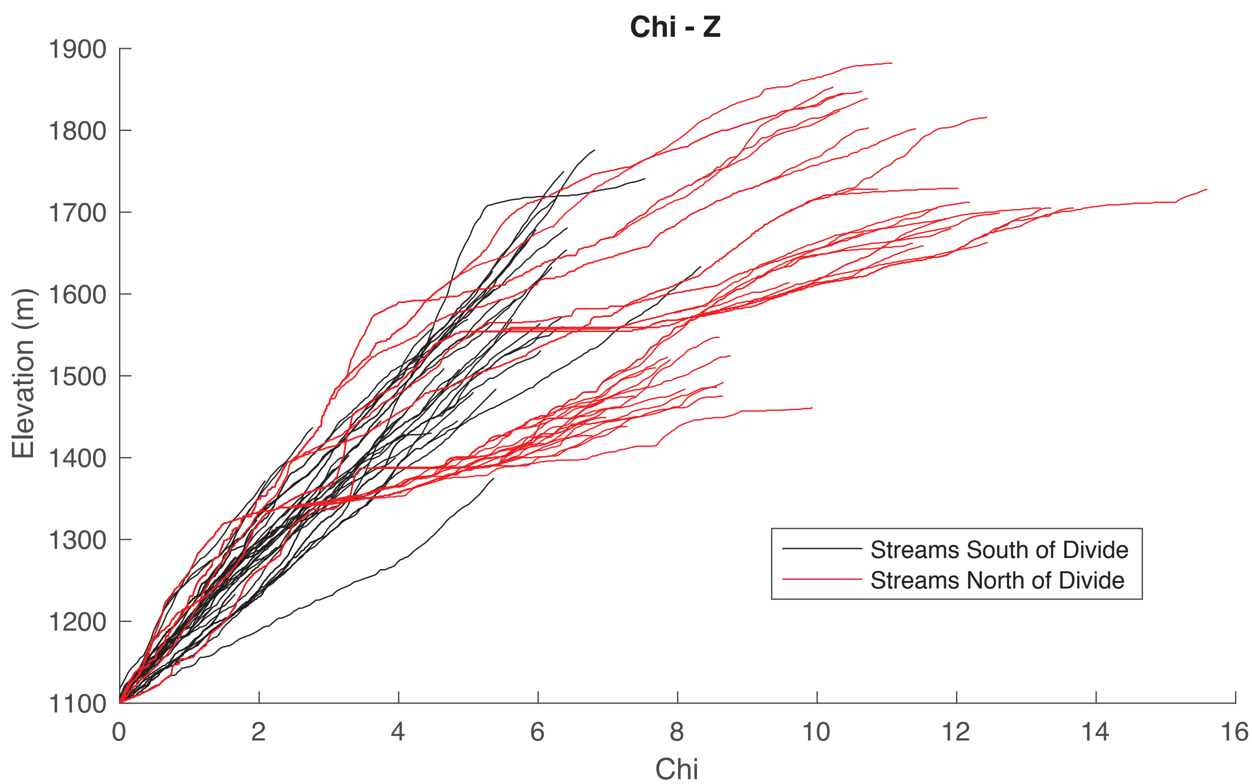

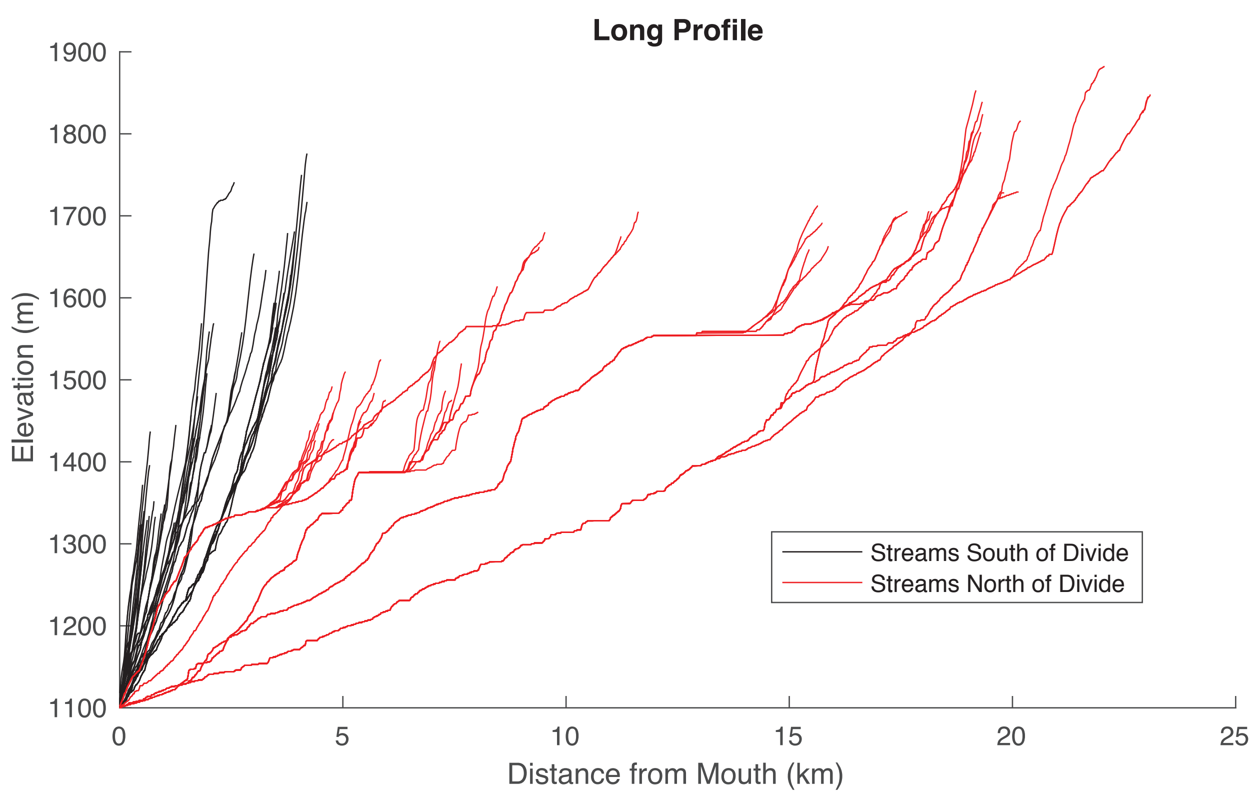

Supplemental Figure 29

Divide SB2

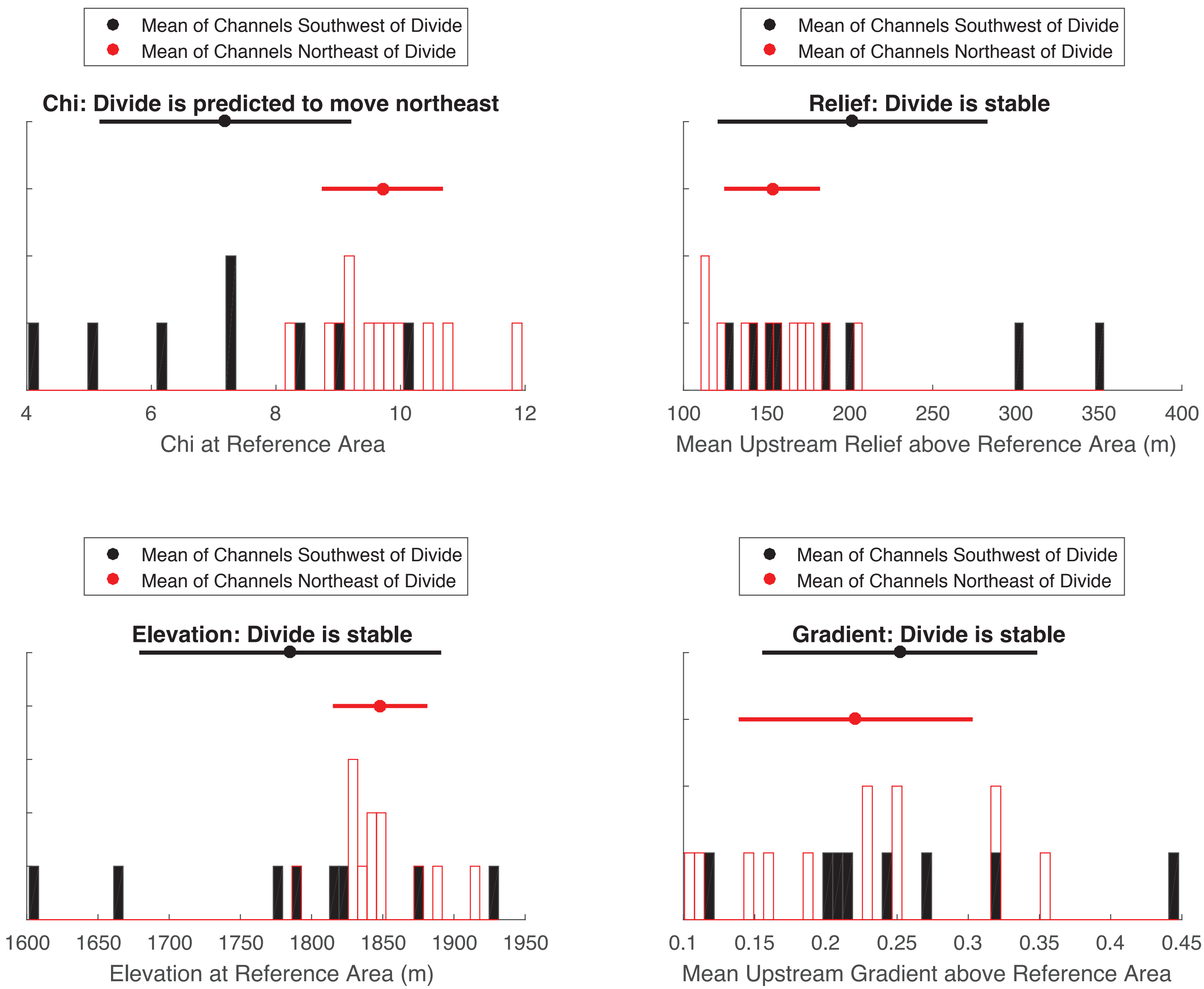

Supplemental Figure 30

Divide SB2

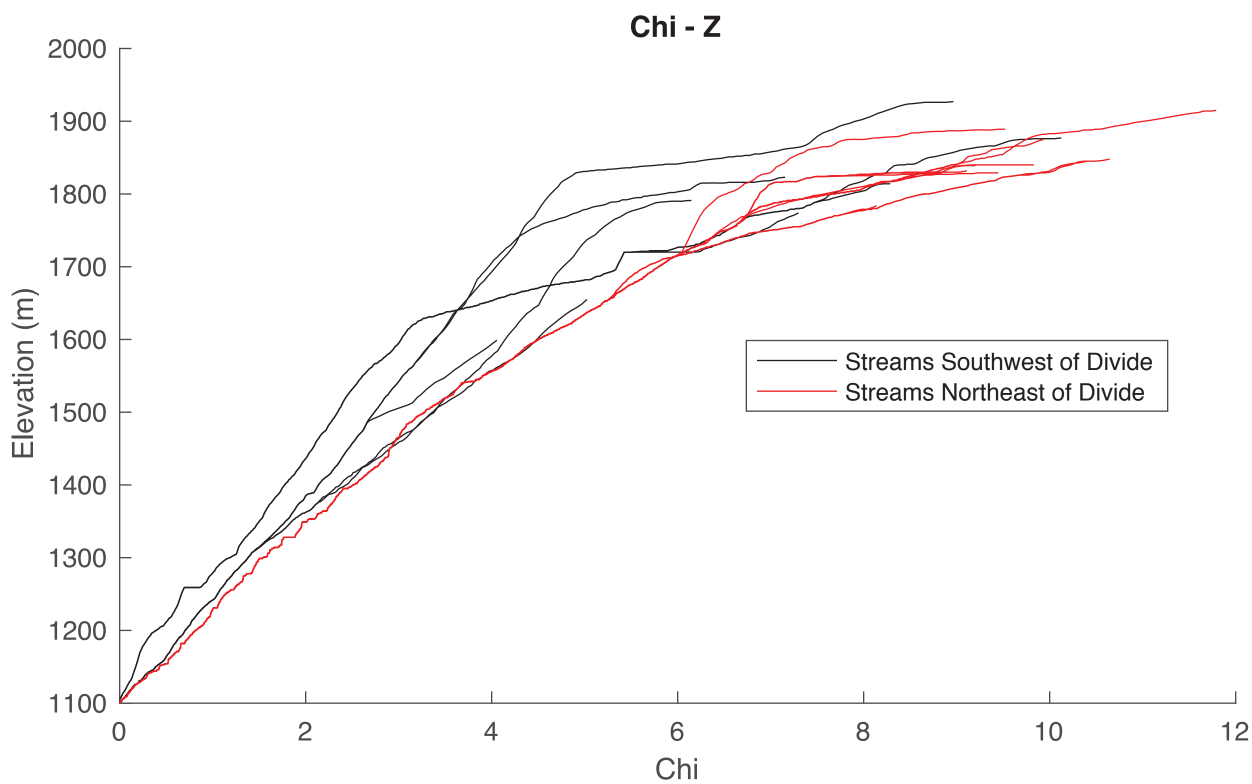

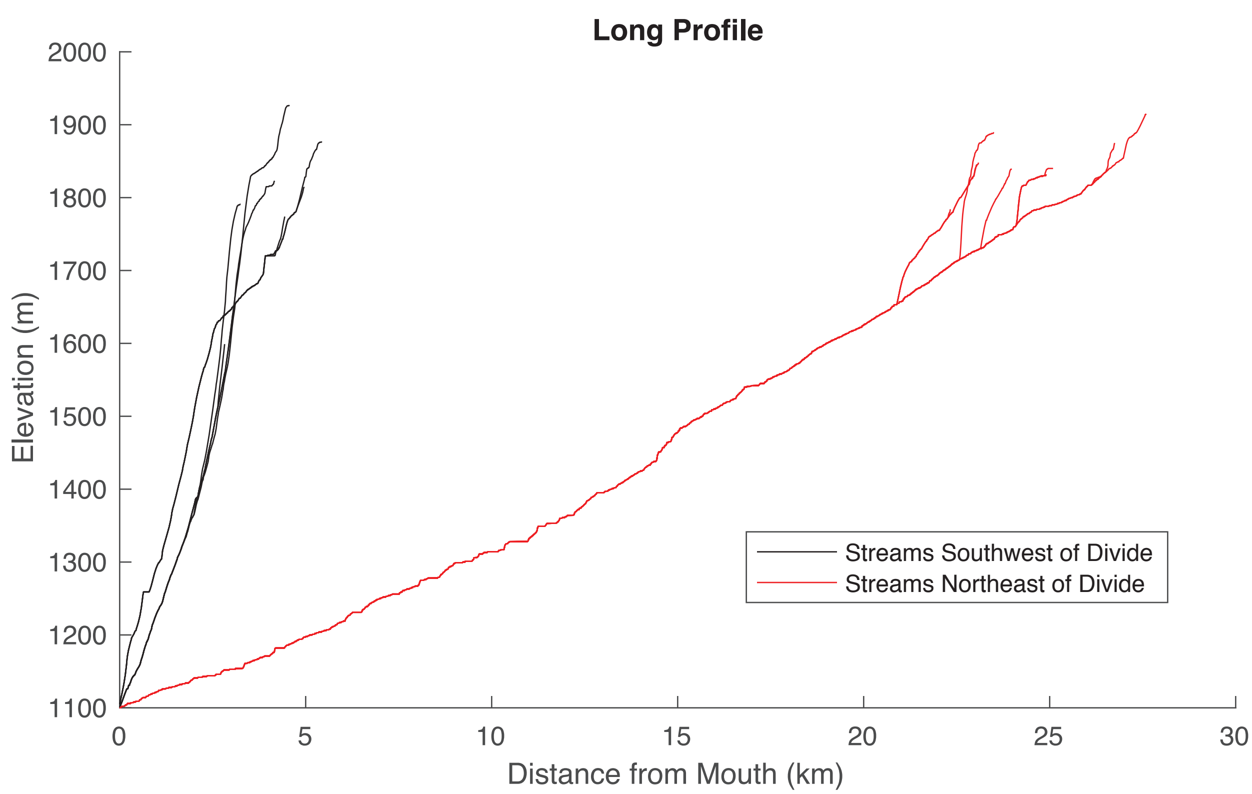

Supplemental Figure 31

Divide SB3

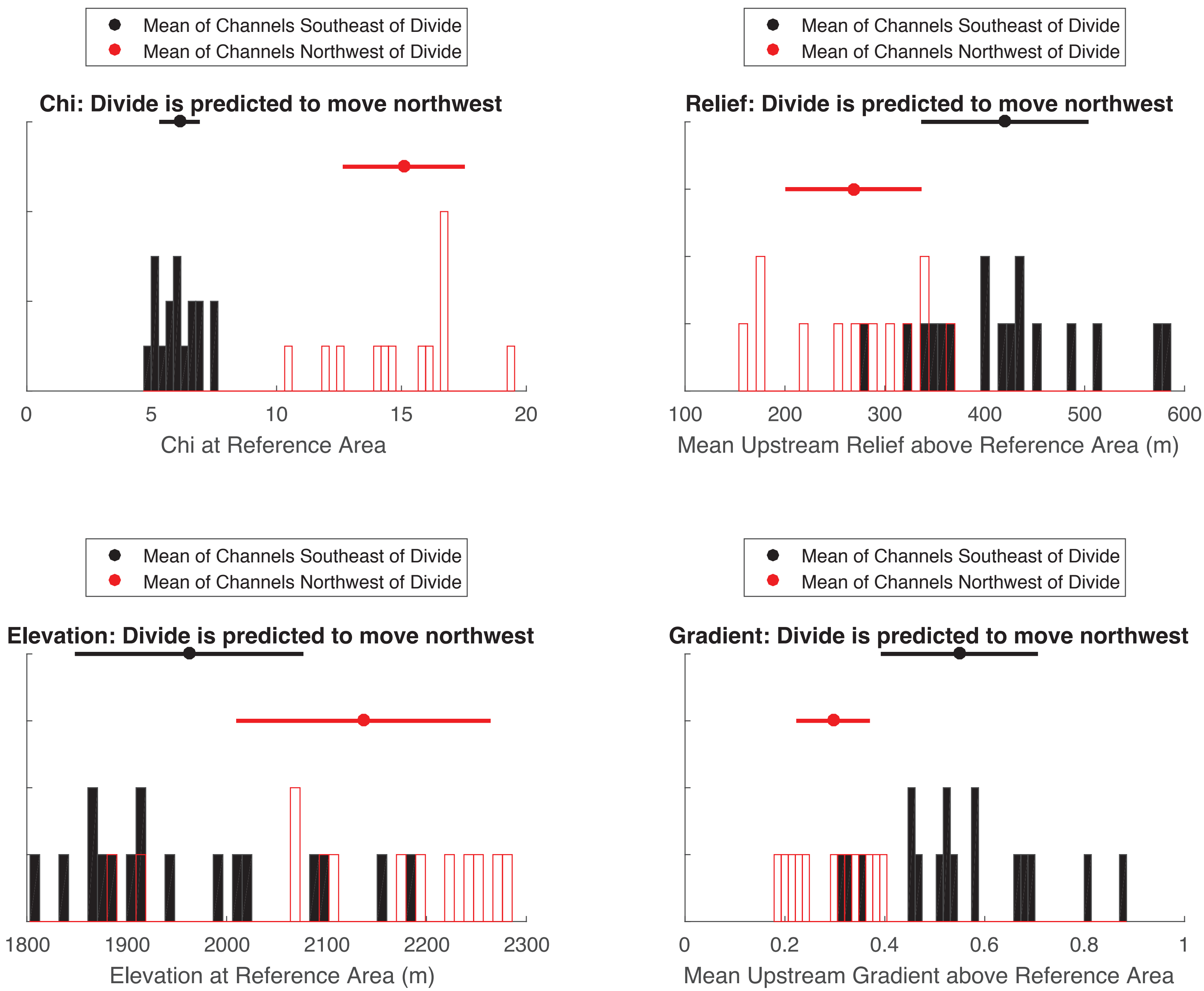

Supplemental Figure 32

Divide SB3

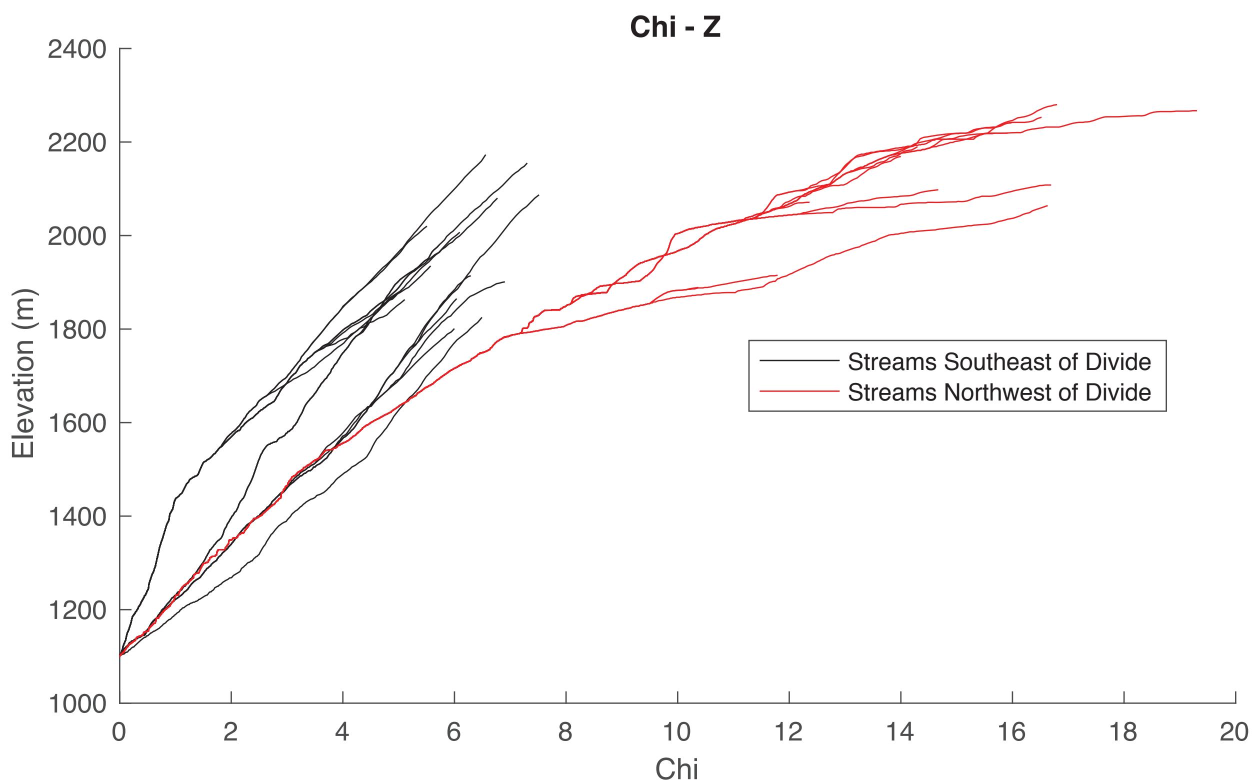

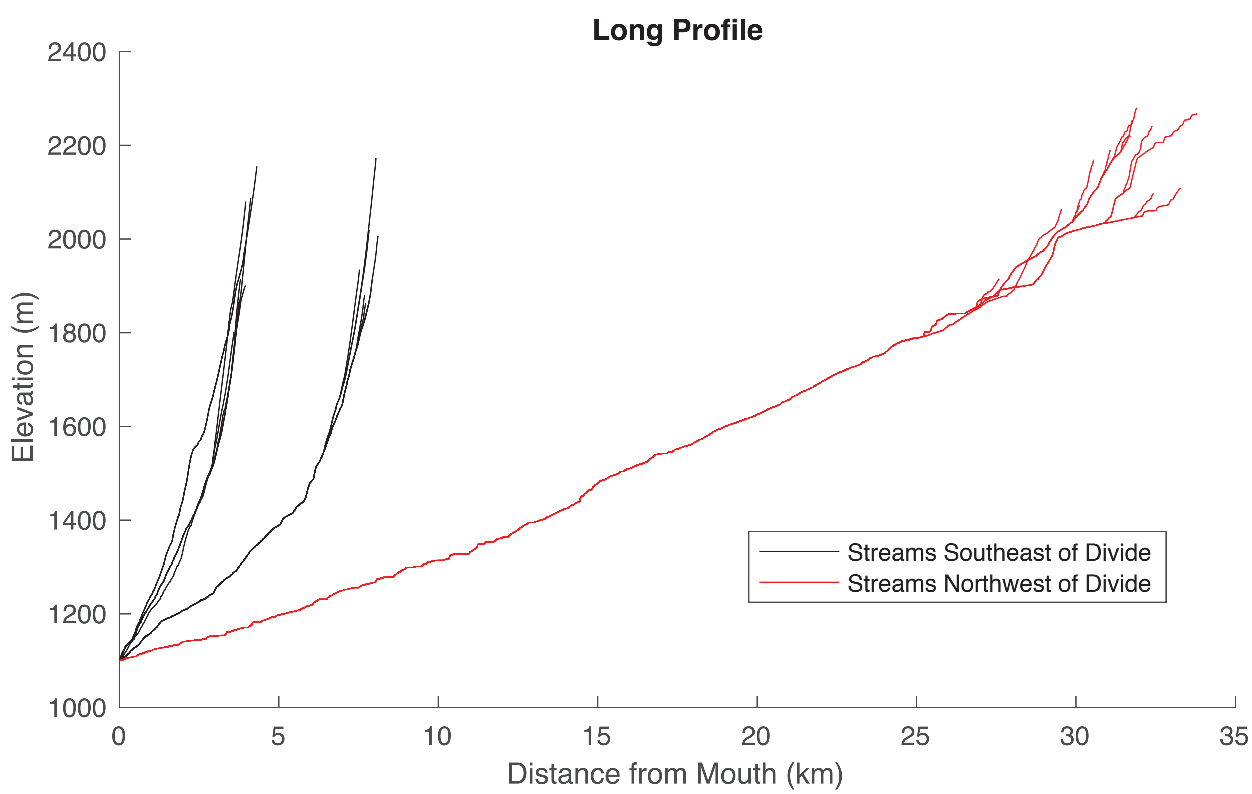

Supplemental Figure 33

Divide SB4

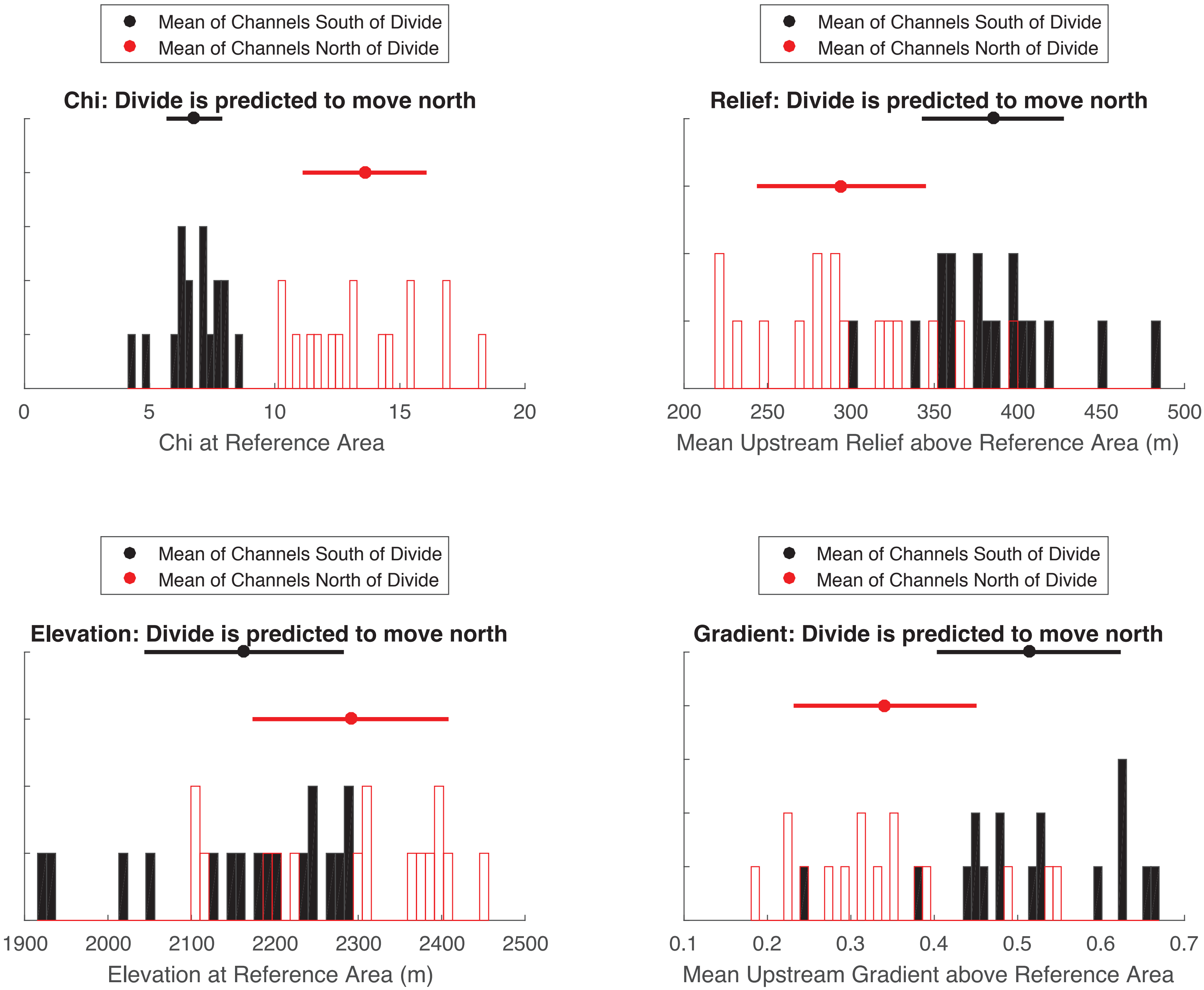

Supplemental Figure 34

Divide SB4

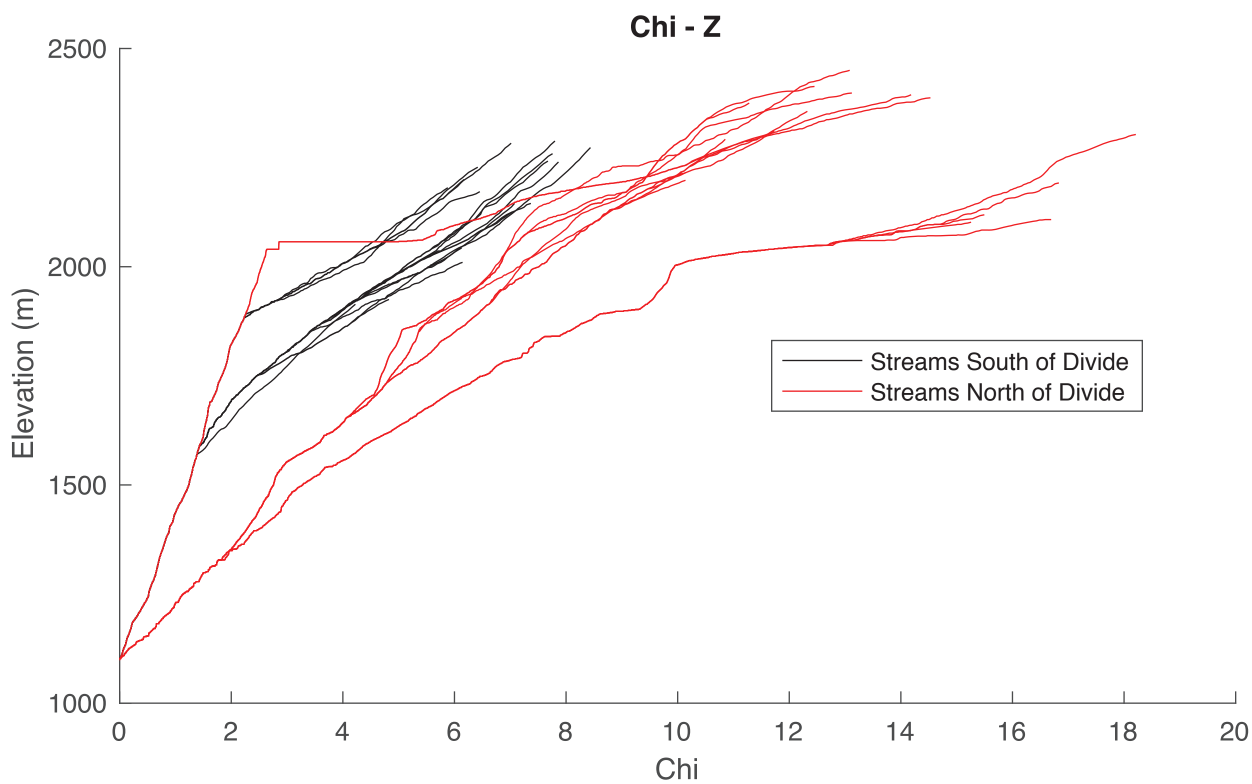

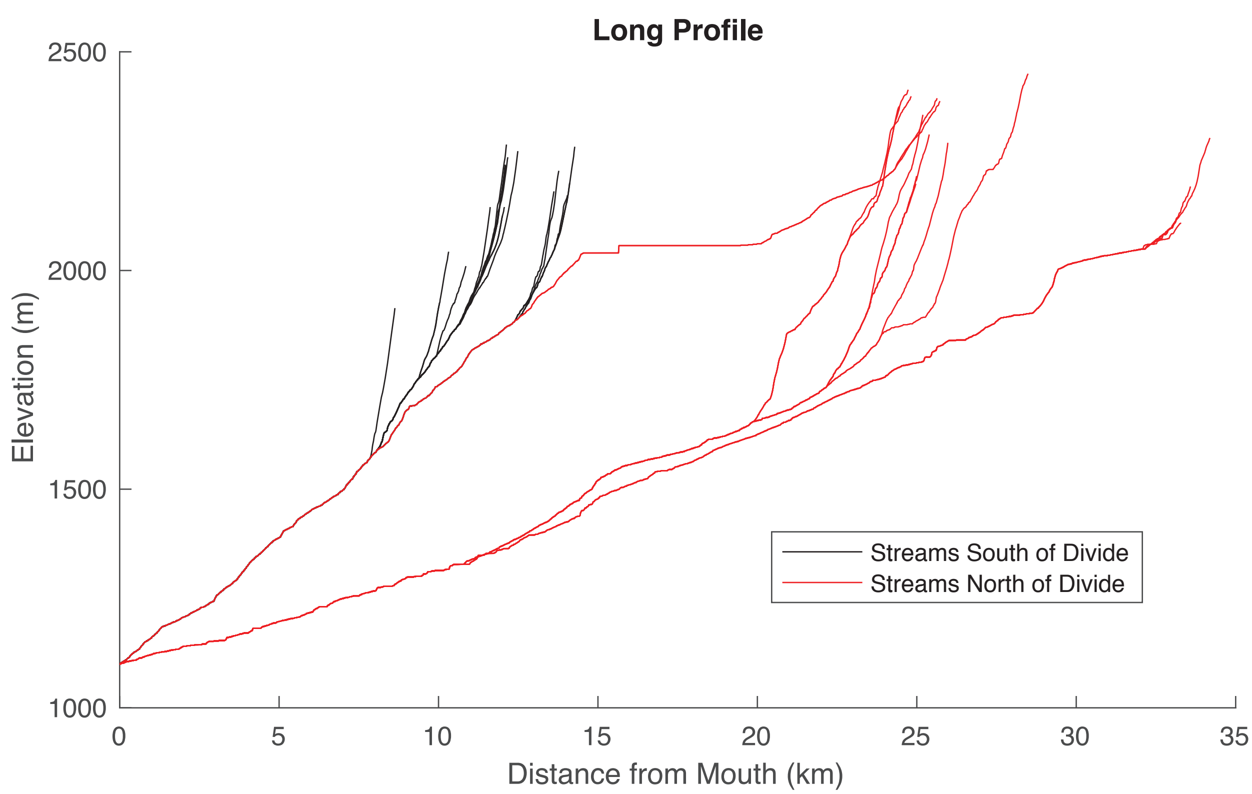

Supplemental Figure 35

Divide SB5

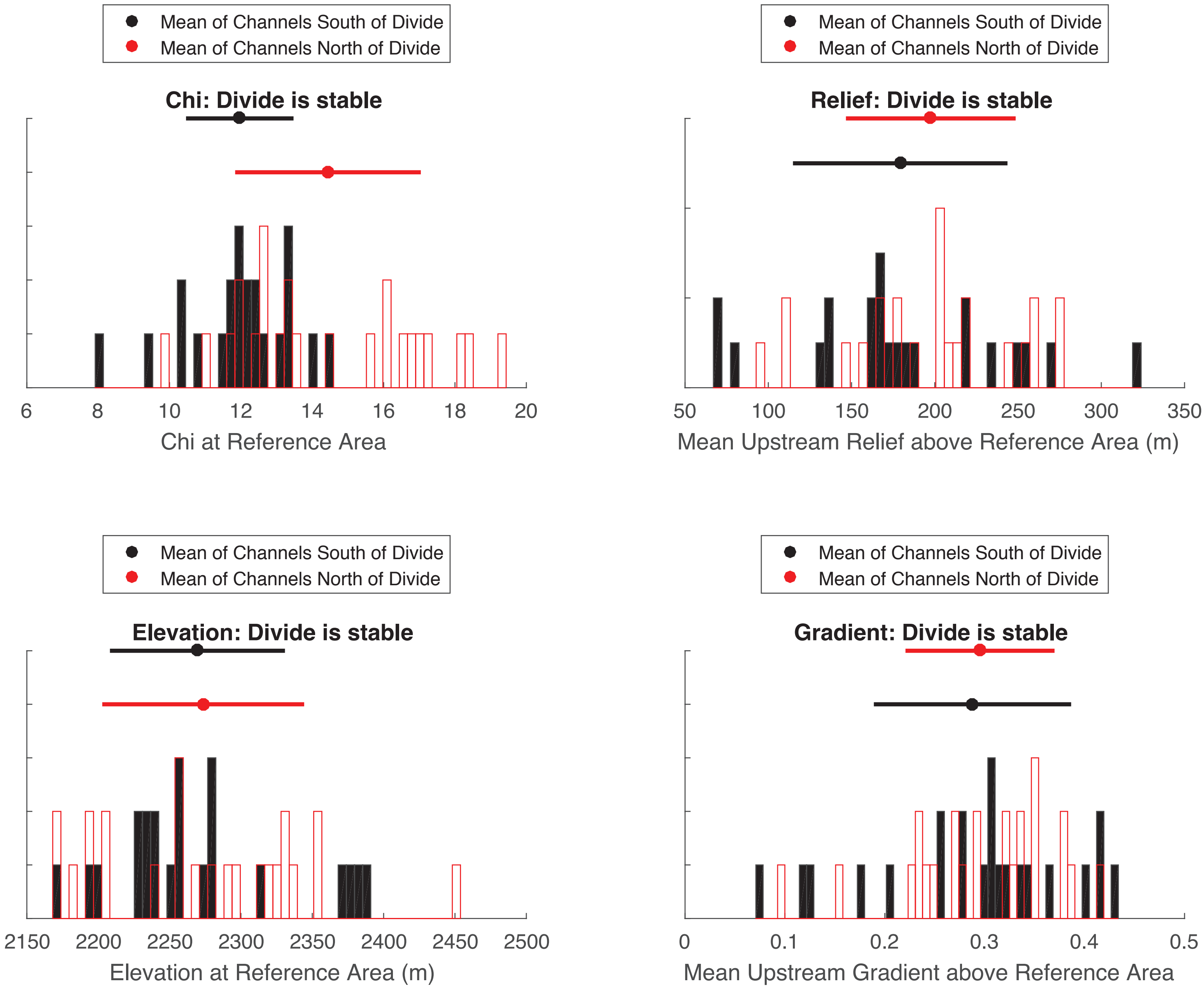

Supplemental Figure 36

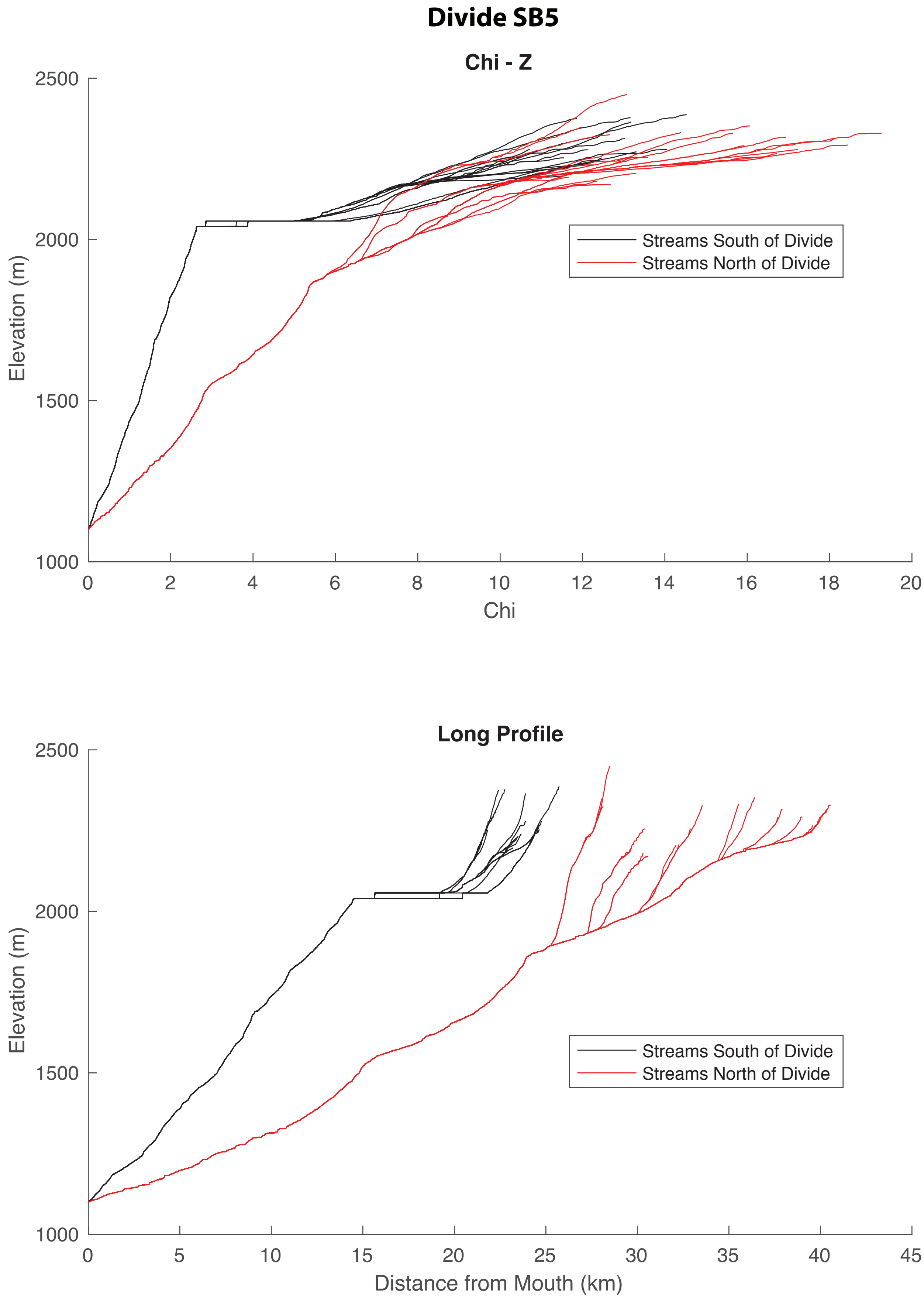

Supplemental Figure 37

Divide SB6

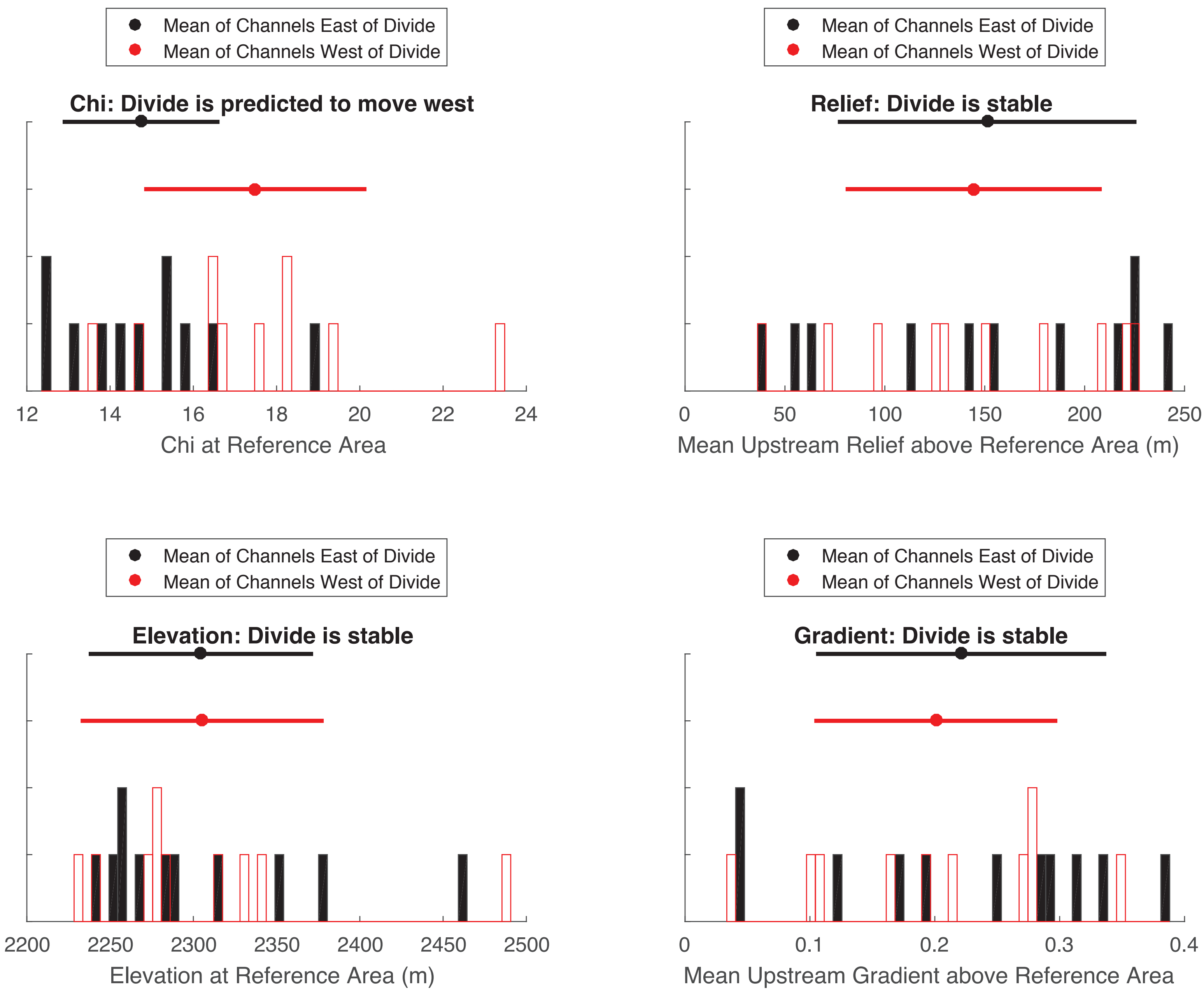

Supplemental Figure 38

Divide SB6

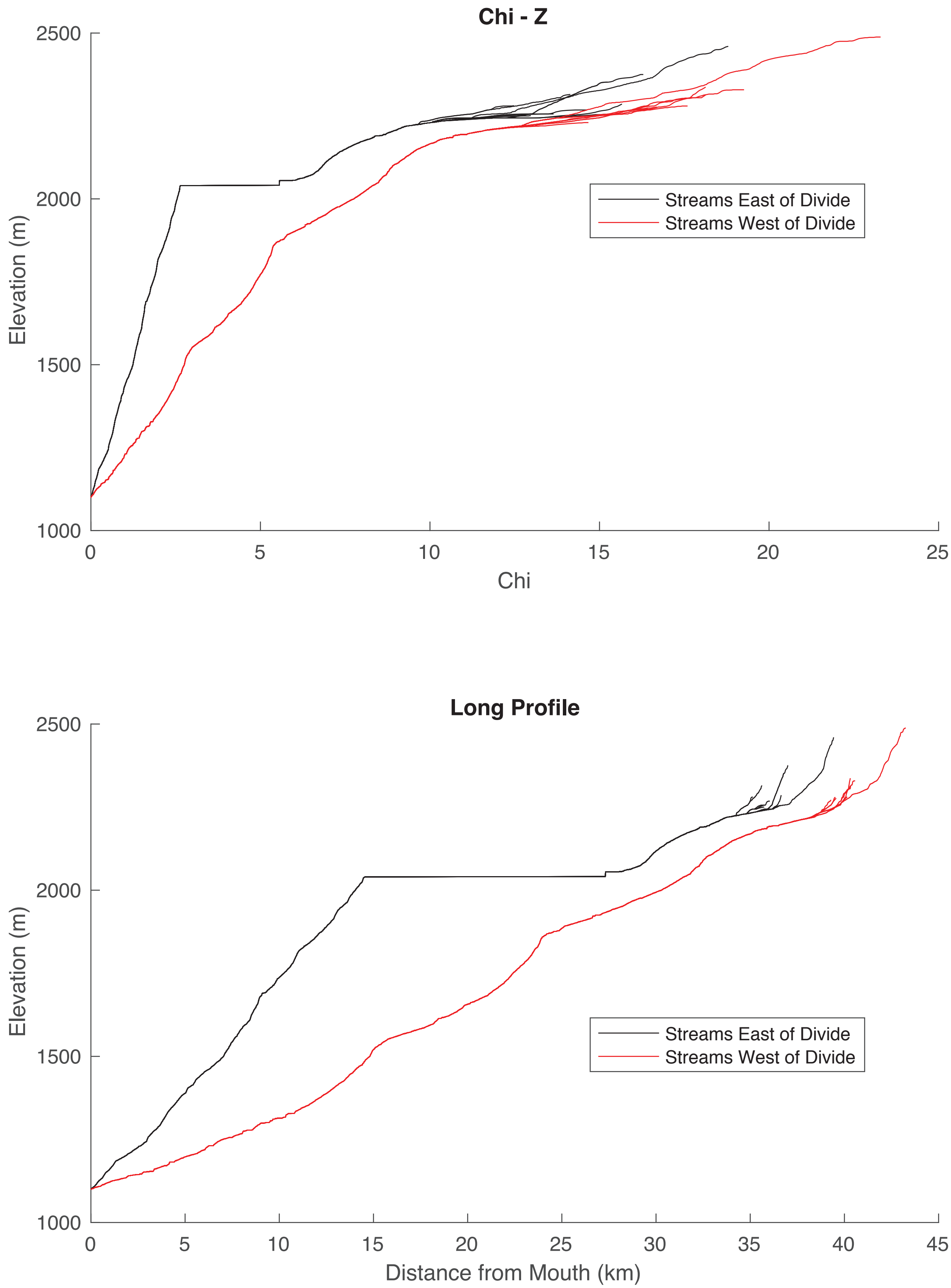

Supplemental Figure 39

Divide SB7

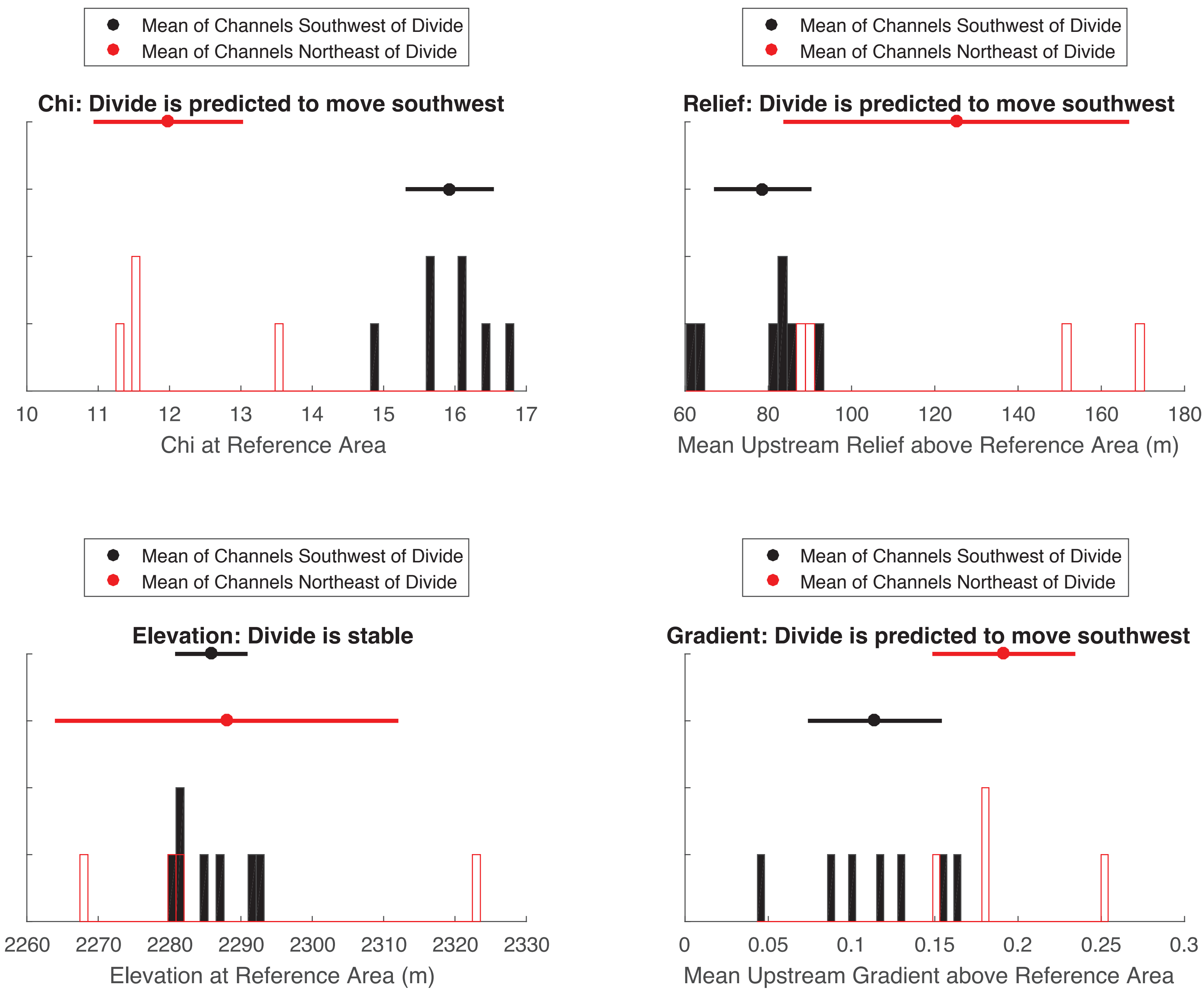

Supplemental Figure 40

Divide SB7

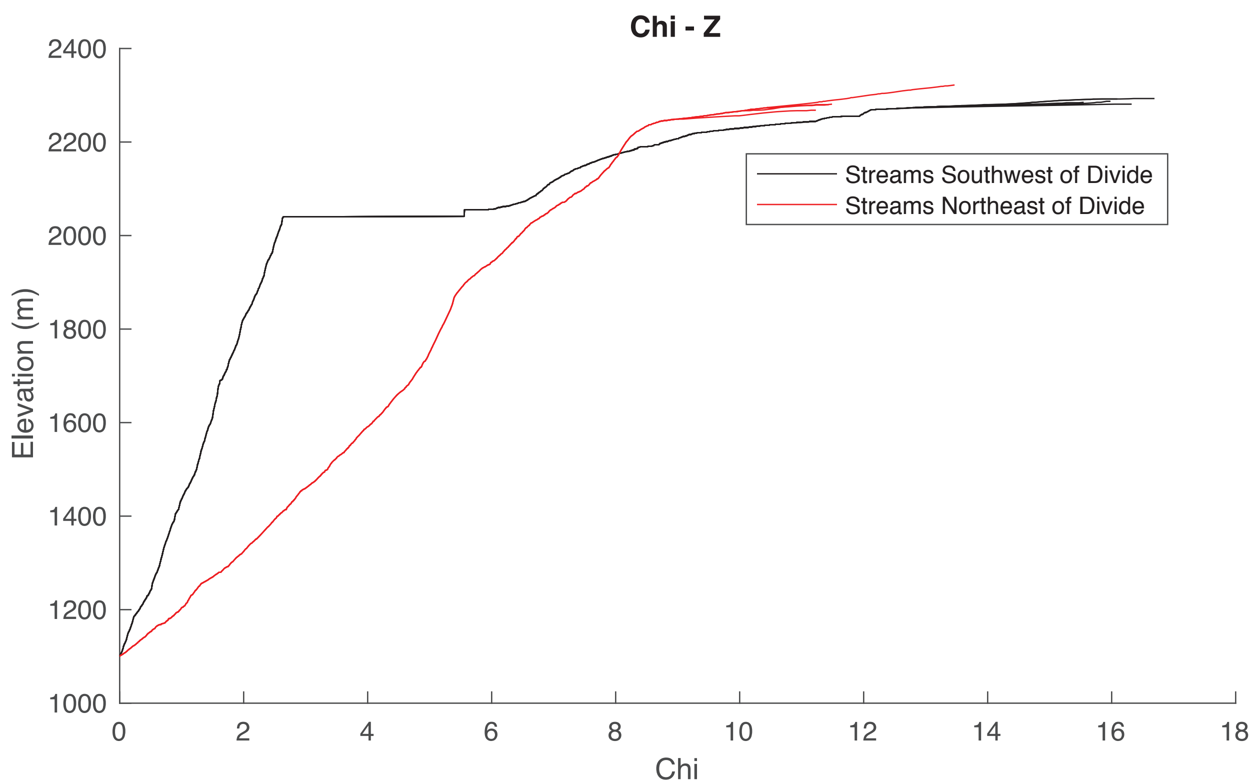

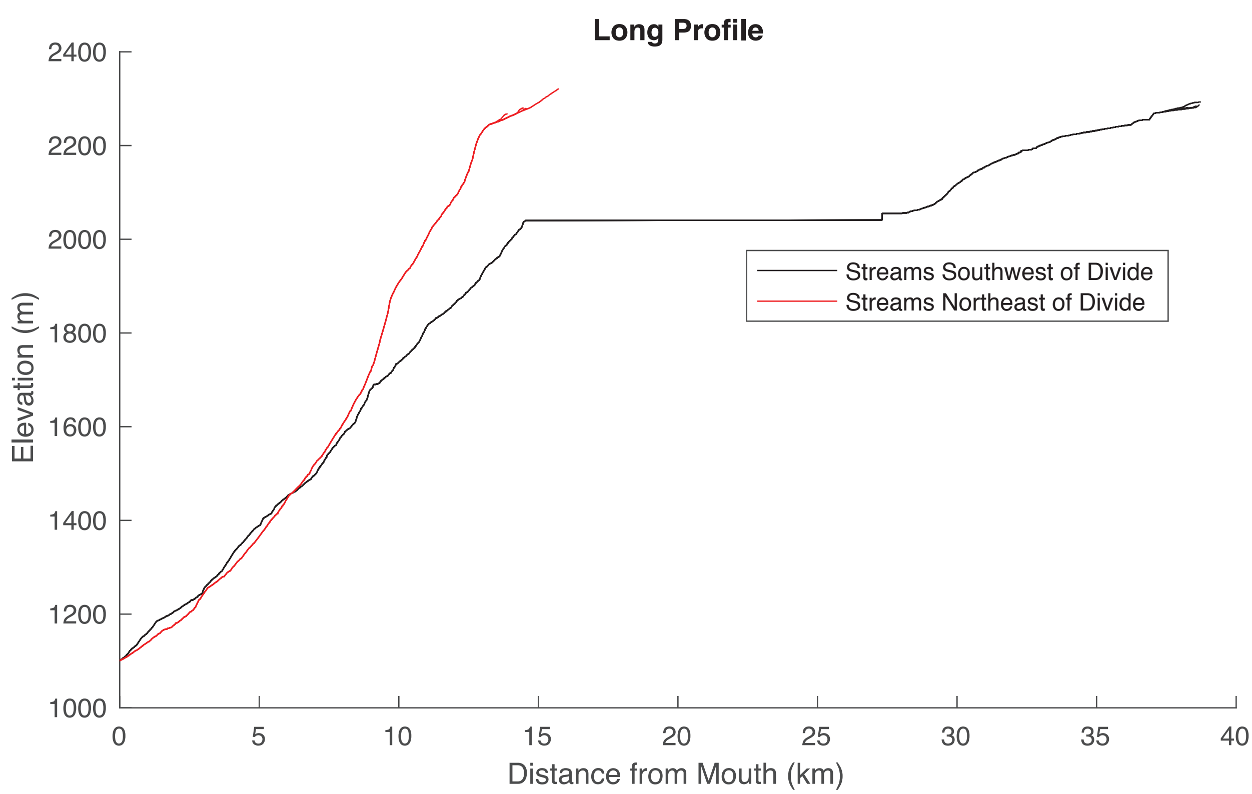

Supplemental Figure 41

Divide SB8

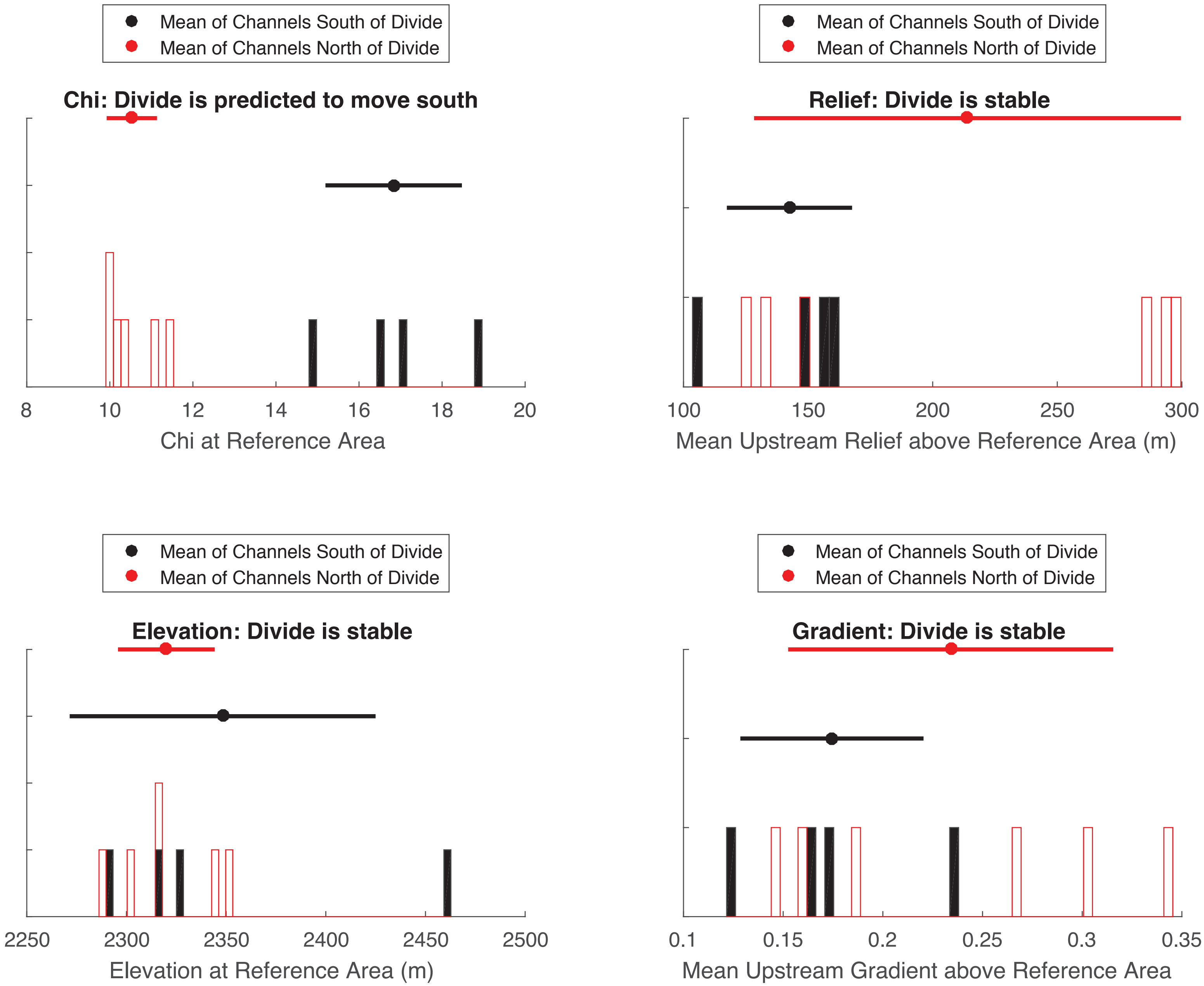

Supplemental Figure 42

Divide SB8

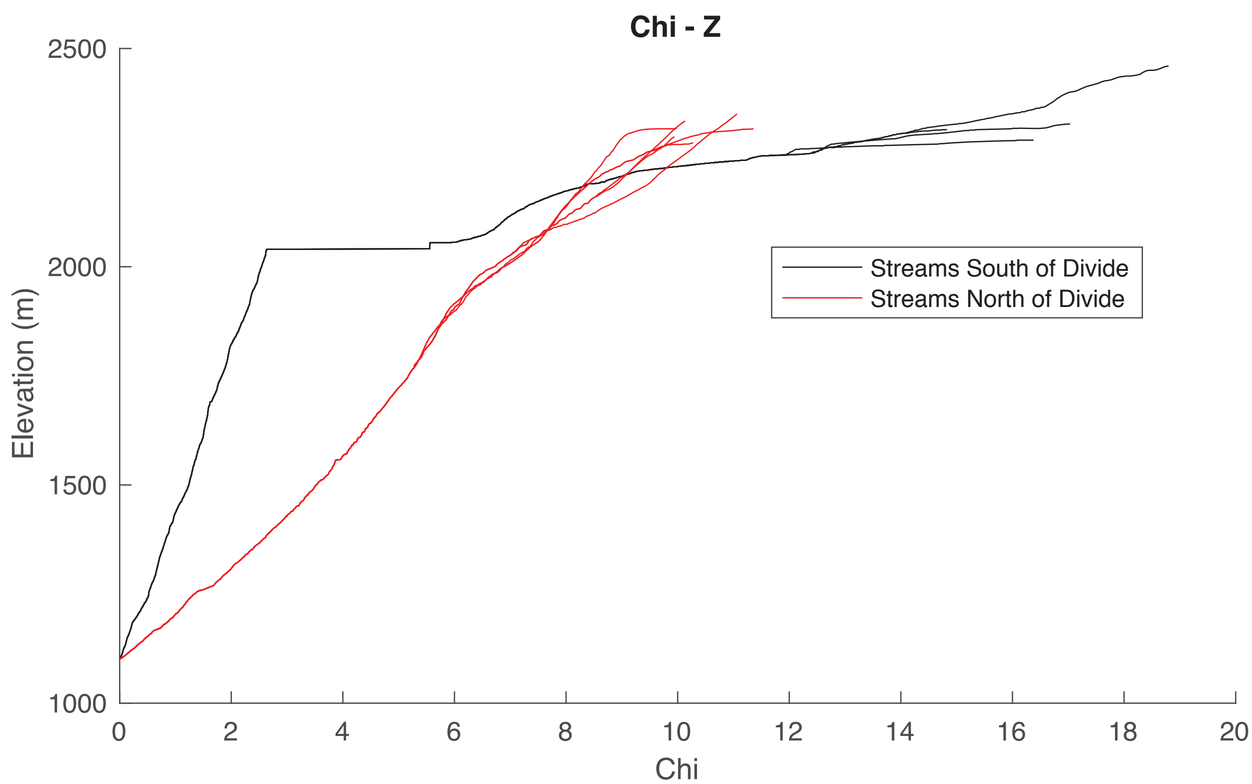

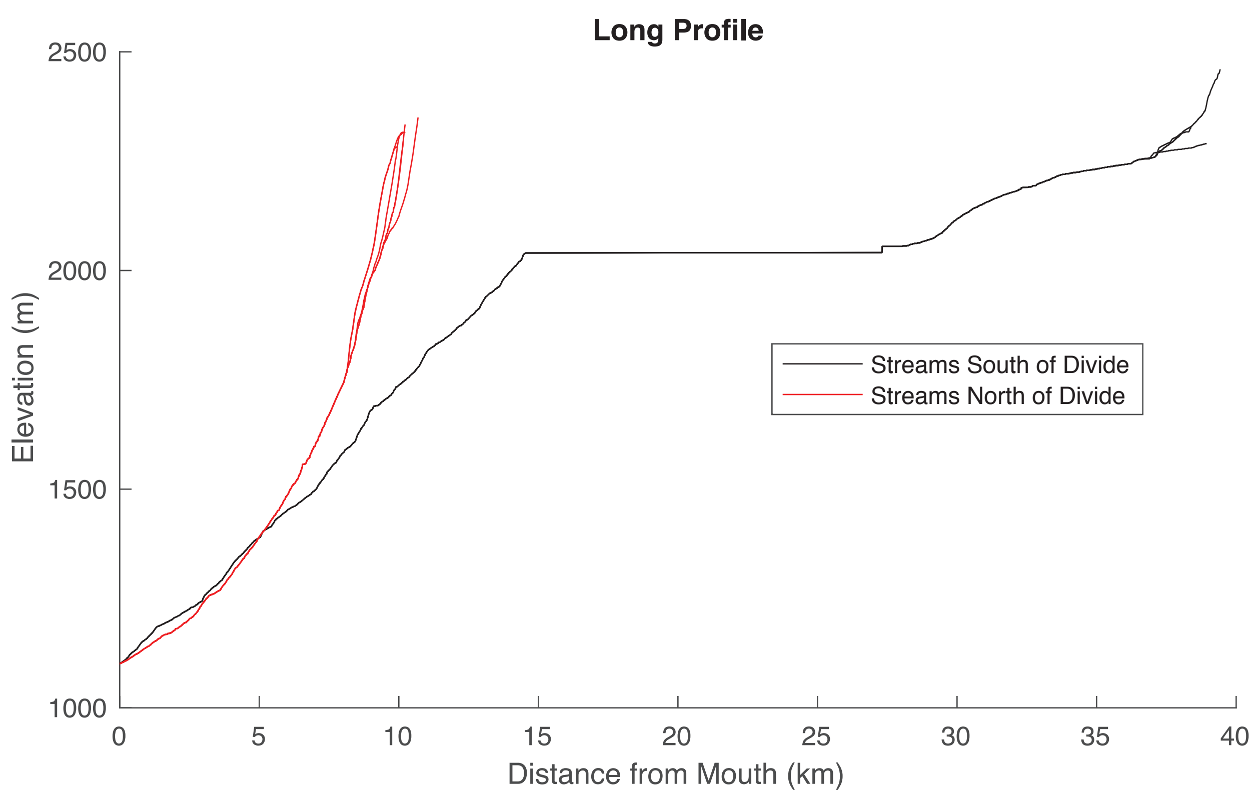

Supplemental Figure 43

Divide SB9

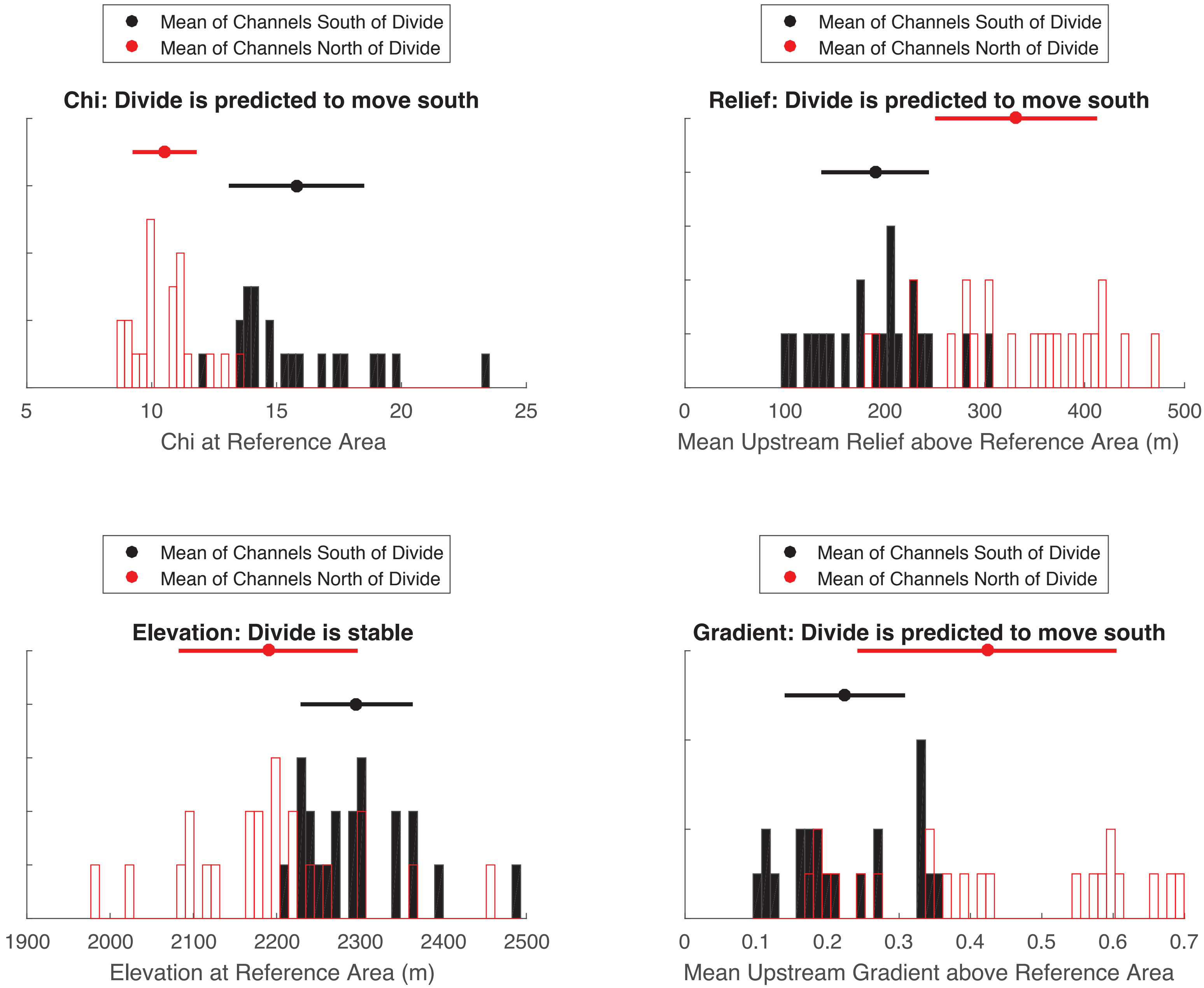

Supplemental Figure 44

Divide SB9

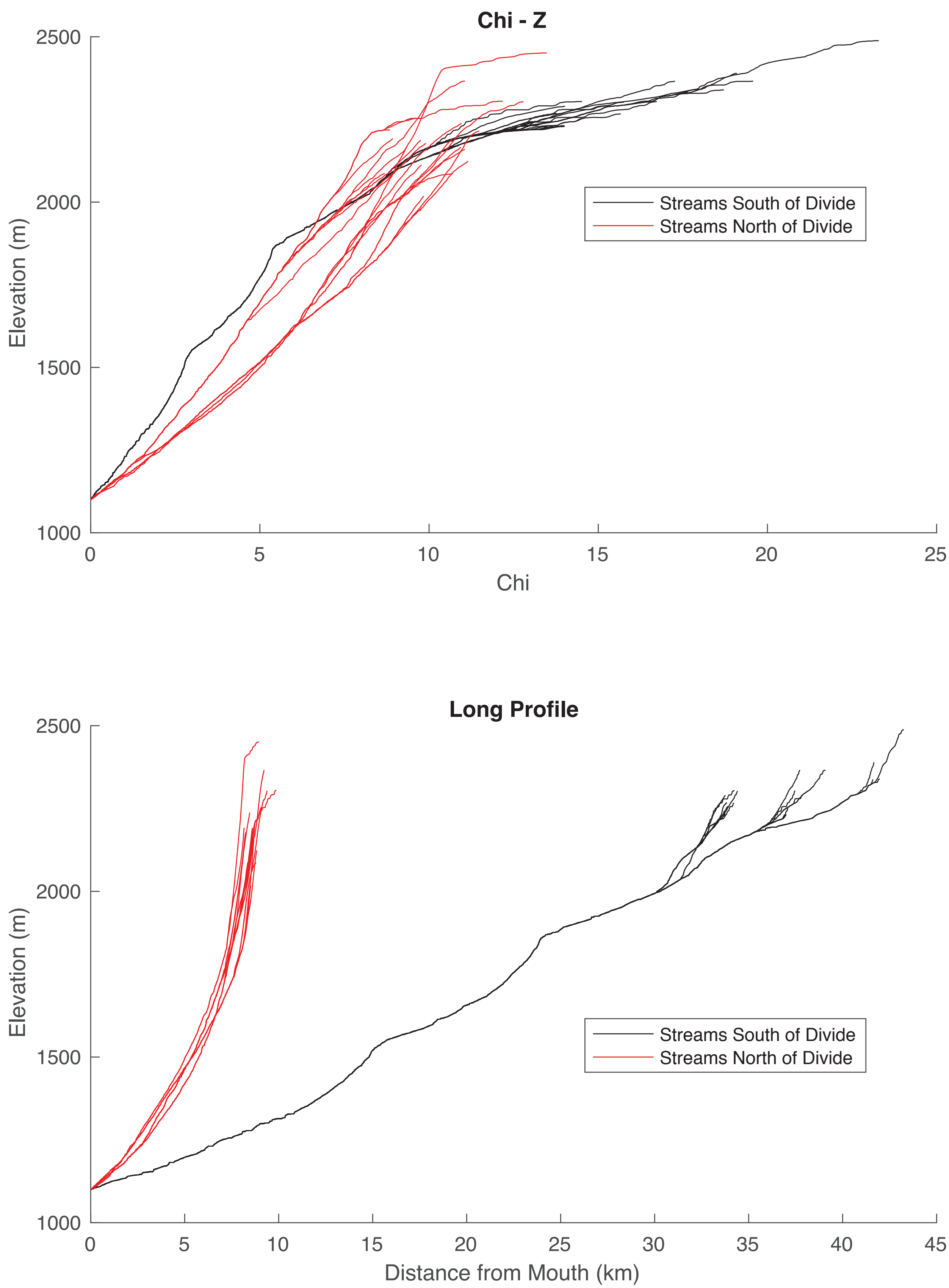

Supplemental Figure 45

Divide SB10

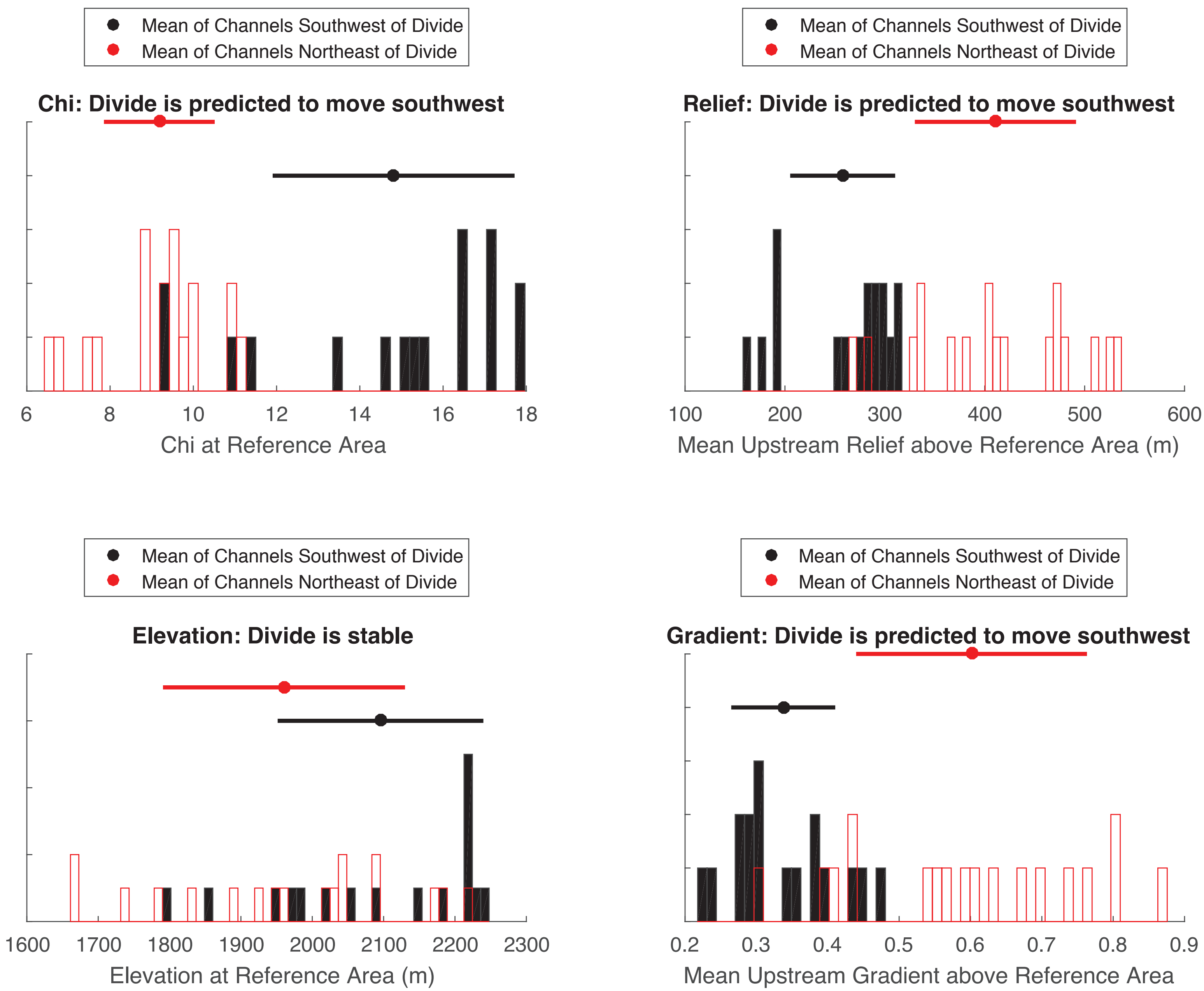

Supplemental Figure 46

Divide SB10

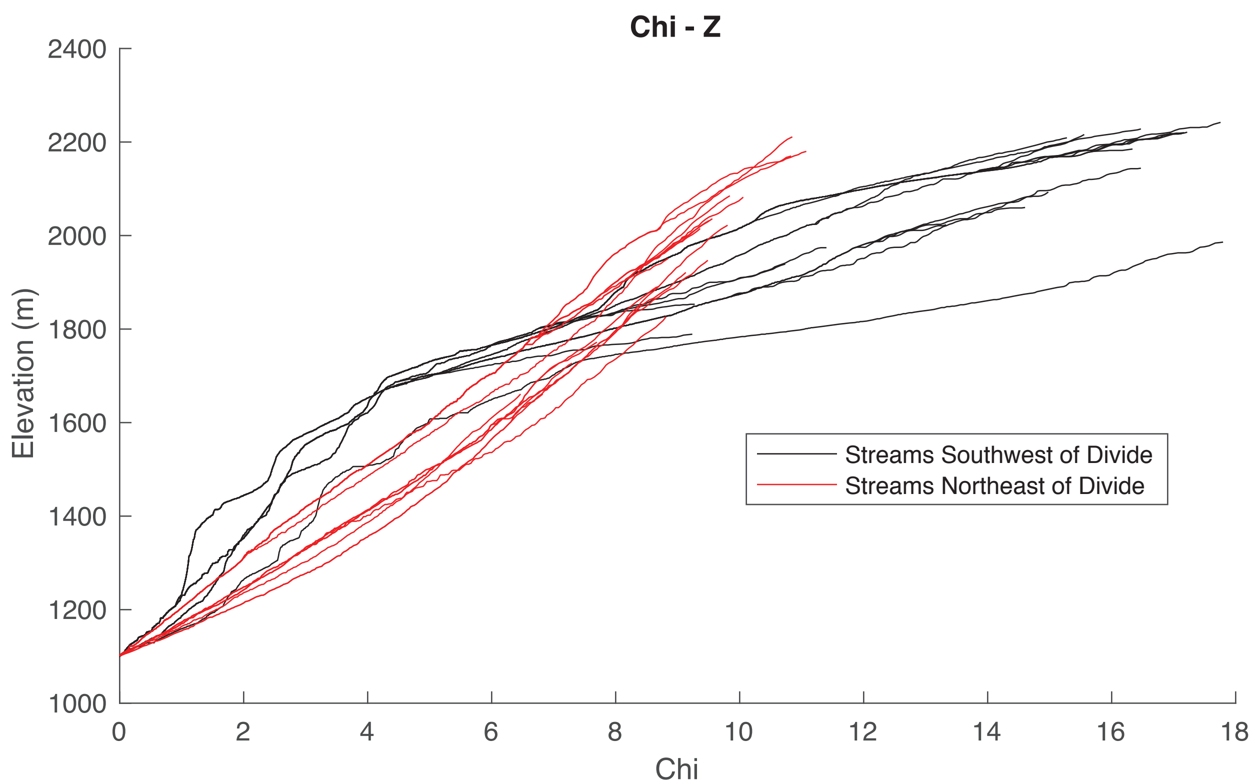

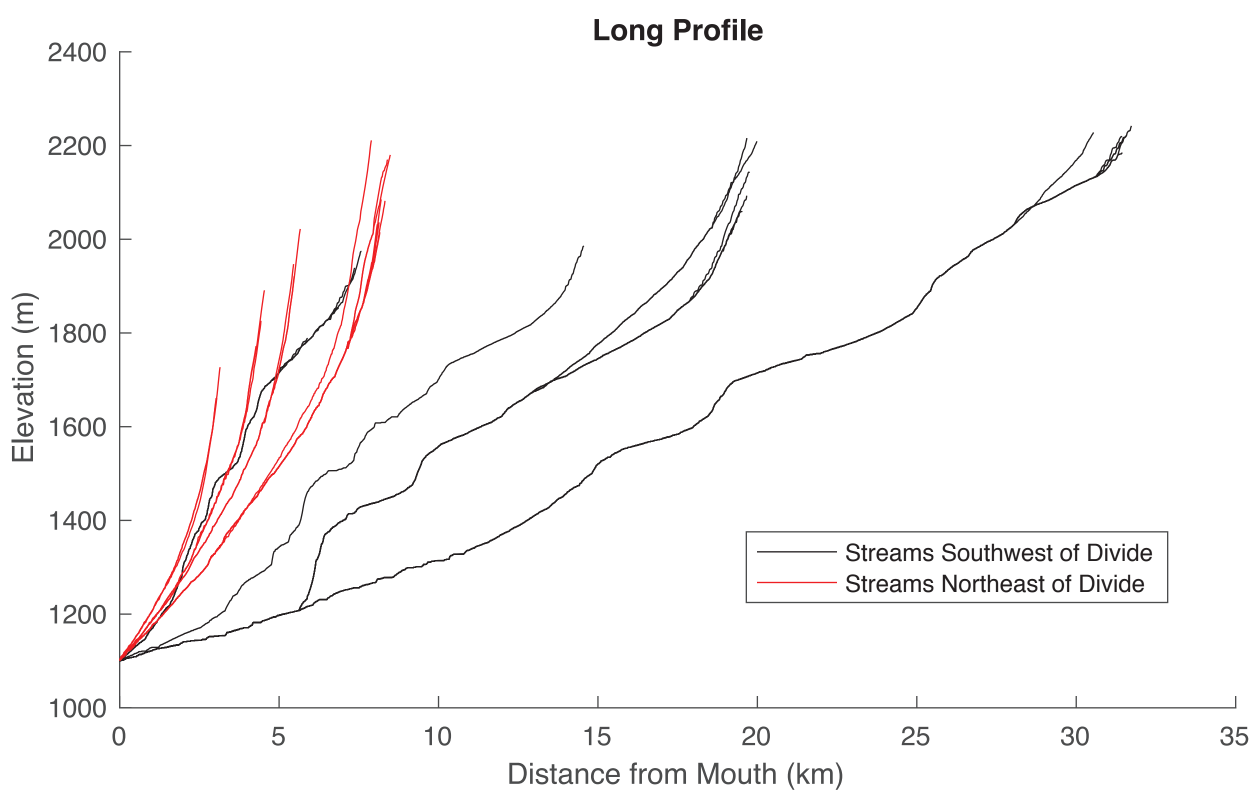

Supplemental Figure 47